CLASSICAL FLIGHT DYNAMICS OF A VARIABLE FORWARD SWEEP WING AIRCRAFT

By

BRETT ALAN NEWMAN

Bachelor of Science

Oklahoma State University

Stillwater, Oklahoma

1983

Submitted to the Faculty of the
Graduate College of the
Oklahoma State University
in partial fulfillment of
the requirements for
the Degree of
MASTER OF SCIENCE
May, 1985

Thesis
1985
N55lc
cop.2

OKLAHOMA STATE UNIVERSITY LIBRARY

CLASSICAL FLIGHT DYNAMICS OF A

VARIABLE FORWARD SWEEP

WING AIRCRAFT

Thesis Approved:

Robert L. Swain
Thesis Adviser

Elmit O. Thom

James K. Good

Norman N. Durham
Dean of the Graduate College

1216348

ACKNOWLEDGMENTS

I want to thank the following people and organizations for their assistance in completing this research effort: Dr. R. L. Swaim for his experience and guidance throughout the research; Dr. F. O. Thomas for his helpful suggestions and thoughts; Dr. J. K. Good for serving as a committee member; Mr. S. Mohan for his numerical and graphics computer program library and assistance in using the Hewlett-Packard 9000 minicomputer and the Theoretical Mechanics Branch, Langley Research Center, National Aeronautics and Space Administration, for their vast resources.

Thanks also go to Mr. and Mrs. G. E. Newman and Mr. M. Maxwell for their encouragement and support during this research effort and the four years of college leading up to this effort. Finally, much appreciation goes to Mrs. G. E. Newman for typing this thesis.

TABLE OF CONTENTS

LIST OF TABLES

LIST OF FIGURES

LIST OF SYMBOLS

English Symbols:

A	aspect ratio or area
b	span
C_{A_x}	x axis aerodynamic force coefficient
C_{A_y}	y axis aerodynamic force coefficient
C_{A_z}	z axis aerodynamic force coefficient
C_D	drag coefficient
C_L	lift coefficient
C_l	roll coefficient
C_m	pitch coefficient
C_n	yaw coefficient
C_{T_x}	x axis thrust force coefficient
$C_{T_{\bar{x}}}$	$\bar{x}$ axis thrust force coefficient
C_{T_y}	y axis thrust force coefficient
$C_{T_{\bar{y}}}$	$\bar{y}$ axis thrust force coefficient
C_{T_z}	z axis thrust force coefficient
$C_{T_{\bar{z}}}$	$\bar{z}$ axis thrust force coefficient
C_y	side force coefficient
c	chord
$\bar{c}$	mean aerodynamic chord
c_m	airfoil pitch coefficient
D	drag
d	diameter

SYMBOLS (Continued)

e	aerodynamic efficiency factor
F	force
F_y	side force
f_{A_x}	x axis perturbation aerodynamic force
f_{A_y}	y axis perturbation aerodynamic force
f_{A_z}	z axis perturbation aerodynamic force
f_{T_x}	x axis perturbation thrust force
f_{T_y}	y axis perturbation thrust force
f_{T_z}	z axis perturbation thrust force
g	gravity
h	altitude
I	incidence angle or moment of inertia
K_{A_x}	x axis aerodynamic moment coefficient
K_{A_y}	y axis aerodynamic moment coefficient
K_{A_z}	z axis aerodynamic moment coefficient
K_{T_x}	x axis thrust moment coefficient
$K_{T_{\bar{x}}}$	$\bar{x}$ axis thrust moment coefficient
K_{T_y}	y axis thrust moment coefficient
$K_{T_{\bar{y}}}$	$\bar{y}$ axis thrust moment coefficient
K_{T_z}	z axis thrust moment coefficient
$K_{T_{\bar{z}}}$	$\bar{z}$ axis thrust moment coefficient
L	lift or roll moment
l	length
M	Mach number or pitch moment
m	mass
m_{A_x}	x axis perturbation aerodynamic moment

SYMBOLS (Continued)

m_{A_y}	y axis perturbation aerodynamic moment
m_{A_z}	z axis perturbation aerodynamic moment
m_{T_x}	x axis perturbation thrust moment
m_{T_y}	y axis perturbation thrust moment
m_{T_z}	z axis perturbation thrust moment
N	yaw moment
q	dynamic pressure
S	area
s	Laplacian variable
sm	static margin
T	thrust force
t	thickness
t^{ε}	wing downwash lag time
t^{σ}	vertical stabilizer sidewash lag time
V	velocity or volume
v	perturbation velocity
x	distance along x
$\bar{x}$	distance along $\bar{x}$
$\bar{\bar{x}}$	distance along $\bar{\bar{x}}$
x'	distance along x'
x''	distance along x''
x'''	distance along x'''
y	distance along y
$\bar{y}$	distance along $\bar{y}$
$\bar{\bar{y}}$	distance along $\bar{\bar{y}}$
y'	distance along y'

y''	distance along y''
y'''	distance along y'''
z	distance along z
$\bar{z}$	distance along $\bar{z}$
$\bar{\bar{z}}$	distance along $\bar{\bar{z}}$
z'	distance along z'
z''	distance along z''
z'''	distance along z'''

Greek Symbols:

∇	angle of attack
α	perturbation angle of attack
β	perturbation sideslip angle or compressibility factor
Δ	control deflection
δ	perturbation control deflection
ε	downwash
ζ	damping ratio
η	dynamic pressure ratio or percent location of control surface root or tip chord
Θ	pitch angle
θ	perturbation pitch angle
κ	airfoil lift curve slope ratio
Λ	sweep angle
λ	taper ratio
ρ	density
σ	sidewash
τ	time constant

ϕ	perturbation roll angle
ψ	perturbation yaw angle
ω	angular velocity or frequency

Superscript Symbols:

A	aileron
B	body
E	elevator, engine or exhaust
F	flap or fuel
H	horizontal stabilizer
I	intake
P	payload
R	rudder
T	thrust
V	vertical stabilizer
W	wing
-W	aircraft excluding wing

Subscript Symbols:

A	aileron
AC	aerodynamic center
A_1	aileron inboard chord
A_2	aileron outboard chord
base	base of body
CG	center of gravity
DR	dutch-roll mode
E	elevator

SYMBOLS (Continued)

E_1	elevator inboard chord
E_2	elevator outboard chord
F	flap
F_1	flap inboard chord
F_2	flap outboard chord
LE	leading edge
max	maximum
min	minimum
nose	nose of body
P	phugoid mode or wing pivot
R	rudder or right
R_1	rudder inboard chord
R_2	rudder outboard chord
root	root chord
S	sonic, spiral mode or structure
stall	stall angle of attack
SP	short period mode
wet	wetted area
wet ex. base	wetted area excluding body base
x	along x axis
$\bar{x}$	along $\bar{x}$ axis
y	along y axis
$\bar{y}$	along $\bar{y}$ axis
z	along z axis
$\bar{z}$	along $\bar{z}$ axis
v_x	partial derivative with respect to v_x
α	partial derivative with respect to α

$\dot{\alpha}$	partial derivative with respect to $\dot{\alpha}$
β	partial derivative with respect to β
$\dot{\beta}$	partial derivative with respect to $\dot{\beta}$
δ^A	partial derivative with respect to δ^A
δ^E	partial derivative with respect to δ^E
δ^F	partial derivative with respect to δ^F
δ^R	partial derivative with respect to δ^R
δ^T	partial derivative with respect to δ^T
ω_x	partial derivative with respect to ω_x
ω_y	partial derivative with respect to ω_y
ω_z	partial derivative with respect to ω_z
0	zero lift
1	steady state

Mathematical Symbols:

d( ) or •	derivative
∂( )	partial derivative
$\Big\vert_1$	evaluated at steady state
[ ]	matrix
{ }	vector
$\angle$	vector notation

Unit Symbols:

kg	kilogram
m	meter
N	Newton
rad	radian

SYMBOLS (Continued)

s	second
°	degree

CHAPTER I

INTRODUCTION

Variable Forward Sweep

The reemerging forward sweep wing is generating a growing interest in the aerospace community. One can see from a brief survey of the current aerospace research literature, the advantages and disadvantages of forward sweep are being throughly investigated for future applications. Research indicates forward sweep is feasible and will be used in future aircraft designs.

A conceivable variation of forward sweep is the merging of forward sweep with variable sweep. Both forward sweep and variable sweep offer significant gains in performance by themselves. The coupling of forward sweep and variable sweep could possibly offer even higher performance levels.

A conventional variable sweep aircraft with backward sweep, or positive sweep angles, is typically designed with minimum longitudinal stability when minimum sweep and subsonic speeds occur. The aircraft's aerodynamic center is at its most forward location in this flight condition. The aerodynamic center and center of gravity both move backward as the sweep is increased, with the aerodynamic center typically moving farther back than the center of gravity. Excessive longitudinal stability which degrades performance and maneuverability can occur at the maximum sweep angle. Supersonic speeds increase the

stability even more by the characteristic backward shift of the aerodynamic center. Elevator control effectiveness reductions can also occur at the maximum sweep angle due to large longitudinal wing moment arms.

The variable forward sweep wing aircraft would logically be designed with minimum longitudinal stability when maximum sweep and supersonic speeds occur. As the sweep decreases or becomes less negative, the aerodynamic center and center of gravity are expected to both move backward, with the aerodynamic center typically moving farther back than the center of gravity. The longitudinal stability will increase with decreasing sweep until subsonic speeds occur. At that time, the stability will decrease due to the characteristic forward shift of the aerodynamic center. If this reduction in stability is significant, the forward variable sweep aircraft will not be hampered as much by the excess stability and control shortage problems that occur with backward variable sweep aircraft.

The lateral-directional characteristics will also be affected by the wing sweep angle. The roll characteristics can be expected to experience the predominate change among the lateral-directional characteristics. For the variable forward sweep wing aircraft, the wing mean aerodynamic chord and aileron moment arm both move inboard as the sweep increases or becomes more negative; consequently, the roll damping and roll response should be reduced, respectively. The inboard movement of the mean aerodynamic chord with increasing sweep should also be expected to reduce the yaw damping.

The longitudinal and lateral-directional characteristics will also be affected through changes in the moments of inertia due to variable sweep. For the variable forward sweep wing aircraft, increasing or more

negative wing sweep should result in pitching and rolling moment of inertia reductions. These reductions should tend to improve the pitching and rolling responses.

A variable forward sweep wing aircraft is an interesting and formidable concept to analyze. For the reasons discussed in this section, the analysis of the flight dynamics of a variable forward sweep wing aircraft was selected as the Master Of Science thesis topic.

Research Scope

The level of complexity of the research is a classical aircraft stability and control analysis such as presented by Roskam (1). Assumptions include rigid body, linearized dynamics and aerodynamics, ideal control surface actuators and no automatic flight control system. The flexibility, linearization, actuator dynamics and automatic flight control system assumptions are introduced because 1) the research is intended to analyze the effects on an aircraft's flight dynamics resulting solely from the variable forward sweep concept and 2) to simplify the analysis.

The equations of motion are uncoupled into a longitudinal set and a lateral-directional set. Laplace transformation and partial fraction expansion theory are used to manipulate and solve the equations of motion. Numerical calculations are performed by programming the equations of motion into a digital computer. Numerical results consist of the characteristic equation root loci, mode shapes and time responses at various wing sweep angles and dynamic pressures. The International System of metric units (SI) is used exclusively throughout this thesis.

Areas to be addressed in the research include aerodynamic center movement, center of gravity movement, characteristic equation root loci behavior, mode shape behavior, time response behavior and dynamic pressure and Mach number effects. The overall goal is to 1) relate the flight dynamics results and trends with the physics of the variable forward sweep concept and 2) indicate any significant advantages or disadvantages associated with the variable forward sweep concept.

CHAPTER II

LITERATURE SURVEY

Variable Sweep

Variable sweep is a design which allows an aircraft's wing sweep angle to be varied during flight and is used to achieve acceptable performance levels throughout the flight envelope. Low and moderate subsonic speeds demand a high aspect ratio, lowly swept wing. High aspect ratio, lowly swept wings result in efficient lift curve slopes and low takeoff and landing speeds. High subsonic speeds and transonic speeds demand a moderate aspect ratio, moderately swept wing to achieve acceptable lift to drag ratios for cruising flight and to delay compressibility drag. Supersonic speeds demand a low aspect ratio, highly swept wing. Low aspect ratio, highly swept wings result in weaker oblique shock waves rather than stronger normal shock waves. Variable sweep is a unique and proven technique which satisfies the diversified wing characteristics required over an aircraft's flight envelope.

A complete history of variable sweep can be found in the papers by Polhamus and Toll (2) and Kress (3). The National Advisory Committee for Aeronautics (NACA) conducted the first extensive research on variable sweep for the purpose of achieving suitable performance levels throughout an aircraft's flight envelope (2). Early wind tunnel research indicated a fixed wing pivot located inboard the aircraft's

fuselage forced extreme wing aerodynamic center travel as the sweep angle varied. With backward sweep, excessive static margins and longitudinal stability resulted. Supersonic speeds aggravated the problem even more by the characteristic backward shift of the aerodynamic center.

The X-5 was the first variable sweep aircraft to fly (2). The X-5 employed variable backward sweep varying from 20° to 60° with an inboard, translating wing pivot to alleviate the excessive stability problem. Flight tests indicated no significant improvements existed over fixed wing aircraft which was later found to result from a poor design. The XF10F-1 was the next variable sweep aircraft to fly (3). The XF10F-1 also employed variable backward sweep varying from 12.5° to 42.5° with an inboard translating wing pivot. Flight tests indicated significant improvements in landing speeds, range and maximum speeds relative to similar fixed wing aircraft.

NACA continued research on variable sweep and discovered in the late 1950's that a fixed forewing and a fixed wing pivot located within the forewing would solve the problem of excessive stability without the complexity of a translating wing pivot (2). Many aircraft using this technique have been produced including the Grumman F-14, General Dynamics F-111 and Rockwell B-1.

All variable sweep aircraft produced to date have employed backward sweep. No research could be found on variable forward sweep except for the mentioning by Polhamus and Toll (2) that variable forward sweep is an unestablished design option.

Forward Sweep

Forward sweep is a design where wings are swept forward to counter certain high speed aerodynamic characteristics. Backward sweep also counters these characteristics. Sweep is used to delay compressibility drag associated with high subsonic and transonic speeds. Sweep also reduces drag at supersonic speeds by causing the formation of weaker oblique shock waves rather than stronger normal shock waves.

The advantages of wing sweep were first realized by Germany in the 1930's (2). The first swept wing aircraft, including both forward and backward sweep, were flown by Germany during World War II. Research from NACA by Diederick and Budiansky (4) in the late 1940's showed the divergence dynamic pressure of forward sweep wings are drastically low compared to the divergence dynamic pressure of backward sweep wings. Consequently, all feasible swept wing designs throughout the mid 1970's employed backward sweep. The forward sweep concept was ignored up to this time until Krone (5) revealed aeroelastic tailoring with composite materials can increase the low divergence limit of forward sweep wings without experiencing the weight penalties associated with the use of conventional metal materials. The solution to the divergence problem has led to the development of the forward sweep X-29 research aircraft which is currently undergoing flight tests conducted by the Defense Advanced Research Projects Agency, National Aeronautics and Space Administration and United States Air Force (USAF). Moore and Frei (6) give a description of the X-29 and its purpose.

The increased interest in using forward sweep once the structural feasibility is verified is due to certain advantages forward sweep has

over backward sweep. Increased lift, reduced drag, improved handling qualities and increased design freedom are some of the major advantages listed by Krone (7). The advantages are difficult to quantify without comparison to a backward sweep wing with certain parameters constrained to equal the forward sweep wing's corresponding parameters.

CHAPTER III

CONFIGURATION DEVELOPMENT

General Description

Figure 1 shows the variable forward sweep wing aircraft studied throughout this research effort. The aircraft incorporates a variable forward sweep wing with sweep angles ranging from -42° to -15°. The wing is pivoted about a fixed pivot located directly above the body centerline. This vertical offset from the body centerline was required due to the internal spacing requirements of the engine. The horizontal stabilizer is a canard while the vertical stabilizer is a single, conventional vertical fin. Conventional aerodynamic control surfaces were selected: elevators on the horizontal stabilizer, rudder on the vertical stabilizer and flaps and ailerons on the wing. The propulsion system consists of a single turbofan engine located internal to the body and exhausting out the base of the body. Intake for the propulsion system consists of a single scoop located on the body underside.

The aircraft is a representative of the light weight fighter category similar to the Northrop F-5 or F-20. The general shape and size of the aircraft is quite similar to the X-29 research aircraft. This similarity is deliberate because the X-29 is the only existing high speed aircraft using a forward sweep angle more negative than -15°. The X-29's basic airframe is unstable; however, by careful selection of the horizontal stabilizer and wing locations relative to the center of

Scale: 1m=1cm

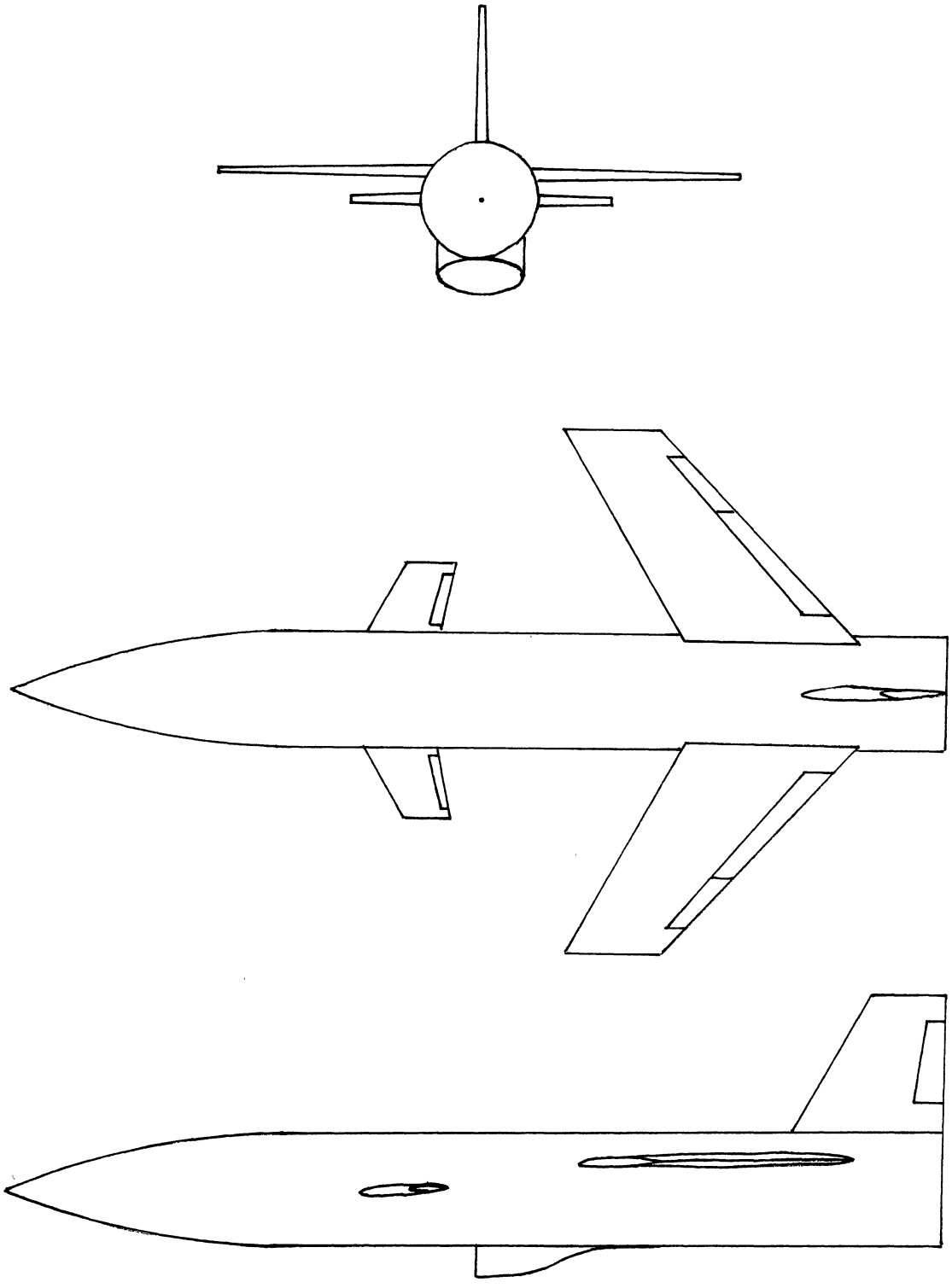

Figure 1. Variable Forward Sweep Wing
Aircraft at -30° Sweep

gravity the basic airframe shown in Figure 1 is stable.

The aircraft was designed with a static margin of -0.25 for a sweep angle of -30°, Mach number of 0.75 and altitude of 6000 m. No design iterations or alterations to improve the aircraft's characteristics for other flight conditions were performed after the off design results were obtained. Instead, the changes in the aircraft's characteristics resulting from changes in the flight condition are the results to be analyzed for this research effort. The aircraft is capable of obtaining low supersonic Mach numbers in level flight. The aircraft's aerodynamic performance such as range, endurance, takeoff and landing speeds, rate of climb, ceiling and maximum speed were not considered in the design. Appendix A contains the specifications for the aircraft.

Design Method

The technique of "design extrapolation" is used to determine the aircraft's basic size and geometry. The size and geometry were extrapolated from the X-29, F-5 and F-20 aircraft. Size and geometry includes the lifting surface and stabilizer planform areas, taper ratios, spans and sweep angles. Body length and diameter, mass, moments of inertia and propulsion are also included in the size and geometry. The flight condition of -30° sweep angle, Mach number of 0.75, and altitude of 6000 m was selected as the design flight condition. This flight condition represents a high subsonic cruise condition where an aircraft of this category will typically spend the majority of it's flight time. References (6), (8), (9) and (10) were used in the "design extrapolation" calculations.

The fundamental design consisted of locating the longitudinal

position of the wing and horizontal stabilizer relative to the center of gravity so that certain design constraints were satisfied. Consider the variable forward sweep wing aircraft shown in Figure 2. The aircraft is in a wing's level steady state rectilinear flight condition. Assuming a small angle of attack ∇_1, neglecting the moments due to the drag and thrust forces and using the derivative and trim results from Chapter IV, the steady trim equations are approximated by equations (1) through (3).

$$n^w \left\{ C_{D_o}^w + C_{D_\alpha}^w (\nabla_1 + I^w - \varepsilon_1^w) \right\} + \frac{S^H}{S^w} \left\{ C_{D_o}^H + C_{D_\alpha}^H (\nabla_1 + I^H) + C_{D_{\delta E}}^H \Delta_1^E \right.$$
$$\left. + \frac{S^B}{S^w} C_{D_o}^B + n^v \frac{S^v}{S^w} C_{D_o}^v - \frac{T_{max}^E \Delta_1^T}{q_1 S^w} = 0 \right. \tag{1}$$

$$n^w C_{L_\alpha}^w (\nabla_1 + I^w - \varepsilon_1^w) + \frac{S^H}{S^w} \left\{ C_{L_\alpha}^H (\nabla_1 + I^H) + C_{L_{\delta E}}^H \Delta_1^E \right\} + \frac{S^B}{S^w} C_{L_\alpha}^B \nabla_1$$
$$- \frac{mg}{q_1 S^w} = 0 \tag{2}$$

$$n^w C_{L_\alpha}^w (\nabla_1 + I^w - \varepsilon_1^w) + \frac{S^H}{S^w} \left\{ \frac{\bar{c}^H}{\bar{x}_{AC}^w} C_{m_{\delta E}}^H \Delta_1^E + \frac{\bar{x}_{AC}^H}{\bar{x}_{AC}^w} C_{L_\alpha}^H (\nabla_1 + I^H) \right.$$
$$\left. + \frac{\bar{x}_{AC}^H}{\bar{x}_{AC}^w} C_{L_{\delta E}}^H \Delta_1^E \right\} + \frac{S^B}{S^w} \frac{\bar{x}_{AC}^B}{\bar{x}_{AC}^w} C_{L_\alpha}^B \nabla_1 = 0 \tag{3}$$

As mentioned in the discussion of the trim calculations in Chapter IV, the three unknowns θ_1, Δ_1^F and q_1 are specified to reduce the total number of unknowns to three. Specifically, θ_1 and Δ_1^F have been selected as zero and q_1 is calculated from a Mach number of 0.75 at an altitude of 6000 m. The wing and stabilizer airfoil sections have been selected as symmetric airfoils. Downwash from the horizontal stabilizer onto the wing and wing and vertical stabilizer dynamic pressure reductions from the horizontal stabilizer and body, respectively, have been included in the trim equations (1) through (3). Equations (1) through (3) contain the three unknowns ∇_1, Δ_1^E and Δ_1^T. Equations (1) through (3) are used in the fundamental design.

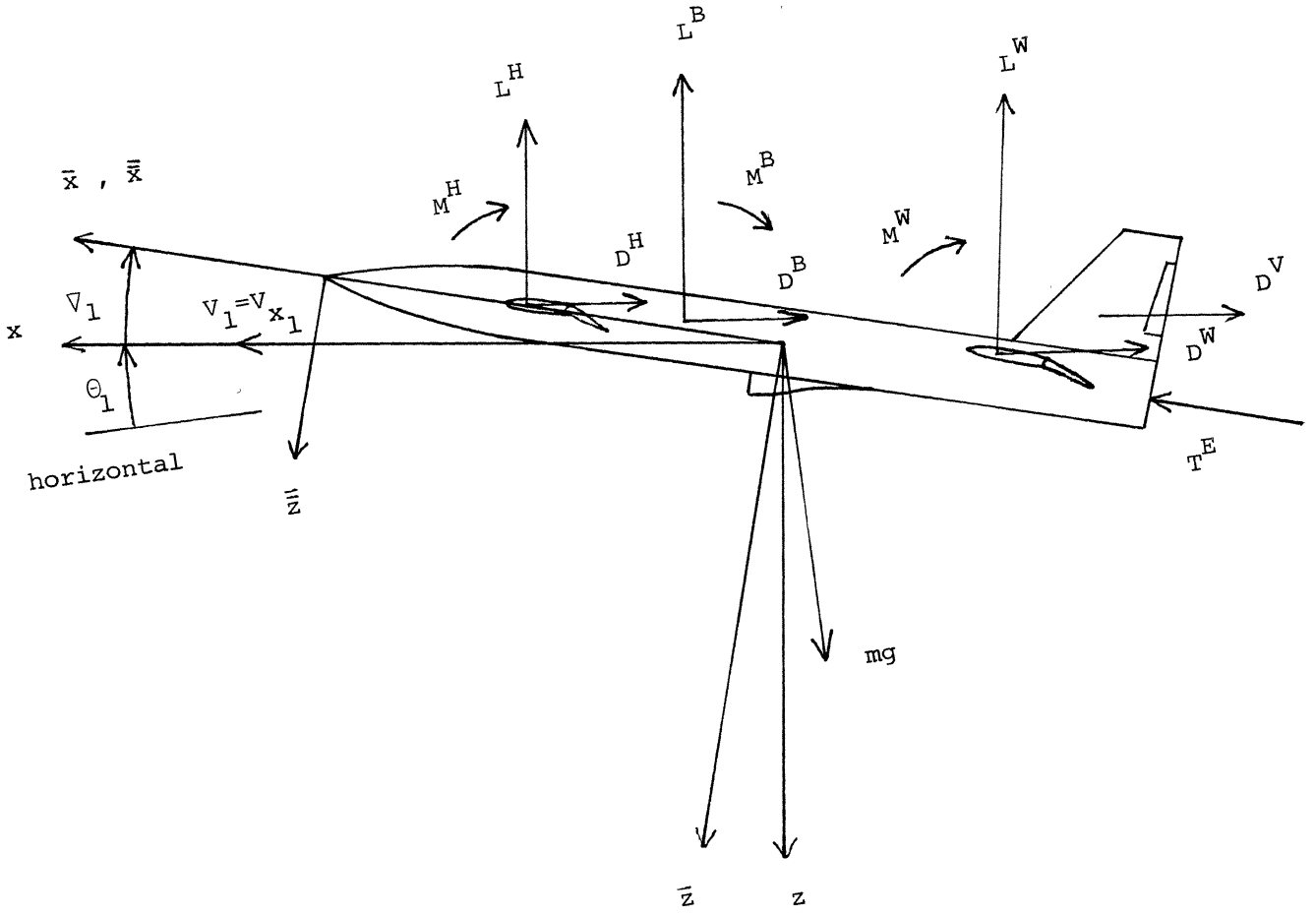

Figure 2. Variable Forward Sweep Wing Aircraft in a Wing's Level Steady State Rectilinear Flight Condition

Taking the partial derivative of equation (3) with respect to ∇_l and expressing the moment arms in the $\bar{\bar{x}}\bar{\bar{y}}\bar{\bar{z}}$ coordinate system results in the expression for the aerodynamic center location given by equation (4). The static margin is given by equation (5).

$$\bar{\bar{X}}_{Ac} = \frac{\eta^W C_{L_\alpha}^W \bar{\bar{X}}_{Ac}^W + \frac{S^H}{S^W} C_{L_\alpha}^H \bar{\bar{X}}_{Ac}^H + \frac{S^B}{S^W} C_{L_\alpha}^B \bar{\bar{X}}_{Ac}^B}{\eta^W C_{L_\alpha}^W + \frac{S^H}{S^W} C_{L_\alpha}^H + \frac{S^B}{S^W} C_{L_\alpha}^B} \tag{4}$$

$$SM = \frac{\bar{\bar{X}}_{Ac} - \bar{\bar{X}}_{CG}}{\bar{c}^W} \tag{5}$$

Equations (4) and (5) are used in the fundamental design.

The center of gravity calculation is performed by dividing the aircraft up into the following seven elements: body, wing, horizontal stabilizer, vertical stabilizer, engine, fuel and payload. Constraining the fuel and payload center of gravities to coincide with the aircraft's center of gravity results in the center of gravity location as equation (6).

$$\bar{\bar{X}}_{CG} = \frac{m^B \bar{\bar{X}}_{CG}^B + m^W \bar{\bar{X}}_{CG}^W + m^H \bar{\bar{X}}_{CG}^H + m^V \bar{\bar{X}}_{CG}^V + m^E \bar{\bar{X}}_{CG}^E}{m - m^F - m^P} \tag{6}$$

E. eng. 24.

Equation (6) is also used in the fundamental design.

The fundamental design is now stated. For the flight condition and extrapolated size and geometry mentioned previously, equations (4) and (5) are used to locate the longitudinal position of the wing and horizontal stabilizer relative to an assumed center of gravity location so that a static margin of -0.25 is attained. Next, equations (1) through (3) are used to solve for the trim unknowns ∇_l, Δ_l^E and Δ_l^T for a specified wing incidence I^W and horizontal stabilizer incidence I^H. Finally, equation (6) is used to calculate the center of gravity location.

The fundamental design is iterated until the following design constraints are met: ∇_1 is in the linear angle of attack range, Δ_1^E is reasonably close to zero, Δ_1^T is between 0 and 1, I^H is larger than I^W and the assumed and calculated center of gravity locations are approximately the same. I^H is constrained to be larger than I^W so that the horizontal stabilizer will stall before the wing stalls. This constraint is a passive safety factor against stalling for a canard configuration.

Wing Description

Figure 3 shows an enlarged view of the right variable forward sweep wing. At the design flight condition mentioned previously, the wing root geometry and pivot location relative to the wing structural planform were selected to allow approximately the same amount of sweep on either side of -30°. The pivot is selected at the 1/2 root chord location in the -30° sweep condition. Note from Figure 3 that the right aerodynamic planform changes shape as the sweep changes but the right structural planform remains the same shape as the sweep changes.

The wing airfoil sections were selected as the NACA 64A010 airfoil. This airfoil is a thin symmetric airfoil with a thickness to chord ratio of 0.10. This airfoil selection allows supersonic flight to be feasible. A more realistic airfoil selection would be a new supercritical airfoil but limited data on these airfoils prevented this selection. The stabilizer airfoil sections are also the NACA 64A010 airfoil.

At -30° sweep, the tip chord is aligned with the longitudinal direction. For sweep less negative than -30°, the tip chord becomes a

Scale: 1m=2cm

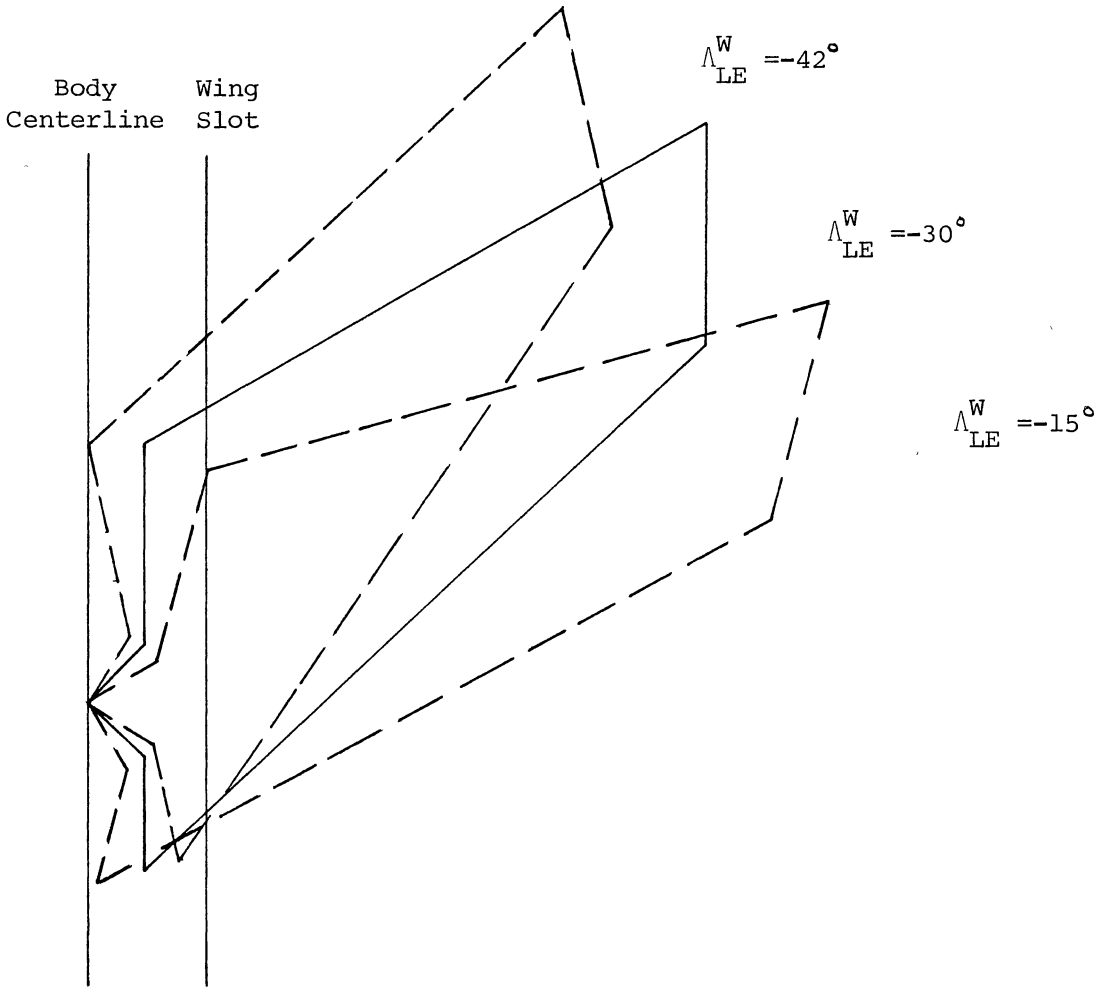

Figure 3. Right Variable Forward Sweep Wing

trailing edge and is not directly facing the aerodynamic flow. For sweep more negative than -30°, the tip chord becomes a leading edge and is directly facing the aerodynamic flow. At these off design sweep angles, the wing span is approximated as the average of the leading edge tip chord span and the trailing edge tip chord span. Any adverse aerodynamic flow patterns resulting from the tip chord becoming a leading edge has been neglected in this research effort.

At -30° sweep, the wing airfoil sections and the aileron and flap inboard and outboard chords are aligned with the longitudinal direction. At off design sweep angles, the airfoils and control surface chords will be skewed to the longitudinal direction. Any resulting adverse aerodynamic effects have been neglected. The structural feasibility of the wing root geometry and pivot is also questionable but is left unspecified at this time. Finally, some type of closure mechanism for the wing slot will be required but is unspecified. These unaddressed areas are felt to be unimportant considerations when regarding the intent and purpose of this research effort.

CHAPTER IV

ANALYSIS METHOD

Equations of Motion Solution

A rigorous application of vectorial Newtonian mechanics leads to the uncoupled longitudinal and lateral-directional sets of small perturbation, scalar, differential equations (7) through (15). A complete derivation is given by Roskam (1).

Longitudinal Set:

$$f_{A_X} + f_{T_X} = mg\cos\Theta_1\,\theta + m\dot{V}_X \tag{7}$$

$$f_{A_Z} + f_{T_Z} = mg\sin\Theta_1\,\theta + mV_{X_1}\dot{\alpha} - mV_{X_1}\omega_Y \tag{8}$$

$$m_{A_Y} + m_{T_Y} = I_{YY}\dot{\omega}_Y \tag{9}$$

$$\omega_Y = \dot{\theta} \tag{10}$$

Lateral-directional Set:

$$f_{A_Y} + f_{T_Y} = -mg\cos\Theta_1\,\phi + mV_{X_1}\dot{\beta} + mV_{X_1}\omega_Z \tag{11}$$

$$m_{A_X} + m_{T_X} = I_{XX}\dot{\omega}_X - I_{XZ}\dot{\omega}_Z \tag{12}$$

$$m_{A_Z} + m_{T_Z} = -I_{XZ}\dot{\omega}_X + I_{ZZ}\dot{\omega}_Z \tag{13}$$

$$\omega_X = -\sin\Theta_1\,\dot{\psi} + \dot{\phi} \tag{14}$$

$$\omega_z = \cos\Theta_1 \dot{\Psi} \tag{15}$$

Equations (7) through (15) are the linearized equations of motion for small perturbations about a wing's level steady state rectilinear flight condition written in the stability axes coordinate system. The xyz coordinate system shown in Figure 4 is the stability axes. The stability axes are denoted by the x axis coinciding with the aircraft's steady state velocity and the origin coinciding with the aircraft's center of gravity. The stability axes are attached to the aircraft and rotate with the aircraft.

The longitudinal unknowns are the perturbation variables V_x, α and Θ which are functions of time. The longitudinal perturbation control variables are δ^E, δ^F and δ^T. Before equations (7) through (10) can be solved, the aerodynamic and thrust forces and moments must be expressed as functions of V_x, α, Θ, δ^E, δ^F, δ^T and their derivatives with respect to time. Similarly, the lateral-directional unknowns are the perturbation variables β, Ψ and ϕ. The lateral-directional perturbation control variables are δ^A and δ^R. Before equations (11) through (15) can be solved, the aerodynamic and thrust forces and moments must be expressed as functions of β, Ψ, ϕ, δ^A, δ^R and their derivatives with respect to time.

For a linear analysis, the longitudinal and lateral-directional forces and moments can be sufficiently represented by the variables V_x, α, $\dot{\alpha}$, ω_y, δ^E, δ^F, δ^T and β, $\dot{\beta}$, ω_x, ω_z, δ^A and δ^R, respectively (1). Note the use of ω_x, ω_y and ω_z inplace of $\dot{\Psi}$, $\dot{\Theta}$ and $\dot{\phi}$. The forces and moments can be expressed as functions of ω_x, ω_y and ω_z much easer

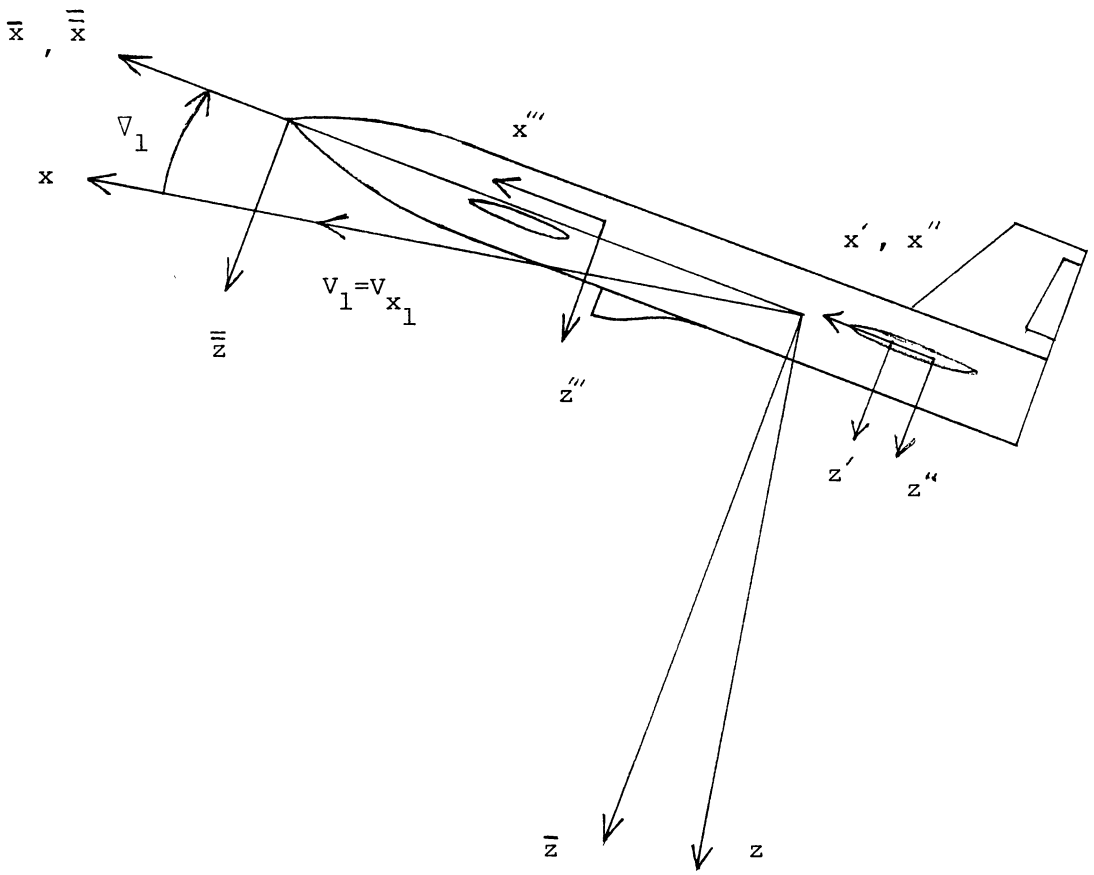

Figure 4. Body Coordinate Systems Used During the Research Effort

than directly expressed as functions of $\dot{\psi}$, $\dot{\theta}$ and $\dot{\phi}$. Equations (10), (14) and (15) are then used to transform from ω_x, ω_y and ω_z to $\dot{\psi}$, $\dot{\theta}$ and $\dot{\phi}$.

Perturbation theory and Taylor series expansion indicates that if F(X,Y), X, and Y can be separated into constant values $F(X_1,Y_1)$, X_1, and Y_1 and perturbation values f(x,y), x, and y, respectively, then the perturbation value f(x,y) is approximated by equation (16).

$$f(x,y) = \frac{\partial F(X,Y)}{\partial x}\bigg|_1 X + \frac{\partial F(X,Y)}{\partial y}\bigg|_1 Y \tag{16}$$

As x and y become smaller, the approximation to f(x,y) in equation (16) becomes more accurate. Equation (16) extends logically to functions of more than two variables. Applying equation (16) to the aerodynamic and thrust forces and moments with the notation F_X for $\frac{\partial F(X,Y)}{\partial x}\Big|_1$ and using dimensionless coefficients results in the following expressions.

Longitudinal Set:

$$f_{A_X} = q_1 S^w \left(C_{A_{X_{V_X}}} V_X + C_{A_{X_\alpha}} \alpha + C_{A_{X_{\dot{\alpha}}}} \dot{\alpha} + C_{A_{X_{\omega_Y}}} \omega_Y + C_{A_{X_{\delta^E}}} \delta^E + C_{A_{X_{\delta^F}}} \delta^F\right) \tag{17}$$

$$f_{A_Z} = q_1 S^w \left(C_{A_{Z_{V_X}}} V_X + C_{A_{Z_\alpha}} \alpha + C_{A_{Z_{\dot{\alpha}}}} \dot{\alpha} + C_{A_{Z_{\omega_Y}}} \omega_Y + C_{A_{Z_{\delta^E}}} \delta^E + C_{A_{Z_{\delta^F}}} \delta^F\right) \tag{18}$$

$$m_{A_Y} = q_1 S^w \bar{c}^w \left(K_{A_{Y_{V_X}}} V_X + K_{A_{Y_\alpha}} \alpha + K_{A_{Y_{\dot{\alpha}}}} \dot{\alpha} + K_{A_{Y_{\omega_Y}}} \omega_Y + K_{A_{Y_{\delta^E}}} \delta^E + K_{A_{Y_{\delta^F}}} \delta^F\right) \tag{19}$$

$$f_{T_X} = q_1 S^w \left(C_{T_{X_{V_X}}} V_X + C_{T_{X_\alpha}} \alpha + C_{T_{X_{\dot{\alpha}}}} \dot{\alpha} + C_{T_{X_{\omega_Y}}} \omega_Y + C_{T_{X_{\delta^T}}} \delta^T\right) \tag{20}$$

$$f_{T_Z} = q_1 S^w \left(C_{T_{Z_{V_X}}} V_X + C_{T_{Z_\alpha}} \alpha + C_{T_{Z_{\dot{\alpha}}}} \dot{\alpha} + C_{T_{Z_{\omega_Y}}} \omega_Y + C_{T_{Z_{\delta^T}}} \delta^T\right) \tag{21}$$

$$m_{T_Y} = q_1 S^w \bar{c}^w \left(K_{T_{Y_{V_X}}} V_X + K_{T_{Y_\alpha}} \alpha + K_{T_{Y_{\dot{\alpha}}}} \dot{\alpha} + K_{T_{Y_{\omega_Y}}} \omega_Y + K_{T_{Y_{\delta^T}}} \delta^T\right) \tag{22}$$

Lateral-directional Set:

$$f_{A_Y} = q_1 S^w \left(C_{A_{Y\beta}} \beta + C_{A_{Y\dot{\beta}}} \dot{\beta} + C_{A_{Y\omega_X}} \omega_X + C_{A_{Y\omega_Z}} \omega_Z + C_{A_{Y\delta A}} \delta^A + C_{A_{Y\delta R}} \delta^R \right) \quad (23)$$

$$m_{A_X} = q_1 S^w b^w \left(K_{A_{X\beta}} \beta + K_{A_{X\dot{\beta}}} \dot{\beta} + K_{A_{X\omega_X}} \omega_X + K_{A_{X\omega_Z}} \omega_Z + K_{A_{X\delta A}} \delta^A + K_{A_{X\delta R}} \delta^R \right) \quad (24)$$

$$m_{A_Z} = q_1 S^w b^w \left(K_{A_{Z\beta}} \beta + K_{A_{Z\dot{\beta}}} \dot{\beta} + K_{A_{Z\omega_X}} \omega_X + K_{A_{Z\omega_Z}} \omega_Z + K_{A_{Z\delta A}} \delta^A + K_{A_{Z\delta R}} \delta^R \right) \quad (25)$$

$$f_{T_Y} = q_1 S^w \left(C_{T_{Y\beta}} \beta + C_{T_{Y\dot{\beta}}} \dot{\beta} + C_{T_{Y\omega_X}} \omega_X + C_{T_{Y\omega_Z}} \omega_Z \right) \quad (26)$$

$$m_{T_X} = q_1 S^w b^w \left(K_{T_{X\beta}} \beta + K_{T_{X\dot{\beta}}} \dot{\beta} + K_{T_{X\omega_X}} \omega_X + K_{T_{X\omega_Z}} \omega_Z \right) \quad (27)$$

$$m_{T_Z} = q_1 S^w b^w \left(K_{T_{Z\beta}} \beta + K_{T_{Z\dot{\beta}}} \dot{\beta} + K_{T_{Z\omega_X}} \omega_X + K_{T_{Z\omega_Z}} \omega_Z \right) \quad (28)$$

Combining equations (7) through (10) and (17) through (22), taking the Laplace transformation, and using matrix algebra results in the longitudinal matrix equation (29). Applying the same process to equations (11) through (15) and (23) through (28) results in the lateral-directional matrix equation (30). The variables in equation (29) and (30) are now functions of the Laplacian variable s rather than time. Also note the initial conditions are zero because the equations of motion are for perturbations about a steady state rectilinear flight condition. Both the longitudinal and the lateral-directional matrix equations can be represented by equation (31) with the Laplacian solution given by equation (32).

$$[A]\{x\} = [B]\{\delta\} \quad (31)$$

$$\{X\} = [A]^{-1}[B]\{\delta\} \quad (32)$$

$$
\begin{bmatrix}
\{m\}s + \{-q_1 S^w (C_{Ax_{V_x}} + C_{T x_{V_x}})\} & \{-q_1 S^w (C_{Ax_{\dot\alpha}} + C_{T x_{\dot\alpha}})\}s + \{-q_1 S^w (C_{Ax_\alpha} + C_{T x_\alpha})\} & \{-q_1 S^w (C_{Ax_{\omega_y}} + C_{T x_{\omega_y}})\}s + \{mg\cos\Theta_1\} \\
\{-q_1 S^w (C_{Az_{V_x}} + C_{T z_{V_x}})\} & \{mV_{x_1} - q_1 S^w (C_{Az_{\dot\alpha}} + C_{T z_{\dot\alpha}})\}s + \{-q_1 S^w (C_{Az_\alpha} + C_{T z_\alpha})\} & \{-mV_{x_1} - q_1 S^w (C_{Az_{\omega_y}} + C_{T z_{\omega_y}})\}s + \{mg\sin\Theta_1\} \\
\{-q_1 S^w \bar{c}^w (K_{Ay_{V_x}} + K_{T y_{V_x}})\} & \{-q_1 S^w \bar{c}^w (K_{Ay_{\dot\alpha}} + K_{T y_{\dot\alpha}})\}s + \{-q_1 S^w \bar{c}^w (K_{Ay_\alpha} + K_{T y_\alpha})\} & \{I_{yy}\}s^2 + \{-q_1 S^w \bar{c}^w (K_{Ay_{\omega_y}} + K_{T y_{\omega_y}})\}s
\end{bmatrix}
\begin{Bmatrix} V_x \\ \alpha \\ \Theta \end{Bmatrix}
$$

$$
\begin{bmatrix}
\{q_1 S^w C_{Ax_{\delta^E}}\} & \{q_1 S^w C_{Ax_{\delta^F}}\} & \{q_1 S^w C_{Tx_{\delta^T}}\} \\
\{q_1 S^w C_{Az_{\delta^E}}\} & \{q_1 S^w C_{Az_{\delta^F}}\} & \{q_1 S^w C_{Tz_{\delta^T}}\} \\
\{q_1 S^w \bar{c}^w K_{Ay_{\delta^E}}\} & \{q_1 S^w \bar{c}^w K_{Ay_{\delta^F}}\} & \{q_1 S^w \bar{c}^w K_{Ty_{\delta^T}}\}
\end{bmatrix}
\begin{Bmatrix} \delta^E \\ \delta^F \\ \delta^T \end{Bmatrix}
\qquad (29)
$$

$$
\begin{bmatrix}
\{mV_{x_1} - q_1 S^w (C_{A_{y\dot{\beta}}} + C_{T_{y\dot{\beta}}})\} s \\
+ \{-q_1 S^w (C_{A_{y\beta}} + C_{T_{y\beta}})\}
&
\{mV_{x_1} \cos\Theta_1 + \\
+ q_1 S^w [(C_{A_{y\omega_x}} + C_{T_{y\omega_x}}) \sin\Theta_1 \\
- (C_{A_{y\omega_z}} + C_{T_{y\omega_z}}) \cos\Theta_1]\} s
&
\{-q_1 S^w (C_{A_{y\omega_x}} + C_{T_{y\omega_x}})\} s \\
+ \{-mg \cos\Theta_1\}
\\
\hline
\{-q_1 S^w b^w (K_{A_{x\dot{\beta}}} + K_{T_{x\dot{\beta}}})\} s \\
+ \{-q_1 S^w b^w (K_{A_{x\beta}} + K_{T_{x\beta}})\}
&
\{-I_{xx} \sin\Theta_1 - I_{xz} \cos\Theta_1\} s^2 \\
+ \{q_1 S^w b^w [(K_{A_{x\omega_x}} + K_{T_{x\omega_x}}) \sin\Theta_1 \\
- (K_{A_{x\omega_z}} + K_{T_{x\omega_z}}) \cos\Theta_1]\} s
&
\{I_{xx}\} s^2 \\
+ \{-q_1 S^w b^w (K_{A_{x\omega_x}} + K_{T_{x\omega_x}})\} s
\\
\hline
\{-q_1 S^w b^w (K_{A_{z\dot{\beta}}} + K_{T_{z\dot{\beta}}})\} s \\
+ \{-q_1 S^w b^w (K_{A_{z\beta}} + K_{T_{z\beta}})\}
&
\{I_{xz} \sin\Theta_1 + I_{zz} \cos\Theta_1\} s^2 \\
+ \{q_1 S^w b^w [(K_{A_{z\omega_x}} + K_{T_{z\omega_x}}) \sin\Theta_1 \\
- (K_{A_{z\omega_z}} + K_{T_{z\omega_z}}) \cos\Theta_1]\} s
&
\{-I_{xz}\} s^2 \\
+ \{-q_1 S^w b^w (K_{A_{z\omega_x}} + K_{T_{z\omega_x}})\} s
\end{bmatrix}
\begin{Bmatrix} \beta \\ \psi \\ \phi \end{Bmatrix}
$$

$$
\begin{bmatrix}
\{q_1 S^w C_{A_{y\delta^A}}\}
&
\{q_1 S^w C_{A_{y\delta^R}}\}
\\
\hline
\{q_1 S^w b^w K_{A_{x\delta^A}}\}
&
\{q_1 S^w b^w K_{A_{x\delta^R}}\}
\\
\hline
\{q_1 S^w b^w K_{A_{z\delta^A}}\}
&
\{q_1 S^w b^w K_{A_{z\delta^R}}\}
\end{bmatrix}
\begin{Bmatrix} \delta^A \\ \delta^R \end{Bmatrix}
\tag{30}
$$

As mentioned previously, the numerical results consist of the characteristic equation root loci, mode shapes and time responses. The characteristic equation is the denominator of $[A]^{-1}$ and is given by the determinant of $[A]$. The longitudinal and lateral-directional characteristic root loci are obtained by solving for the characteristic equation roots at various flight conditions. Applying partial fraction expansion to equation (32) and taking the inverse Laplace transformation leads to the time responses. The longitudinal time responses are for V_X, α and Θ due to the control inputs δ^E, δ^F and δ^T. The lateral-directional time responses are for β, Ψ and ϕ due to the control inputs δ^A and δ^R. Again, the time responses are obtained for various flight conditions.

The mode shapes are calculated from equation (33) which is obtained from equation (31) by setting $\{\delta\}$ equal to the zero vector, $\{o\}$.

$$[A]\{x\} = \{o\} \tag{33}$$

Matrix equation (33) is three scalar homogeneous equations generally with a rank of two implying infinitely many solutions. In accordance with mode shape theory, only information about the relative magnitudes of the elements of $\{x\}$ can be determined. Arbitrarily selecting Θ equal to $1\angle 0°$ and using the longitudinal equations corresponding to equation (33), V_X and α can be determined as functions of s. Arbitrarily selecting β equal to $1\angle 0°$ and using the lateral-directional equations corresponding to equation (33), Ψ and ϕ can be determined as functions of s. The mode shapes for a particular characteristic root are finally obtained by substituting the particular characteristic root of interest in for s. Also the mode shapes are obtained for various flight conditions.

Aircraft Force and Moment Calculations

Before equations (29) and (30) can be solved the aircraft stability and control derivatives must be calculated. To accomplish this the aircraft is divided up into the following five elements: wing, horizontal stabilizer, vertical stabilizer, body and propulsion intake and exhaust. The aircraft forces and moments are the summation of the element forces and moments. In this way, the aircraft stability and control derivatives are determined as functions of the element stability and control derivatives. As discussed in this chapter, reference (11) and simple theoretical principles are used to calculate the element stability and control derivatives.

Figure 5 is used to calculate the aircraft longitudinal stability and control derivatives in terms of the element stability and control derivatives. This calculation consists of expressing the aircraft forces and moments in terms of the element forces and moments. Next, Taylor series expansion is used to express each force and moment in terms of the longitudinal variables. Finally, the aircraft stability and control derivatives are obtained by factoring with respect to the longitudinal variables. Applying the same process to Figure 6 results in the aircraft lateral-directional stability and control derivatives. Appendix B lists the results.

The aircraft stability and control derivatives appearing in equations (29) and (30) correspond to the stability axes. However, the aircraft stability and control derivatives resulting from Figures 5 and 6 do not correspond to the stability axes. This result occurs because reference (11) and the simple theoretical principles used to calculate the element stability and control derivatives do not correspond to the

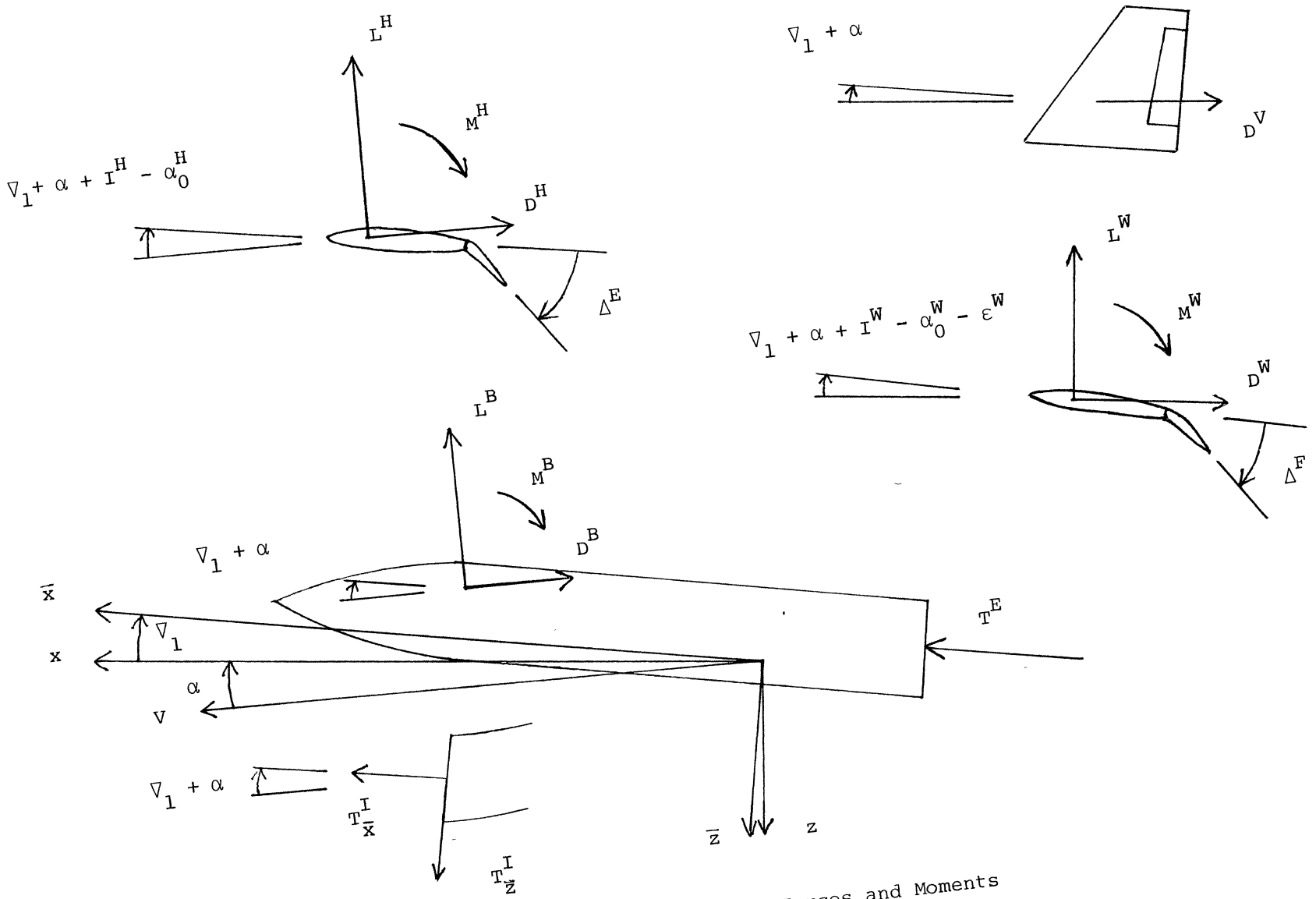

Figure 5. Element Longitudinal Forces and Moments

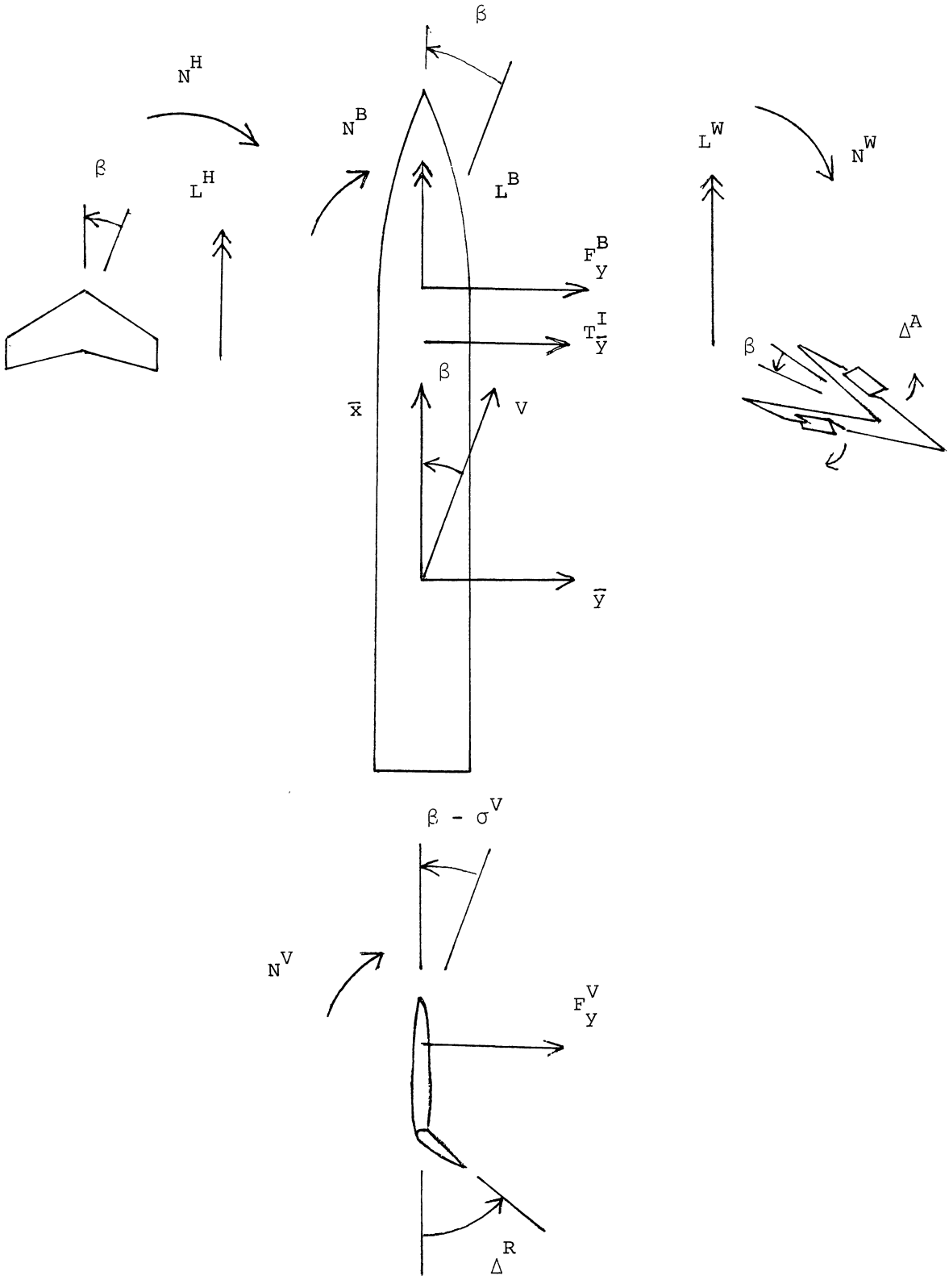

Figure 6. Element Lateral-directional Forces and Moments

stability axes. Therefore, a transformation to the stability axes is required. Figure 7 is used for the longitudinal transformation and Figure 8 is used for the lateral-directional transformation. The transformations are given by equations (34) through (45). Computing the partial derivatives of the perturbation forces and moments and using equations (34) through (45) lead to the stability and control derivative transformations which are also listed in Appendix B. There is no standard notation for the thrust derivatives like there is for the aerodynamic derivatives C_D, C_L, C_m, C_Y, C_ℓ and C_n. Therefore, the subscript notation $\bar{x}, \bar{y}$, and $\bar{z}$ is used to denote the thrust derivatives as determined in the $\bar{x}\bar{y}\bar{z}$ coordinate system.

$$C_{A_X} = -C_D + \alpha C_L \tag{34}$$

$$C_{A_Z} = -C_L - \alpha C_D \tag{35}$$

$$K_{A_Y} = C_m \tag{36}$$

$$C_{T_X} = C_{T_{\bar{x}}} + \bar{V}_1 C_{T_{\bar{z}}} \tag{37}$$

$$C_{T_Z} = C_{T_{\bar{z}}} - \bar{V}_1 C_{T_{\bar{x}}} \tag{38}$$

$$K_{T_Y} = K_{T_{\bar{y}}} \tag{39}$$

$$C_{A_Y} = C_Y \tag{40}$$

$$K_{A_X} = C_\ell + \bar{V}_1 C_n \tag{41}$$

$$K_{A_Z} = C_n - \bar{V}_1 C_\ell \tag{42}$$

$$C_{T_Y} = C_{T_{\bar{y}}} \tag{43}$$

$$K_{T_X} = K_{T_{\bar{x}}} + \bar{V}_1 K_{T_{\bar{z}}} \tag{44}$$

$$K_{T_Z} = K_{T_{\bar{z}}} - \bar{V}_1 K_{T_{\bar{x}}} \tag{45}$$

As mentioned in the previous section the longitudinal forces and moments can be sufficiently represented by the longitudinal variables $v_x, \alpha, \dot{\alpha}, \omega_y, \delta^E, \delta^F$ and δ^T. Also, the lateral-directional forces and moments can be sufficiently represented by the lateral-directional variables $\beta, \dot{\beta}, \omega_x, \omega_z, \delta^A$ and δ^R. Note the forces and moments do not depend upon the variable derivatives except for $\dot{\alpha}$ and $\dot{\beta}$. If the

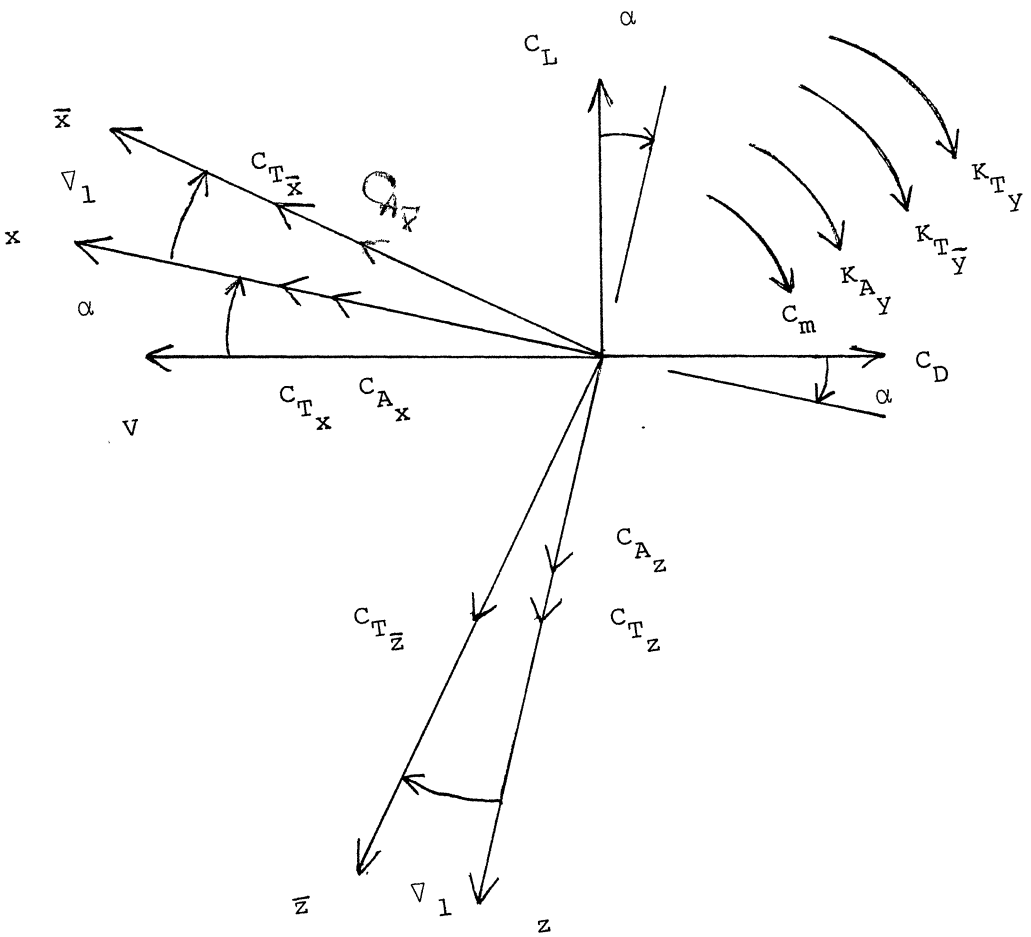

Figure 7. Longitudinal Transformation To the Stability Axes

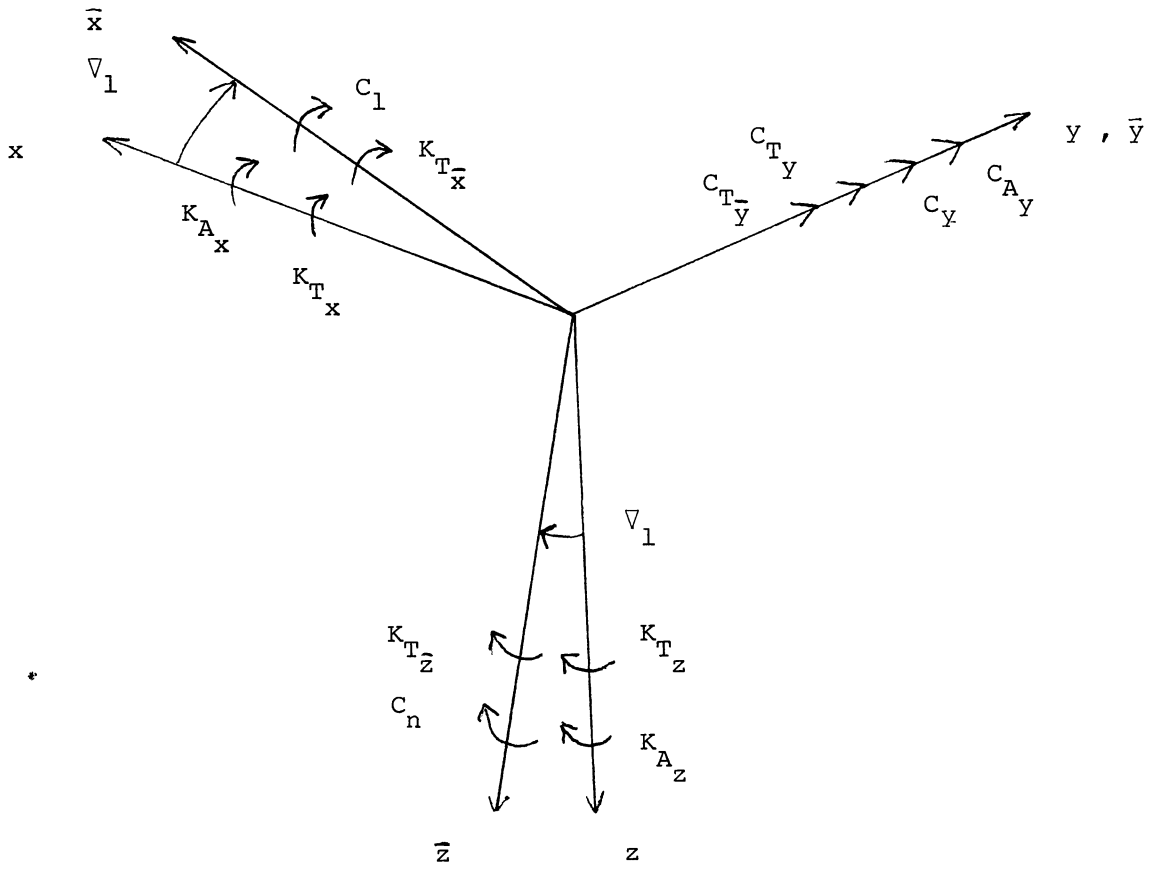

Figure 8. Lateral-directional Transformation To the Stability Axes

downwash lag theory (1) is used to calculate $\dot{\alpha}$ and $\dot{\beta}$, the derivative independence implies the same forces and moments are obtained for the same state no matter how the state was arrived at. The aerodynamic and thrust pressures change instantaneously whenever the state changes. This assumption which is used exclusively in the force and moment model is called quasi steady flow (1).

In order to make the aerodynamic force and moment model more realistic, four interference effects are incorporated into the stability and control derivative calculations. Downwash from the horizontal stabilizer on the wing, dynamic pressure reduction from the horizontal stabilizer on the wing, sidewash from the body on the vertical stabilizer and dynamic pressure reduction from the body on the vertical stabilizer are included in Figures 5 and 6.

For the purpose of computing moments due to the element forces, the element forces are assumed to lie along the axes of the $\bar{x}\bar{y}\bar{z}$ coordinate system. This assumption is reasonable because ∇_1 and the perturbation variables have been assumed small. Roskam (1) also makes this assumption.

Lacking propulsion data, the thrust force at the exhaust location is considered to be solely a function of Δ^T. This assumption implies the inlet conditions do not affect the exhaust thrust force. The thrust force of the inlet location is calculated from the fluid mechanics momentum principle given approximately by equation (46)

$$F = (\rho V_{x_1} A^I) V \tag{46}$$

where V is determined as a function of the perturbation variables. The assumption that the inlet thrust force occurs in the $\bar{x}\bar{y}\bar{z}$ coordinate system is taken. Note that equation (46) is applied three times for each axis of the $\bar{x}\bar{y}\bar{z}$ coordinate system.

Element Force and Moment Calculations

The fundamental aerodynamic stability derivatives and all aerodynamic control derivatives are calculated from the USAF Stability and Control DATCOM (11). The remaining aerodynamic stability derivatives are calculated from the fundamental aerodynamic stability derivatives using simple theoretical principles. The fundamental aerodynamic stability derivatives include the wing and stabilizer C_{D_0}, C_{D_α} (supersonic), C_{L_α}, C_{m_0} and the body C_{D_0}, C_{D_α}, C_{L_α}, C_{m_0} and aerodynamic center location. The body aerodynamic center location is where the body C_{m_α} is zero and is therefore considered indirectly as a stability derivative. All thrust stability and control derivatives are calculated from simple theoretical principles. Appendix C lists the results.

Reference (11) is an extremely extensive handbook for calculating the stability and control derivatives of rigid aircraft. Only the simplest methods of reference (11) are selected for the derivative calculations. Many of the empirical correction factors for interference effects between the aircraft elements are neglected. However, the major interference effects of downwash and dynamic pressure reductions have been included as mentioned previously. Roskam (1) states that for a linear analysis this simplification is a reasonable selection. For a single person using reference (11) with hand calculations, this simplification is also the only practical selection possible.

Reference (11) was originally developed for aircraft employing backward sweep. The applicability of reference (11) to forward sweep is questionable. Consequently, USAF is conducting research to determine the applicability of reference (11) to forward sweep and to develop any

necessary modifications for this application to forward sweep (12). Reference (12) states that C_{L_α} is estimated quite accurately from the existing methods. The methods for C_{D_o}, C_{D_α} (supersonic), C_{m_o} and the aerodynamic control derivatives with regard to forward sweep are not mentioned in reference (12). For this research effort, the existing methods for these derivatives are applied to the forward sweep wing with the question of applicability still unspecified.

The simple theoretical principles used to calculate the element stability derivatives are discussed below. The wing, horizontal stabilizer and vertical stabilizer aerodynamic centers are assumed to be at the 1/4 mean aerodynamic chord for subsonic Mach numbers and at the 1/2 mean aerodynamic chord for supersonic Mach numbers. The velocity derivatives are estimated from the well known Prandtl-Glauert transformation for subsonic Mach numbers (1). Using the theoretical lift curve slope for a flat plate at supersonic Mach numbers, Etkin (13) shows the structure of the Prandtl-Glauert transformation also applies to supersonic Mach numbers. As mentioned previously, the inlet thrust force is calculated from the fluid mechanics momentum principle.

The angular velocity derivatives are calculated by determinin an induced perturbational velocity, angle of attack or sideslip angle due to the angular velocity perturbation. The velocity, angle of attack or sideslip angle derivatives are combined with these induced perturbations to form the angular velocity derivatives. For the angular velocity derivative calculations, the angular velocities ω_x, ω_y and ω_z are assumed to lie along the axes of the $\bar{x}\bar{y}\bar{z}$ coordinate system since $\bar{V}_1$ and the perturbation variables are assumed to be small. Roskam (1) has a complete development of this computational method for the angular velocity derivatives.

The $\dot{\alpha}$ and $\dot{\beta}$ derivatives are calculated from the downwash lag theory (1). This theory implies there is a finite time delay between the time the downwash distribution changes and the time this new downwash distribution is propagated downstream and sensed or felt elsewhere. The downwash and sidewash are given by equations (47) through (50).

$$\varepsilon^w = \varepsilon_1^w + \frac{d\varepsilon^w}{d\alpha}\alpha - \frac{d\varepsilon^w}{d\alpha}\dot{\alpha}\, t^{\varepsilon} \tag{47}$$

$$\sigma^v = \sigma_1^v + \frac{d\sigma^v}{d\beta}\beta - \frac{d\sigma^v}{d\beta}\dot{\beta}\, t^{\sigma} \tag{48}$$

$$t^{\varepsilon} = \frac{\bar{x}_{AC}^{H} - \bar{x}_{AC}^{w}}{V_{x_1}} \tag{49}$$

$$t^{\sigma} = \frac{\bar{x}_{AC}^{B} - \bar{x}_{AC}^{v}}{V_{x_1}} \tag{50}$$

As mentioned in reference (11), the vertical stabilizer and body derivatives $C_{Y_\beta}^{v}$ and $C_{Y_\beta}^{B}$ are approximated by $-C_{L_\beta}^{v}$ and $-C_{L_\beta}^{B}$, respectively. One final point is reference (11) does not have a method to predict $C_{\ell_\beta}^{B}$ and $C_{n_\beta}^{B}$. These derivatives are approximated by $C_{m_\alpha}^{B}$ referenced to the body aerodynamic center location.

Trim Calculations

Equations (29) and (30) correspond to small perturbations about a wing's level steady state rectilinear flight condition. Before these equations can be solved the wing's level steady state rectilinear flight condition or trim condition must be determined. Consider Figure 2 again which depicts a variable forward sweep wing aircraft in a wing's level steady state rectilinear flight condition. The corresponding trim equations are given by equations (51) through (53).

$$q_1 S^w C_{A_x} + q_1 S^w C_{T_x} = mg \sin\Theta_1 \tag{51}$$

$$q_1 S^w C_{A_z} + q_1 S^w C_{T_z} = -mg \cos\Theta_1 \tag{52}$$

$$q_1 S^w \bar{c}^w K_{A_y} + q_1 S^w \bar{c}^w K_{T_y} = 0 \qquad (53)$$

The trim equations (51) through (53) are longitudinal equations. For a steady state rectilinear flight condition, symmetric aircraft and no lateral-directional control surface deflections, the terms in the lateral-directional trim equations are identically zero.

Using the stability and control derivative results of this chapter and the configuration results discussed in Chapter III the trim equations are expanded in terms of the aircraft elements and the trim unknowns V_{x_1}, Θ_1, ∇_1, Δ_1^E, Δ_1^F, Δ_1^T and ρ. With only three trim equations, four of the unknowns must be specified. V_{x_1}, Θ_1, Δ_1^F and ρ are specified and the trim equations are used to solve for ∇_1, Δ_1^E and Δ_1^T. The trim calculation is quite similar to how an aircraft is flown. For up and away flight with zero flap deflection (Δ_1^F), the pilot desires a certain speed and direction (V_{x_1}, Θ_1) for a given altitude (ρ). The elevator and throttle controls (Δ_1^E, Δ_1^T) are adjusted with the resulting angle of attack (∇_1) until the desired conditions are attained. Specifically for this research effort, Θ_1 and Δ_1^F are selected as zero and V_{x_1} and ρ are selected to result in a desired Mach number and dynamic pressure. The expanded trim equations are given by equations (54) through (56).

$$\left\{ n^w \frac{2 C_{L_\alpha}^{w^2}}{\pi A^w e^w} + \frac{S^H}{S^w} \frac{2 C_{L_\alpha}^{H^2}}{\pi A^H e^H} \right\} \nabla_1^2 + \left\{ - n^w \frac{4 C_{L_\alpha}^{w^2}}{\pi A^w e^w} \varepsilon_1^w + \frac{S^H}{S^w} \frac{4 C_{L_\alpha}^{H^2}}{\pi A^H e^H} I^H \right\} \nabla_1$$
$$+ \left\{ \frac{S^H}{S^w} C_{D_{\delta_E}}^H \right\} \Delta_1^E + \left\{ - C_{T_{\bar{x}_{\delta_T}}} \right\} \Delta_1^T = - n^w \left(C_{D_o}^w + \frac{2 C_{L_\alpha}^{w^2}}{\pi A^w e^w} \varepsilon_1^{w^2} \right)$$
$$- \frac{S^H}{S^w} \left(C_{D_o}^H + \frac{2 C_{L_\alpha}^{H^2}}{\pi A^H e^H} I^{H^2} \right) - \frac{S^\beta}{S^w} C_{D_o}^\beta - n^v \frac{S^v}{S^w} C_{D_o}^v \qquad (54)$$

$$\left\{ n^w C_{L_\alpha}^w + \frac{S^H}{S^w} C_{L_\alpha}^H + \frac{S^\beta}{S^w} C_{L_\alpha}^\beta \right\} \nabla_1 + \left\{ \frac{S^H}{S^w} C_{L_{\delta_E}}^H \right\} \Delta_1^E + \left\{ C_{T_{\bar{x}_{\delta_T}}} \right\} \nabla_1 \Delta_1^T$$
$$= \frac{mg}{q_1 S^w} + n^w C_{L_\alpha}^w \varepsilon_1^w - \frac{S^H}{S^w} C_{L_\alpha}^H I^H \qquad (55)$$

$$\left\{ n^{w} \frac{\bar{z}_{Ac}^{w}}{\bar{c}^{w}} \frac{2 C_{L_\alpha}^{w^2}}{\pi A^{w} e^{w}} + \frac{S^{H}}{S^{w}} \frac{\bar{z}_{Ac}^{H}}{\bar{c}^{w}} \frac{2 C_{L_\alpha}^{H^2}}{\pi A^{H} e^{H}} \right\} \nabla_1^2 + \left\{ -n^{w} \left(\frac{\bar{x}_{Ac}^{w}}{\bar{c}^{w}} C_{L_\alpha}^{w} + \frac{\bar{z}_{Ac}^{w}}{\bar{c}^{w}} \frac{4 C_{L_\alpha}^{w^2}}{\pi A^{w} e^{w}} \varepsilon_1^{w} \right) \right.$$

$$+ \frac{S^{H}}{S^{w}} \left(- \frac{\bar{x}_{Ac}^{H}}{\bar{c}^{w}} C_{L_\alpha}^{H} + \frac{\bar{z}_{Ac}^{H}}{\bar{c}^{w}} \frac{4 C_{L_\alpha}^{H^2}}{\pi A^{H} e^{H}} I^{H} \right) - \frac{S^{B}}{S^{w}} \frac{\bar{x}_{Ac}^{B}}{\bar{c}^{w}} C_{L_\alpha}^{B} \Big\} \nabla_1 + \left\{ \frac{S^{H}}{S^{w}} \left(- \frac{\bar{c}^{H}}{\bar{c}^{w}} C_{m_{\delta\varepsilon}}^{H} \right.\right.$$

$$\left.\left. - \frac{\bar{x}_{Ac}^{H}}{\bar{c}^{w}} C_{L_{\delta\varepsilon}}^{H} + \frac{\bar{z}_{Ac}^{H}}{\bar{c}^{w}} C_{D_{\delta\varepsilon}}^{H} \right) \right\} \Delta_1^{E} + \left\{ -K_T \bar{y}_{\delta T} \right\} \Delta_1^{T} = -n^{w} \left\{ \frac{\bar{x}_{Ac}^{w}}{\bar{c}^{w}} C_{L_\alpha}^{w} \varepsilon_1^{w} \right.$$

$$+ \frac{\bar{z}_{Ac}^{w}}{\bar{c}^{w}} \left(C_{D_o}^{w} + \frac{2 C_{L_\alpha}^{w^2}}{\pi A^{w} e^{w}} \varepsilon_1^{w^2} \right) \Big\} + \frac{S^{H}}{S^{w}} \left\{ \frac{\bar{x}_{Ac}^{H}}{\bar{c}^{w}} C_{L_\alpha}^{H} I^{H} - \frac{\bar{z}_{Ac}^{H}}{\bar{c}^{w}} \left(C_{D_o}^{H} \right.\right.$$

$$\left.\left. + \frac{2 C_{L_\alpha}^{H^2}}{\pi A^{H} e^{H}} I^{H^2} \right) \right\} - \frac{S^{B}}{S^{w}} \frac{\bar{z}_{Ac}^{B}}{\bar{c}^{w}} C_{D_o}^{B} - n^{v} \frac{S^{v}}{S^{w}} \frac{\bar{z}_{Ac}^{v}}{\bar{c}^{w}} C_{D_o}^{v} \qquad (56)$$

Equations (54) through (56) correspond to a subsonic trim speed. For a supersonic trim speed the corresponding wing and horizontal stabilizer derivative must be used.

The trim calculation is a nonlinear calculation due to the terms ∇_1^2 and $\nabla_1 \Delta_1^T$ appearing in equations (54) through (56). Even though linearized aerodynamics are used, the inclusion of the nonlinear terms is essential in obtaining the correct trim solution because of their magnitude relative to the other terms. The use of linearized aerodynamics implies ∇_1 is in the linear angle of attack range. The nonlinear term ∇_1^2 appears from the wing and horizontal stabilizer C_{D_α}. C_{D_α} is a function of C_L which is a function of ∇_1 ; consequently, ∇_1^2 appears. The nonlinear term $\nabla_1 \Delta_1^T$ appears from equation (37) and (38). Again for the moment considerations, the element forces are assumed to lie along the $\bar{x}\bar{y}\bar{z}$ coordinate system.

CHAPTER V

RESULTS AND DISCUSSION

Preliminary Discussion

Three different dynamic pressures are selected for the research effort. Each dynamic pressure is separated by approximately 10,000 N/m^2. These three dynamic pressures correspond to a mid subsonic speed, high subsonic speed and low supersonic speed. Table I lists h, ρ, V_S, V_{x_1}, M_1 and q_1 for these three speed and altitude conditions.

TABLE I
SPEED AND ALTITUDE CONDITIONS INVESTIGATED
IN THE RESEARCH

h (m)	ρ (kg/m^3)	V_S (m/s)	V_{x_1} (m/s)	M_1	q_1 (N/m^2)
6000	0.6597	316.4	158.2	0.5	8255
6000	0.6597	316.4	237.3	0.75	18570
12500	0.2873	442.7	295.1	1.5	28150

At each of the dynamic pressures listed in Table I, the sweep angle is varied through its full range of -42° to -15°. For each sweep angle the aerodynamic center location, center of gravity location, characteristic roots, mode shapes and time responses are calculated and graphed. Appendix D contains these graphs. The scale of each graph in Appendix D must be carefully noted when viewing the graphs. Some scales

have been increased or decreased so that the information can be seen clearly. Only the mode shape and time response graphs corresponding to the sweep angles of -42°, -30° and -15° are contained in Appendix D. Also, the time response to δ^T and δ^F are not included because an aircraft is typically flown longitudinally with the elevator. All the time responses are for step inputs with each plot indicating the corresponding control surface and the magnitude of the step.

Before any discussion of the graphical results is undertaken, realize the following point. Each graph in Appendix D is for one specific Mach number and dynamic pressure. It would be highly irregular to fly at a subsonic speed at maximum sweep or at a supersonic speed at minimum sweep. The graphs are generated in this way simply to indicate the variable forward sweep wing aircraft characteristics as a function of sweep, Mach number and dynamic pressure.

Aerodynamic Center and Center of Gravity

The aerodynamic center and center of gravity location versus sweep angle graphs verify the expected trends. As the sweep is increased or becomes more negative, both the aerodynamic center and center of gravity move forward with the aerodynamic center movement larger than the center of gravity movement. In other words, the static margin is decreasing.

At the dynamic pressures 8,255 N/m^2, 18,570 N/m^2, and 28,150 N/m^2, the static margins range from -0.5830 to 0.01083, -0.6138 to 0.01747 and -0.6926 to -0.2460, respectively. Both subsonic aerodynamic center location curves are approximately the same while the supersonic aerodynamic center location curve is shifted backward due to the

characteristic shift of the aerodynamic center at supersonic speeds. Note the center of gravity locations are independent of the Mach number and dynamic pressure.

Consider a variable forward sweep design with a static margin of approximately zero at the most forward aerodynamic center location and a subsonic Mach number and dynamic pressure of 0.75 and 18,570 N/m^2, respectively. If sweep less negative than -30° is used for subsonic speeds and sweep more negative than -30° is used for supersonic speeds, the aerodynamic center and center of gravity location versus sweep angle would look similar to Figure 9.

If the reduction of the static margins denoted by ΔSm_1 and ΔSm_3 are much larger than the increase in the static margin denoted by ΔSm_2, Figure 9 a applies. The characteristic backward shift of the aerodynamic center will not significantly change the stability. If ΔSm_2 is approximately equal to ΔSm_1 and ΔSm_3, Figure 9 b applies. The characteristic backward shift of the aerodynamic center will significantly change the stability. Consequently, the latter case will reduce the excessive stability problems for a variable forward sweep design. Figure 10 illustrates the similar graph for a variable backward sweep design. Clearly, the aerodynamic center movement caused by variable sweep and the characteristic shift are in the same direction causing excessive stability.

Using the graphical results, ΔSm_1 and ΔSm_3 are approximately 0.35 and 0.23, respectively, while ΔSm_2 is approximately -0.23. Because these static margin changes are approximately the same size, the characteristic shift of the aerodynamic center will indeed be significant. Consequently, a variable forward sweep design

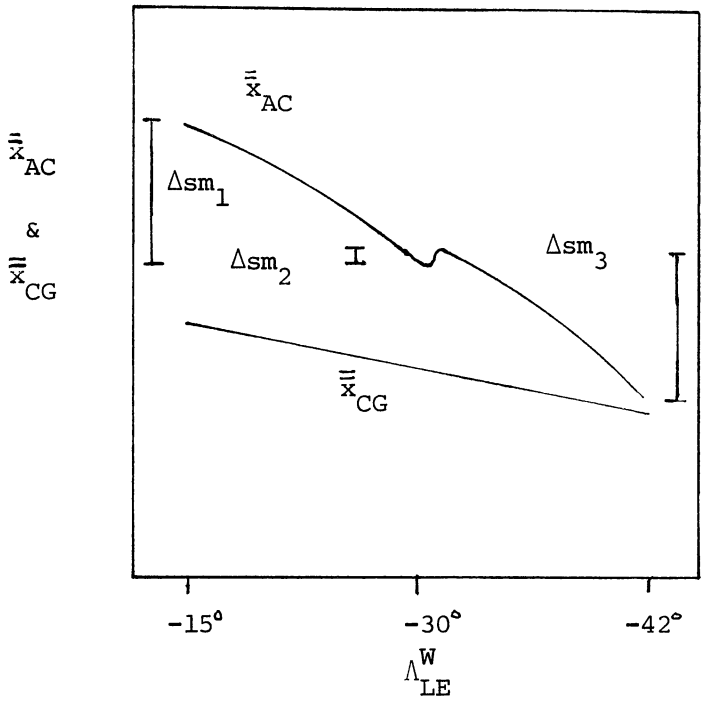

a

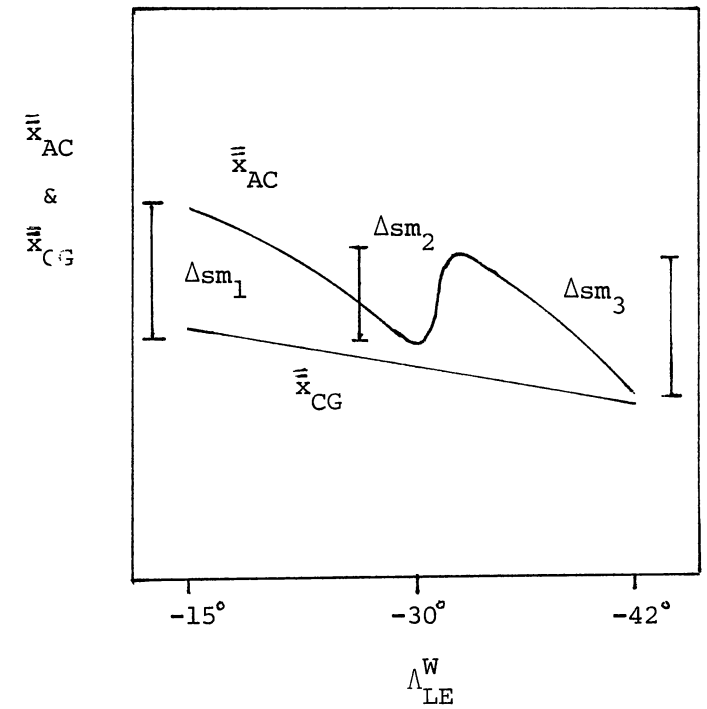

b

Figure 9. Typical Aerodynamic Center and Center of Gravity Locations Versus Sweep for a Variable Forward Sweep Design

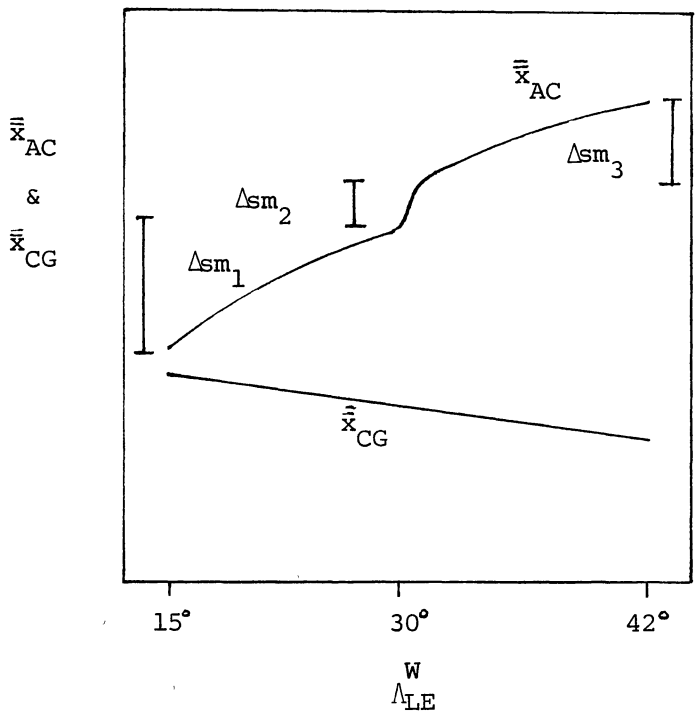

Figure 10. Typical Aerodynamic Center and Center of Gravity Locations Versus Sweep for a Variable Backward Sweep Design

should not experience excessive stability problems caused by variable sweep.

Characteristic Root Locus

At the design condition of -30° sweep, Mach number of 0.75 and dynamic pressure of 18,570 N/m^2, the variable forward sweep wing aircraft in Figure 1 has the classical longitudinal and lateral-directional characteristic modes. These modes are the longitudinal short period and phugoid modes and the lateral-directional dutch-roll, roll and spiral modes. Note the spiral mode is stable for this aircraft. The damping ratios, natural frequencies and time constants at the design condition are listed below.

Longitudinal:	$\zeta_{SP} = 0.1929$	$\omega_{SP} = 3.559$ rad/s
	$\zeta_P = 0.2270$	$\omega_P = 0.06880$ rad/s
Lateral-directional:	$\zeta_{DR} = 0.1246$	$\omega_{DR} = 1.751$ rad/s
	$\tau_R = 2.637$ s	$\tau_S = 26.03$ s

These values yield level 2 handling qualities for this aircraft according to Roskam (1). Note the longitudinal and lateral-directional characteristic equations are 4th and 5th order, respectively. One lateral-directional root is identically zero and corresponds to yaw angle neutral stability.

The short period roots remain stable for each sweep angle and dynamic pressure; however, significant changes in the roots do occur. At the dynamic pressures 8,255 N/m^2 and 18,570 N/m^2, increasing or more negative sweep causes the short period roots to approach the real axis on an almost vertical path and upon reaching the real axis split into

two real roots. At the dynamic pressure 28,150 N/m^2, the same trend appears but the roots do not reach the real axis.

The phugoid root loci at the dynamic pressures 8,255 N/m^2 and 18,570 N/m^2 are quite similar. As sweep increases or becomes more negative, the roots move on an almost vertical path away from the origin which gradually changes to a nearly clockwise arc about the origin. Starting from a stable location, the roots travel a significant distance into the unstable region. At the dynamic pressure 28,150 N/m^2, the phugoid roots consist of one real stable root and one real unstable root, each moving away from the origin as sweep increases. Note the instability is quite small though. Also, if low sweep is used for subsonic speeds and high sweep for supersonic speeds, the significant phugoid instability at the dynamic pressures 8,255 N/m^2 and 18,570 N/m^2 can probably be avoided.

For the dynamic pressures 8,255 N/m^2 and 18,570 N/m^2, the phugoid roots become unstable at approximately the same sweep where the aerodynamic center moves forward of the center of gravity. This is also noted by the well known stability derivative $K_{A_{Y_\alpha}}$ or C_{m_α} changing from negative to positive values. Obviously, the aerodynamic center forward of the center of gravity is causing the instability. Some other occurrence is causing the instability at the dynamic pressure 28,150 N/m^2 because the aerodynamic center is always behind the center of gravity. A closer examination of the stability derivative $K_{A_{Y_{V_x}}}$ reveals the reason for the instability.

Positive values for $K_{A_{Y_{V_x}}}$ are desired because a forward speed perturbation will cause a pitch up moment. With a negative value for $C_{A_{X_{\omega_y}}}$, the pitch up will cause a force along the negative x axis countering the

initial forward speed perturbation. At the dynamic pressures 8,255 N/m^2 and 18,570 N/m^2 $K_{A_{Y_{V_X}}}$ is positive, but at 28,150 N/m^2 $K_{A_{Y_{V_X}}}$ is negative. The Prandtl-Glauert transformation is used exclusively for calculating the perturbational velocity aerodynamic stability derivatives. This transformation changes sign between subsonic and supersonic speeds and causes the sign change of $K_{A_{Y_{V_X}}}$. Therefore, the phugoid instability at the dynamic pressure 28,150 N/m^2 is due to the characteristics of supersonic flow.

The dutch-roll root loci do not indicate any significant changes with respect to sweep or dynamic pressure. Increasing or more negative sweep does lead to a slight movement of the roots on an almost vertical path away from the origin. The dutch-roll mode consists predominately of sideslip motions. The wing contribution to the sideslip stability derivatives is quite small; consequently, the dutch-roll mode is a relatively weak function of wing sweep.

The roll and spiral roots remain stable for each sweep angle and dynamic pressure; however, significant changes are indicated. As sweep increases or becomes more negative, the roll root moves toward the origin and the stable spiral root moves away from the origin. At the dynamic pressure 8,255 N/m^2 and very high sweep angles, the roll and spiral roots have moved enough to eventually meet and combine to form a pair of complex conjugate roots. The roll and spiral modes are then coupled into a decaying, oscillatory mode. Again, if low sweep is used at subsonic speeds and high sweep is used at supersonic speeds, this coupled roll-spiral mode can be avoided.

The wing contribution to roll damping is a major portion. Wing roll damping decreases as sweep increases or becomes more negative due

to the mean aerodynamic chord moving inboard; consequently, the roll stability is reduced and the roll root moves toward the origin. As expected, the wing subsonic and supersonic yaw damping decreases and increases, respectively, as the sweep increases because of the inboard movement of the mean aerodynamic chord and the sign of the Prandtl-Glauert transformation at subsonic and supersonic speeds. However, the numerical results indicated the aircraft yaw damping increases with increasing sweep regardless of the Mach number. This result is a little unexpected but there is a reason. As sweep increases, the wing and hence the aircraft center of gravity moves forward. Consequently, the vertical stabilizer's yaw moment arm increases. The vertical stabilizer's increase in yaw damping apparently masks any change in the wing or body yaw damping as sweep increases. The aircraft yaw stability increase causes the spiral stability to increase and the stable spiral root moves away from the origin.

Mode Shape and Time Response

The longitudinal mode shapes at the dynamic pressures 8,255 N/m^2 and 18,570 N/m^2 indicate the phugoid mode is the dominate mode in the V_X motions for -15° and -30° sweep. The short period mode is the dominate mode in the α motions and the short period and phugoid modes both contribute to the θ motions for -15° and -30° sweep. At -42° sweep, both the phugoid and short period modes contribute to the V_X, α and Θ motions. The time responses indicate these same results.

The V_X responses to the δ^E step for -15° and -30° sweep are slow oscillatory responses (phugoid). The α responses to the δ^E step for -15° and -30° sweep are fast oscillatory responses (short period).

The θ responses to the δ^E step for -15° and -30° sweep are a combination of slow and fast oscillatory responses (phugoid, short period). At -42° sweep, the V_X, α and θ responses to the δ^E step are a combination of oscillatory and exponential responses (phugoid, short period) even though the time responses look like purely exponential responses for the first 5 seconds. Realize the short period roots at -42° sweep and dynamic pressures 8,255 N/m^2 and 18,570 N/m^2 are two real roots leading to two exponential modes. Also note at -15° and -30° sweep the time responses are stable, but at -42° sweep the responses are significantly unstable because of the significant phugoid instability discussed previously.

At the dynamic pressure 28,150 N/m^2, the longitudinal mode shapes again indicate V_X motions are dominated by the phugoid mode, α motions are dominated by the short period mode and θ motions are a combination of the phugoid and short period modes. This is true for all sweep angles. The time responses verify these same results.

The V_X responses to the δ^E step are exponential responses (phugoid). The α responses to the δ^E step are fast oscillatory responses (short period). The θ responses to the δ^E step are a combination of exponential and fast oscillatory responses (phugoid, short period). Realize the phugoid roots at the dynamic pressure 28,150 N/m^2 are two real roots leading to two exponential modes. Also note that even though the phugoid roots are slightly unstable at this dynamic pressure, the time responses are well behaved with regards to stability. In other words, the phugoid instability is insignificant as discussed previously.This is a well known fact that when the characteristic roots become slightly unstable, there is not a sudden change from good flight dynamics to bad flight dynamics (1).

The lateral-directional mode shapes at all the dynamic pressures and sweep angles are all quite similar. The β motions are dominated by the dutch-roll mode while the ψ and ϕ motions are dominated by the roll and spiral modes. The time responses verify these same results. The β responses to the δ^A and δ^R steps are oscillatory responses (dutch-roll). The ψ responses to the δ^A and δ^R steps are a combination of exponential and linear responses (roll, spiral, ψ neutral stability). The wiggle in the ψ responses which look like an oscillatory response is actually caused by the combination of the exponential and linear responses. The appearance of the linear terms is discussed later. The ϕ responses to the δ^A and δ^R steps are exponential responses (roll, spiral). Note the coupled roll-spiral mode at the dynamic pressure 8,255 N/m^2 and -42° sweep is insignificant or not visible in the ψ and ϕ responses. The β and ϕ responses are stable even though the ϕ response looks unstable. The ψ responses are unstable. This response stability is also discussed below.

The V_x, α and θ Laplace transform numerators are complete polynomials. Complete means that the zero power of s coefficient in the polynomial is not zero. The characteristic roots lead to the characteristic modes. The control step inputs (zero root) lead to a constant mode because the numerator polynomials are complete and no cancellation of the zero root occurs. The time response stability thus depends upon the characteristic roots. The β and ϕ Laplace transform numerators are not complete polynomials. Remembering that one lateral-directional characteristic root is identically zero, cancellation occurs and the characteristic and constant modes appear just as in the longitudinal case. The ψ Laplace transform numerator is

a complete polynomial. Cancellation does not occur, and the double zero root results in an extra linear mode.

Since all the lateral-directional characteristic roots are stable, the β and ϕ responses are also stable even though the ϕ response looks like an unstable response. The ψ response is an unstable response because of the linear mode. This means that an aileron roll maneuver, ζ^A step, will result in a constant ϕ after the transient response has decayed. This roll stability indicates a "mathematical" maneuver restriction occurs because the responses indicate the steady state constant ϕ is only 1.6 complete rolls at the dynamic pressure 8,255 N/m^2 and -42° sweep. At higher dynamic pressures and lower or less negative sweep the restriction is insignificant because the steady state constant ϕ is well over several or more complete rolls. Note that if the spiral root is unstable, the β, ψ and ϕ responses would all diverge and this restriction would not occur. Realize a complete roll maneuver due to a ζ^A step can not be considered as a small perturbation motion, hence the steady state results discussed here are not valid. In fact, the small perturbation responses are only valid initially when the magnitude of the perturbation can still be considered as small. An impulse would be a more realistic input for the small perturbation lateral-directional analysis because this would result in the responses all returning asymptotically to zero and the small perturbation equations would then still be valid.

CHAPTER VI

CONCLUSIONS AND RECOMMENDATIONS

Conclusions

A conceivable variation of the revived forward sweep concept is the merging of forward sweep and variable sweep. Both forward sweep and variable sweep offer significant performance gains over fixed backward sweep wing designs. The coupling of forward sweep and variable sweep might result in even higher performance levels. The goal of this research is to 1) study the flight dynamics of the variable forward sweep concept and 2) indicate any significant advantages or disadvantages associated with the variable forward sweep concept. Goal 1 is accomplished by conducting and discussing this research. Goal 2 is accomplished by stating the following conclusions.

1. Variable forward sweep designs should have far fewer problems with excessive longitudinal stability and elevator control effectiveness reduction than variable backward sweep designs.

2. Significant changes occur in the short period and phugoid modes over the variable forward sweep range and dynamic pressures. A fixed forewing and fixed wing pivot located in the forewing, artificial longitudinal stability or center of gravity control might be required to reduce these effects.

3. The dutch-roll mode is affected very little by the variable forward sweep; however, the roll and spiral modes are significantly

affected by variable forward sweep. Artificial lateral-directional stability might be required to reduce these effects.

4. A "mathematical" roll maneuver restriction occurs if all the lateral-directional modes are stable. However, this restriction breaks down as the small perturbation assumption fails. An unstable spiral root may be advantageous to the "mathematical" roll performance.

5. The flight dynamics of a variable forward sweep wing aircraft present no major difficulties for the variable forward sweep concept to become a feasible design option.

Recommendations

Many unaddressed areas of the variable forward sweep concept need to be studied further. These unaddressed areas include the effects of flexibility, nonlinear dynamics and aerodynamics, nonideal control surface actuators and automatic flight control systems. The forward sweep wing is a flexible structure and its affects upon the linear dynamics and aerodynamics assumptions need to be analyzed. Any high performance aircraft that is designed today employs some type of automatic flight control system to squeeze the maximum possible performance out of an aircraft. The variable forward sweep wing aircraft will not be excluded; hence, the incorporation of automatic flight control systems should be addressed. Finally, to insure the accuracy of the research, nonlinear dynamics and aerodynamics and nonideal control surface actuators should also be used.

BIBLIOGRAPHY

(1) Roskam, J. Airplane Flight Dynamics And Automatic Flight Controls. Lawrence: Roskam Aviation and Engineering Corporation, 1979.

(2) Polhamus, E. C. and T. A. Toll. "Research Related To Variable Sweep Aircraft Development." NASA-TM-83121, May, 1981.

(3) Kress, R. W. "Variable Sweep Wing Design." AIAA-80-3043, March, 1980.

(4) Diederick, F. W. and B. Budiansky. "Divergence of Swept Wings." NACA-TN-1680, 1948.

(5) Krone, N. J. "Divergence Elimination With Advanced Composites." AIAA-75-1009, August, 1975.

(6) Moore, M. and D. Frei. "X-29 Forward Swept Wing Aerodynamic Overview." AIAA-83-1834, July, 1983.

(7) Krone, N. J. "Forward Swept Wing Flight Demonstrator." AIAA-80-1882, August, 1980.

(8) Nicolai, L. M. Fundamentals Of Aircraft Design. Fairborn: E. P. Domicone Printing Services, 1975.

(9) Jane's All The World's Aircraft 1984-85. London: Jane's Publishing Company Limited, 1984.

(10) "Specifications." Aviation Week & Space Technology, Vol. 120, No. 11 (12 March 1984), pp. 131-173.

(11) Finck, R. D. USAF Stability and Control DATCOM. Wright-Patterson Air Force Base: Air Force Flight Dynamics Laboratory, April, 1978.

(12) Sharpes, D. G. "Qualification of the Datcom for Sweptforward Wing Planforms-A Summary of Work to Date." AIAA-83-1836, July, 1983.

(13) Etkin, B. Dynamics of Flight-Stability and Control. New York: John Wiley & Sons, 1982.

APPENDIX A

CONFIGURATION SPECIFICATIONS

The specifications of the aircraft shown in Figure 1 are listed in this appendix. The appendix is divided into the following sections: body, wing, horizontal stabilizer, vertical stabilizer, propulsion, mass and center of gravity and moments of inertia. Some sections include a discussion of the methodology used in calculating the specifications.

Figure 4 shows the body coordinate systems used in the research effort. The xyz stability axes were mentioned previously. The $\bar{x}\bar{y}\bar{z}$ coordinate system is attached to the aircraft's center of gravity, $\bar{\bar{x}}\bar{\bar{y}}\bar{\bar{z}}$ coordinate system is attached to the aircraft's nose, $x'y'z'$ coordinate system is attached to the wing pivot, $x''y''z''$ coordinate system is attached to the wing's center of gravity and $x'''y'''z'''$ coordinate system is attached to the aircraft minus the wing center of gravity. All the coordinate systems shown in Figure 4 with the exception of the stability axes have their x axis parallel to the body centerline.

Body:

$\ell^B = 14.63$ m

$d^B = 1.829$ m

$S^B_{base} = 2.627$ m^2

$V^B = 33.31$ m^3

$\ell^B_{nose} = 4.389$ m

$S^B = 2.627$ m^2

$S^B_{wet\ ex.base} = 76.06$ m^2

The volume is based on a conical nose shape with a nose length of 20% of the body length. However, the nose length listed is 30% of the body length. These lengths were selected because the nose taper ratio

is only significant in the leading 20% of the nose. The volume is used in the body subsonic aerodynamic center calculation. The exact nose profile is unspecified but a parabolic profile is assumed when the methods of reference (11) are used.

Wing:

	NACA 64A010 airfoil	$-42° \leq \Lambda^W_{LE} \leq -15°$
	$\bar{\bar{x}}_p = -12.55$ m	$\bar{\bar{y}}_p = 0$
	$\bar{\bar{z}}_p = -0.4445$ m	$I^W = 0°$
	$\alpha^W_o = 0°$	$\alpha^W_{stall} = 12°$
	$e^W_{(subsonic)} = 0.85$	$\eta^W = 0.9$
	$\varepsilon^W_i = 0.6°$	$d\varepsilon^W/d\alpha = 0.1$
At $\Lambda^W_{LE} = -30°$:	$S^W = 18.58$ m^2	$S^W_{wet} = 28.00$ m^2
	$\bar{c}^W = 2.341$ m	$b^W = 8.230$ m
	$c^W_{root} = 3.010$ m	$\lambda^W = 0.5$
	$c^W_F/c^W = 0.2$	$c^W_A/c^W = 0.2$
	$\eta^W_{F_1} = 0.3$	$\eta^W_{A_1} = 0.7$
	$\eta^W_{F_2} = 0.7$	$\eta^W_{A_2} = 0.9$

The flaps and ailerons are plain flaps. There is no available method to calculate η^W, e^W, ε^W_i and $\frac{d\varepsilon^W}{d\alpha}$ for a canard forward sweep wing configuration. Therefore, values for these variables were selected as reasonably conservative values compared to typical values for a conventional configuration. As a first degree estimate, α^W_o and α^W_{stall} are set equal to the airfoil α_o and α_{stall}.

Horizontal Stabilizer:

NACA 64A010 airfoil	$\Lambda^H_{LE} = 30°$
$S^H = 4.645$ m^2	$S^H_{wet} = 4.396$ m^2

$\bar{c}^H = 1.171\ m$ $\qquad$ $b^H = 4.115\ m$

$c^H_{root} = 1.505\ m$ $\qquad$ $\lambda^H = 0.5$

$c^H_E / c^H = 0.2$ $\qquad$ $\eta^H_{E_1} = 0.5$

$\eta^H_{E_2} = 0.9$ $\qquad$ $I^H = 2°$

$\alpha^H_o = 0°$ $\qquad$ $\alpha^H_{Stall} = 12°$

$e^H(subsonic) = 0.85$

The elevators are plain flaps. e^H, α^H_o and α^H_{Stall} are estimated by the same method as stated in the wing section.

Vertical Stabilizer:

NACA 64A010 airfoil $\qquad$ $\Lambda^V_{LE} = 30°$

$S^V = 3.716\ m^2$ $\qquad$ $S^V_{wet} = 7.432\ m^2$

$\bar{c}^V = 1.814\ m$ $\qquad$ $b^V = 2.134\ m$

$c^V_{root} = 2.357\ m$ $\qquad$ $\lambda^V = 0.4774$

$c^V_R / c^V = 0.2$ $\qquad$ $\eta^V_{R_1} = 0.2$

$\eta^V_{R_2} = 0.8$ $\qquad$ $I^V = 0°$

$\beta^V_o = 0°$ $\qquad$ $\beta^V_{Stall} = 12°$

$e^V(subsonic) = 0.85$ $\qquad$ $\eta^V = 0.9$

$\sigma^V_1 = 0°$ $\qquad$ $d\sigma^V/d\beta = 0.1$

The rudder is a plain flap. λ^V is selected so that the trailing edge sweep angle is zero. η^V, e^V, σ^V_1, $\frac{d\sigma^V}{d\beta}$, β^V_o and β^V_{Stall} are estimated by the same method as stated in the wing section. Figure 11 shows the definition of S^V and b^V.

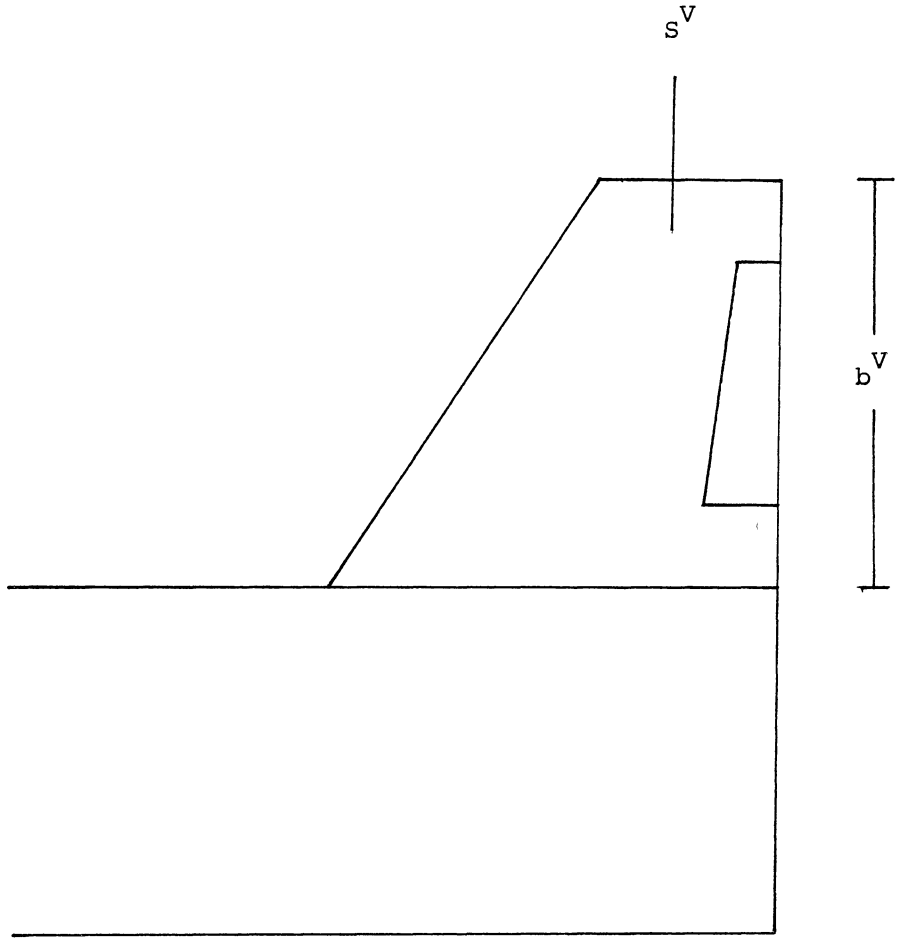

Figure 11. Vertical Stabilizer Planform Definitions

Propulsion: General Electric F404-GE-400 turbofan

$T^E_{max} = 71{,}170\ N$ $\quad A^I = 0.5\ m^2$

$\ell^E = 4.039\ m$ $\quad d^E = 0.8890\ m$

$\bar{\bar{x}}^I = -7.315\ m$ $\quad \bar{\bar{y}}^I = 0$

$\bar{\bar{z}}^I = 1.402\ m$ $\quad \bar{\bar{x}}^E = -14.63\ m$

$\bar{\bar{y}}^E = 0$ $\quad \bar{\bar{z}}^E = 0$

The engine centerline coincides with the body centerline and the engine base coincides with the body base.

Mass and Center of Gravity:

$m_{max} = 12{,}000\ Kg$ $\quad m_{min} = 6000\ Kg$

$m^W = 1{,}565\ Kg$ $\quad m^E = 785\ Kg$

$0 \leq (m^P + m^F) \leq 6000\ Kg$ $\quad \bar{\bar{x}}^{-W}_{CG} = -7.459\ m$

$\bar{\bar{y}}^{-W}_{CG} = 0$ $\quad \bar{\bar{z}}^{-W}_{CG} = -0.02749\ m$

At $\Lambda^W_{LE} = -30°$: $\bar{\bar{x}}_{CG} = -8.090\ m$ $\quad \bar{\bar{y}}_{CG} = 0$

$\bar{\bar{z}}_{CG} = -0.1\ m$

The aircraft's center of gravity location will vary depending upon the sweep angle. Therefore, the analysis required a method to estimate the wing's center of gravity location as a function of sweep. Combining this method with the stationary center of gravity for the remaining elements of the aircraft, the aircraft's center of gravity location can be calculated as a function of sweep.

For this method, the wing is modeled as a solid homogeneous panel. Equation (57) and the geometry shown in Figure 12 are used to calculate

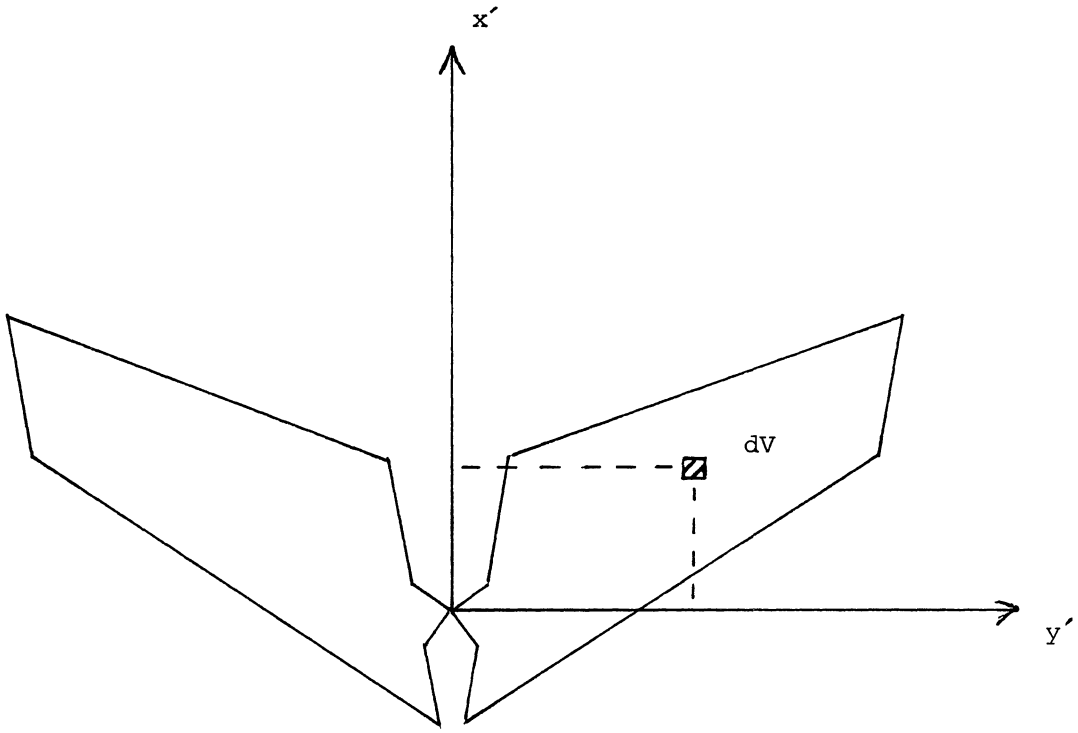

Figure 12. Wing Geometry for Center of Gravity and Moments of Inertia Calculations

the wing center of gravity location.

$$\bar{\bar{x}}^{w}_{cG} = \bar{\bar{x}}_{p} + \frac{\rho^{w}}{m^{w}} \iiint x' dV \tag{57}$$

The aircraft center of gravity location is then calculated from equation (58).

$$\bar{\bar{x}}_{cG} = \frac{\bar{m}^{w}\bar{\bar{x}}^{-w}_{cG} + m^{w}\bar{\bar{x}}^{w}_{cG}}{m} \tag{58}$$

Note $\bar{\bar{y}}^{w}_{cG}$ and $\bar{\bar{z}}^{w}_{cG}$ and hence $\bar{\bar{y}}_{cG}$ and $\bar{\bar{z}}_{cG}$ do not vary with sweep.

The wing density in equation (57) is given by equation (59).

$$\rho^{w} = \frac{m^{w}}{S^{w}_{s} t^{w}} \tag{59}$$

Assuming the wing to be thin, the z integrals with the limits of $-t^{w}/2$ to $t^{w}/2$ will cancel the t^{w} in equation (59). Therefore, a value for t^{w} is not required. After examining Nicolai's (8) weight estimations, the wing mass was selected as 30% of the aircraft's minimum mass excluding the engine mass. $\bar{\bar{z}}_{cG}$ was designed to be -0.1m because the wing and vertical stabilizer are located above the body centerline.

Moments of Inertia:

$I^{-w}_{\bar{x}\bar{x}} = 33,930 \ Kg m^2$ $\quad I^{-w}_{\bar{y}\bar{y}} = 49,870 \ Kg m^2$

$I^{-w}_{\bar{z}\bar{z}} = 122,320 \ Kg m^2$ $\quad I^{-w}_{\bar{x}\bar{z}} = -2,087 \ Kg m^2$

At $\Lambda^{w}_{LE} = -30°$: $\quad I_{\bar{x}\bar{x}} = 42,000 \ Kg m^2$ $\quad I_{\bar{y}\bar{y}} = 69,000 \ Kg m^2$

$I_{\bar{z}\bar{z}} = 149,000 \ Kg m^2$ $\quad I_{\bar{x}\bar{z}} = 0$

Similar to the previous section, a method to estimate the wing moments of inertia as a function of sweep is required. Combining this method with the constant moments of inertia for the remaining elements of the aircraft, the aircraft's moments of inertia can be calculated as a function of sweep. The wing is again modeled as a solid homogeneous panel.

Equations (60) through (63) and the geometry of Figure 12 are used to calculate the wing moments of inertia.

$$I^{w}_{x''x''} = -m^{w}(\bar{\bar{z}}_{p} - \bar{\bar{z}}^{w}_{cG})^2 + \rho^{w}\iiint (y'^2 + z'^2)\, dV \tag{60}$$

$$I^{w}_{y''y''} = -m^{w}\{(\bar{\bar{x}}_{p} - \bar{\bar{x}}^{w}_{cG})^2 + (\bar{\bar{z}}_{p} - \bar{\bar{z}}^{w}_{cG})^2\} + \rho^{w}\iiint (x'^2 + z'^2)\, dV \tag{61}$$

$$I^{w}_{z''z''} = -m^{w}(\bar{\bar{x}}_{p} - \bar{\bar{x}}^{w}_{cG})^2 + \rho^{w}\iiint (x'^2 + y'^2)\, dV \tag{62}$$

$$I^{w}_{x''z''} = -m^{w}(\bar{\bar{x}}_{p} - \bar{\bar{x}}^{w}_{cG})(\bar{\bar{z}}_{p} - \bar{\bar{z}}^{w}_{cG}) + \rho^{w}\iiint x'z'\, dV \tag{63}$$

The aircraft moments of inertia are then calculated from equations (64) through (67).

$$I_{\bar{x}\bar{x}} = m^{-w}(\bar{\bar{z}}_{cG} - \bar{\bar{z}}^{-w}_{cG})^2 + I^{-w}_{x'''x'''} + m^{w}(\bar{\bar{z}}_{cG} - \bar{\bar{z}}^{w}_{cG})^2 + I^{w}_{x''x''} \tag{64}$$

$$I_{\bar{y}\bar{y}} = m^{-w}\{(\bar{\bar{x}}_{cG} - \bar{\bar{x}}^{-w}_{cG})^2 + (\bar{\bar{z}}_{cG} - \bar{\bar{z}}^{-w}_{cG})^2\} + I^{-w}_{y'''y'''} + m^{w}\{(\bar{\bar{x}}_{cG} - \bar{\bar{x}}^{w}_{cG})^2 + (\bar{\bar{z}}_{cG} - \bar{\bar{z}}^{w}_{cG})^2\} + I^{w}_{y''y''} \tag{65}$$

$$I_{\bar{z}\bar{z}} = m^{-w}(\bar{\bar{x}}_{cG} - \bar{\bar{x}}^{-w}_{cG})^2 + I^{-w}_{z'''z'''} + m^{w}(\bar{\bar{x}}_{cG} - \bar{\bar{x}}^{w}_{cG})^2 + I^{w}_{z''z''} \tag{66}$$

$$I_{\bar{x}\bar{z}} = m^{-w}(\bar{\bar{x}}_{cG} - \bar{\bar{x}}^{-w}_{cG})(\bar{\bar{z}}_{cG} - \bar{\bar{z}}^{-w}_{cG}) + I^{-w}_{x'''z'''} + m^{w}(\bar{\bar{x}}_{cG} - \bar{\bar{x}}^{w}_{cG})(\bar{\bar{z}}_{cG} - \bar{\bar{z}}^{w}_{cG}) + I^{w}_{x''z''} \tag{67}$$

The thin wing assumption is used again.

As shown by Roskam (1), equations (68) through (71) are finally used to transform the moments of inertia from the $\bar{\bar{x}}\bar{\bar{y}}\bar{\bar{z}}$ coordinate system to the xyz coordinate system shown in Figure 4.

$$I_{xx} = \cos^2\nabla_1\, I_{\bar{x}\bar{x}} + \sin^2\nabla_1\, I_{\bar{z}\bar{z}} - 2\cos\nabla_1 \sin\nabla_1\, I_{\bar{x}\bar{z}} \tag{68}$$

$$I_{yy} = I_{\bar{y}\bar{y}} \tag{69}$$

$$I_{zz} = \sin^2\nabla_1\, I_{\bar{x}\bar{x}} + \cos^2\nabla_1\, I_{\bar{z}\bar{z}} + 2\cos\nabla_1 \sin\nabla_1\, I_{\bar{x}\bar{z}} \tag{70}$$

$$I_{xz} = \cos\nabla_1 \sin\nabla_1 (I_{\bar{x}\bar{x}} - I_{\bar{z}\bar{z}}) + (\cos^2\nabla_1 - \sin^2\nabla_1)\, I_{\bar{x}\bar{z}} \tag{71}$$

This is required because the moments of inertia appearing in the equations of motion correspond to the xyz coordinate system.

APPENDIX B

AIRCRAFT STABILITY AND CONTROL DERIVATIVES

The aircraft stability and control derivatives in terms of the element stability and control derivatives as mentioned in Chapter IV are contained in this appendix. The stability and control derivative transformations to the stability axes as mentioned in Chapter IV are also contained in this appendix.

Aircraft Aerodynamic Derivatives:

$$C_D = \eta^w C_D^w + \frac{S^H}{S^w} C_D^H + \frac{S^B}{S^w} C_D^B + \eta^v \frac{S^v}{S^w} C_D^v$$

$$C_{D_{V_X}} = \eta^w C_{D_{V_X}}^w + \frac{S^H}{S^w} C_{D_{V_X}}^H + \frac{S^B}{S^w} C_{D_{V_X}}^B + \eta^v \frac{S^v}{S^w} C_{D_{V_X}}^v$$

$$C_{D_\alpha} = \eta^w C_{D_\alpha}^w + \frac{S^H}{S^w} C_{D_\alpha}^H + \frac{S^B}{S^w} C_{D_\alpha}^B$$

$$C_{D_{\dot\alpha}} = \eta^w C_{D_{\dot\alpha}}^w$$

$$C_{D_{\omega_Y}} = \eta^w C_{D_{\omega_Y}}^w + \frac{S^H}{S^w} C_{D_{\omega_Y}}^H + \frac{S^B}{S^w} C_{D_{\omega_Y}}^B + \eta^v \frac{S^v}{S^w} C_{D_{\omega_Y}}^v$$

$$C_{D_{\delta E}} = \frac{S^H}{S^w} C_{D_{\delta E}}^H$$

$$C_{D_{\delta F}} = \eta^w C_{D_{\delta F}}^w$$

$$C_L = \eta^w C_L^w + \frac{S^H}{S^w} C_L^H + \frac{S^B}{S^w} C_L^B$$

$$C_{L_{V_X}} = \eta^w C_{L_{V_X}}^w + \frac{S^H}{S^w} C_{L_{V_X}}^H + \frac{S^B}{S^w} C_{L_{V_X}}^B$$

$$C_{L_\alpha} = \eta^w C_{L_\alpha}^w + \frac{S^H}{S^w} C_{L_\alpha}^H + \frac{S^B}{S^w} C_{L_\alpha}^B$$

$$C_{L_{\dot\alpha}} = \eta^w C_{L_{\dot\alpha}}^w$$

$$C_{L_{\omega_Y}} = \eta^w C_{L_{\omega_Y}}^w + \frac{S^H}{S^w} C_{L_{\omega_Y}}^H + \frac{S^B}{S^w} C_{L_{\omega_Y}}^B$$

$$C_{L_{\delta E}} = \frac{S^H}{S^w} C_{L_{\delta E}}^H$$

$$C_{L_{\delta F}} = \eta^w C_{L_{\delta F}}^w$$

$$C_m = \eta^w \left(C_m^w + \frac{\bar{x}_{Ac}^w}{\bar{c}^w} C_L^w - \frac{\bar{z}_{Ac}^w}{\bar{c}^w} C_D^w \right) + \frac{S^H}{S^w} \left(\frac{\bar{c}^H}{\bar{c}^w} C_m^H + \frac{\bar{x}_{Ac}^H}{\bar{c}^w} C_L^H - \frac{\bar{z}_{Ac}^H}{\bar{c}^w} C_D^H \right) + \frac{S^B}{S^w} \left(\frac{\ell^B}{\bar{c}^w} C_m^B + \frac{\bar{x}_{Ac}^B}{\bar{c}^w} C_L^B - \frac{\bar{z}_{Ac}^B}{\bar{c}^w} C_D^B \right) - \eta^v \frac{S^v}{S^w} \frac{\bar{z}_{Ac}^v}{\bar{c}^w} C_D^v$$

$$C_{m_{V_X}} = \eta^w \left(C_{m_{V_X}}^w + \frac{\bar{x}_{Ac}^w}{\bar{c}^w} C_{L_{V_X}}^w - \frac{\bar{z}_{Ac}^w}{\bar{c}^w} C_{D_{V_X}}^w \right) + \frac{S^H}{S^w} \left(\frac{\bar{c}^H}{\bar{c}^w} C_{m_{V_X}}^H + \frac{\bar{x}_{Ac}^H}{\bar{c}^w} C_{L_{V_X}}^H - \frac{\bar{z}_{Ac}^H}{\bar{c}^w} C_{D_{V_X}}^H \right) + \frac{S^B}{S^w} \left(\frac{\ell^B}{\bar{c}^w} C_{m_{V_X}}^B + \frac{\bar{x}_{Ac}^B}{\bar{c}^w} C_{L_{V_X}}^B - \frac{\bar{z}_{Ac}^B}{\bar{c}^w} C_{D_{V_X}}^B \right) - \eta^v \frac{S^v}{S^w} \frac{\bar{z}_{Ac}^v}{\bar{c}^w} C_{D_{V_X}}^v$$

$$C_{m_\alpha} = \eta^w \left(C_{m_\alpha}^w + \frac{\bar{x}_{Ac}^w}{\bar{c}^w} C_{L_\alpha}^w - \frac{\bar{z}_{Ac}^w}{\bar{c}^w} C_{D_\alpha}^w \right) + \frac{S^H}{S^w} \left(\frac{\bar{c}^H}{\bar{c}^w} C_{m_\alpha}^H + \frac{\bar{x}_{Ac}^H}{\bar{c}^w} C_{L_\alpha}^H - \frac{\bar{z}_{Ac}^H}{\bar{c}^w} C_{D_\alpha}^H \right) + \frac{S^B}{S^w} \left(\frac{\ell^B}{\bar{c}^w} C_{m_\alpha}^B + \frac{\bar{x}_{Ac}^B}{\bar{c}^w} C_{L_\alpha}^B - \frac{\bar{z}_{Ac}^B}{\bar{c}^w} C_{D_\alpha}^B \right)$$

$$C_{m_{\dot\alpha}} = \eta^w \left(C_{m_{\dot\alpha}}^w + \frac{\bar{x}_{Ac}^w}{\bar{c}^w} C_{L_{\dot\alpha}}^w - \frac{\bar{z}_{Ac}^w}{\bar{c}^w} C_{D_{\dot\alpha}}^w \right)$$

$$C_{m_{\omega_Y}} = \eta^w \left(C_{m_{\omega_Y}}^w + \frac{\bar{x}_{Ac}^w}{\bar{c}^w} C_{L_{\omega_Y}}^w - \frac{\bar{z}_{Ac}^w}{\bar{c}^w} C_{D_{\omega_Y}}^w \right) + \frac{S^H}{S^w} \left(\frac{\bar{c}^H}{\bar{c}^w} C_{m_{\omega_Y}}^H + \frac{\bar{x}_{Ac}^H}{\bar{c}^w} C_{L_{\omega_Y}}^H - \frac{\bar{z}_{Ac}^H}{\bar{c}^w} C_{D_{\omega_Y}}^H \right) + \frac{S^B}{S^w} \left(\frac{\ell^B}{\bar{c}^w} C_{m_{\omega_Y}}^B + \frac{\bar{x}_{Ac}^B}{\bar{c}^w} C_{L_{\omega_Y}}^B - \frac{\bar{z}_{Ac}^B}{\bar{c}^w} C_{D_{\omega_Y}}^B \right) - \eta^v \frac{S^v}{S^w} \frac{\bar{z}_{Ac}^v}{\bar{c}^w} C_{D_{\omega_Y}}^v$$

$$C_{m_{\delta E}} = \frac{S^H}{S^w} \left(\frac{\bar{c}^H}{\bar{c}^w} C_{m_{\delta E}}^H + \frac{\bar{x}_{Ac}^H}{\bar{c}^w} C_{L_{\delta E}}^H - \frac{\bar{z}_{Ac}^H}{\bar{c}^w} C_{D_{\delta E}}^H \right)$$

$$C_{m_{\delta F}} = \eta^w \left(C_{m_{\delta F}}^w + \frac{\bar{x}_{Ac}^w}{\bar{c}^w} C_{L_{\delta F}}^w - \frac{\bar{z}_{Ac}^w}{\bar{c}^w} C_{D_{\delta F}}^w \right)$$

$$C_Y = n^v \frac{S^v}{S^w} C_Y^v + \frac{S^B}{S^w} C_Y^B$$

$$C_{Y\beta} = n^v \frac{S^v}{S^w} C_{Y\beta}^v + \frac{S^B}{S^w} C_{Y\beta}^B$$

$$C_{Y\dot{\beta}} = n^v \frac{S^v}{S^w} C_{Y\dot{\beta}}^v$$

$$C_{Y\omega_X} = n^v \frac{S^v}{S^w} C_{Y\omega_X}^v + \frac{S^B}{S^w} C_{Y\omega_X}^B$$

$$C_{Y\omega_Z} = n^v \frac{S^v}{S^w} C_{Y\omega_Z}^v + \frac{S^B}{S^w} C_{Y\omega_Z}^B$$

$$C_{Y\delta A} = 0$$

$$C_{Y\delta R} = n^v \frac{S^v}{S^w} C_{Y\delta R}^v$$

$$C_\ell = n^w C_\ell^w + \frac{S^H}{S^w} C_\ell^H - n^v \frac{S^v}{S^w} \frac{\bar{z}_{Ac}^v}{b^w} C_Y^v + \frac{S^B}{S^w}\left(\frac{\ell^B}{b^w} C_\ell^B - \frac{\bar{z}_{Ac}^B}{b^w} C_Y^B\right)$$

$$C_{\ell\beta} = n^w C_{\ell\beta}^w + \frac{S^H}{S^w} C_{\ell\beta}^H - n^v \frac{S^v}{S^w} \frac{\bar{z}_{Ac}^v}{b^w} C_{Y\beta}^v + \frac{S^B}{S^w}\left(\frac{\ell^B}{b^w} C_{\ell\beta}^B - \frac{\bar{z}_{Ac}^B}{b^w} C_{Y\beta}^B\right)$$

$$C_{\ell\dot{\beta}} = -n^v \frac{S^v}{S^w} \frac{\bar{z}_{Ac}^v}{b^w} C_{Y\dot{\beta}}^v$$

$$C_{\ell\omega_X} = n^w C_{\ell\omega_X}^w + \frac{S^H}{S^w} C_{\ell\omega_X}^H - n^v \frac{S^v}{S^w} \frac{\bar{z}_{Ac}^v}{b^w} C_{Y\omega_X}^v + \frac{S^B}{S^w}\left(\frac{\ell^B}{b^w} C_{\ell\omega_X}^B - \frac{\bar{z}_{Ac}^B}{b^w} C_{Y\omega_X}^B\right)$$

$$C_{\ell\omega_Z} = n^w C_{\ell\omega_Z}^w + \frac{S^H}{S^w} C_{\ell\omega_Z}^H - n^v \frac{S^v}{S^w} \frac{\bar{z}_{Ac}^v}{b^w} C_{Y\omega_Z}^v + \frac{S^B}{S^w}\left(\frac{\ell^B}{b^w} C_{\ell\omega_Z}^B - \frac{\bar{z}_{Ac}^B}{b^w} C_{Y\omega_Z}^B\right)$$

$$C_{\ell\delta A} = n^w C_{\ell\delta A}^w$$

$$C_{\ell\delta R} = -n^v \frac{S^v}{S^w} \frac{\bar{z}_{Ac}^v}{b^w} C_{Y\delta R}^v$$

$$C_n = n^w C_n^w + \frac{S^H}{S^w} C_n^H + n^v \frac{S^v}{S^w}\left(\frac{\bar{c}^v}{b^w} C_n^v + \frac{\bar{x}_{Ac}^v}{b^w} C_Y^v\right) + \frac{S^B}{S^w}\left(\frac{\ell^B}{b^w} C_n^B + \frac{\bar{x}_{Ac}^B}{b^w} C_Y^B\right)$$

$$C_{n\beta} = n^w C_{n\beta}^w + \frac{S^H}{S^w} C_{n\beta}^H + n^v \frac{S^v}{S^w}\left(\frac{\bar{c}^v}{b^w} C_{n\beta}^v + \frac{\bar{x}_{Ac}^v}{b^w} C_{Y\beta}^v\right) + \frac{S^B}{S^w}\left(\frac{\ell^B}{b^w} C_{n\beta}^B + \frac{\bar{x}_{Ac}^B}{b^w} C_{Y\beta}^B\right)$$

$$C_{n\dot{\beta}} = n^v \frac{S^v}{S^w}\left(\frac{\bar{c}^v}{b^w} C_{n\dot{\beta}}^v + \frac{\bar{x}_{Ac}^v}{b^w} C_{Y\dot{\beta}}^v\right)$$

$$C_{n\omega_X} = n^w C_{n\omega_X}^w + \frac{S^H}{S^w} C_{n\omega_X}^H + n^v \frac{S^v}{S^w}\left(\frac{\bar{c}^v}{b^w} C_{n\omega_X}^v + \frac{\bar{x}_{Ac}^v}{b^w} C_{Y\omega_X}^v\right) + \frac{S^B}{S^w}\left(\frac{\ell^B}{b^w} C_{n\omega_X}^B + \frac{\bar{x}_{Ac}^B}{b^w} C_{Y\omega_X}^B\right)$$

$$C_{n\omega_Z} = n^w C_{n\omega_Z}^w + \frac{S^H}{S^w} C_{n\omega_Z}^H + n^v \frac{S^v}{S^w}\left(\frac{\bar{c}^v}{b^w} C_{n\omega_Z}^v + \frac{\bar{x}_{Ac}^v}{b^w} C_{Y\omega_Z}^v\right) + \frac{S^B}{S^w}\left(\frac{\ell^B}{b^w} C_{n\omega_Z}^B + \frac{\bar{x}_{Ac}^B}{b^w} C_{Y\omega_Z}^B\right)$$

$$C_{n\delta A} = n^w C_{n\delta A}^w$$

$$C_{n\delta R} = n^v \frac{S^v}{S^w}\left(\frac{\bar{c}^v}{b^w} C_{n\delta R}^v + \frac{\bar{x}_{Ac}^v}{b^w} C_{Y\delta R}^v\right)$$

Aerodynamic Derivative Transformations:

$$C_{A_X} = -C_D$$

$$C_{A_{X_{V_X}}} = -C_{D_{V_X}} - \frac{2C_D}{V_{X_1}}$$

$$C_{A_{X_\alpha}} = -C_{D_\alpha} + C_L$$

$$C_{A_{X_{\dot{\alpha}}}} = -C_{D_{\dot{\alpha}}}$$

$$C_{A_{X\omega_y}} = -C_{D\omega_y}$$

$$C_{A_{X\delta E}} = -C_{D\delta E}$$

$$C_{A_{X\delta F}} = -C_{D\delta F}$$

$$C_{A_Z} = -C_L$$

$$C_{A_{Z_{V_X}}} = -C_{L_{V_X}} - \frac{2C_L}{V_{X_1}}$$

$$C_{A_{Z_\alpha}} = -C_{L_\alpha} - C_D$$

$$C_{A_{Z_{\dot{\alpha}}}} = -C_{L_{\dot{\alpha}}}$$

$$C_{A_{Z\omega_y}} = -C_{L\omega_y}$$

$$C_{A_{Z\delta E}} = -C_{L\delta E}$$

$$C_{A_{Z\delta F}} = -C_{L\delta F}$$

$$K_{A_y} = C_m$$

$$K_{A_{y_{V_X}}} = C_{m_{V_X}} + \frac{2C_m}{V_{X_1}}$$

$$K_{A_{y_\alpha}} = C_{m_\alpha}$$

$$K_{A_{y_{\dot{\alpha}}}} = C_{m_{\dot{\alpha}}}$$

$$K_{A_{y\omega_y}} = C_{m\omega_y}$$

$$K_{A_{y\delta E}} = C_{m\delta E}$$

$$K_{A_{y\delta F}} = C_{m\delta F}$$

$$C_{A_y} = C_y$$

$$C_{A_{y_\beta}} = C_{y_\beta}$$

$$C_{A_{y_{\dot{\beta}}}} = C_{y_{\dot{\beta}}}$$

$$C_{A_{y\omega_X}} = C_{y\omega_X}$$

$$C_{A y \omega_z} = C_{y \omega_z}$$

$$C_{A y \delta A} = C_{y \delta A}$$

$$C_{A y \delta R} = C_{y \delta R}$$

$$K_{AX} = C_\ell + \nabla_1 C_n$$

$$K_{AX\beta} = C_{\ell\beta} + \nabla_1 C_{n\beta}$$

$$K_{AX\dot{\beta}} = C_{\ell\dot{\beta}} + \nabla_1 C_{n\dot{\beta}}$$

$$K_{AX\omega_X} = C_{\ell\omega_X} + \nabla_1 C_{n\omega_X}$$

$$K_{AX\omega_Z} = C_{\ell\omega_Z} + \nabla_1 C_{n\omega_Z}$$

$$K_{AX\delta A} = C_{\ell\delta A} + \nabla_1 C_{n\delta A}$$

$$K_{AX\delta R} = C_{\ell\delta R} + \nabla_1 C_{n\delta R}$$

$$K_{AZ} = C_n - \nabla_1 C_\ell$$

$$K_{AZ\beta} = C_{n\beta} - \nabla_1 C_{\ell\beta}$$

$$K_{AZ\dot{\beta}} = C_{n\dot{\beta}} - \nabla_1 C_{\ell\dot{\beta}}$$

$$K_{AZ\omega_X} = C_{n\omega_X} - \nabla_1 C_{\ell\omega_X}$$

$$K_{AZ\omega_Z} = C_{n\omega_Z} - \nabla_1 C_{\ell\omega_Z}$$

$$K_{AZ\delta A} = C_{n\delta A} - \nabla_1 C_{\ell\delta A}$$

$$K_{AZ\delta R} = C_{n\delta R} - \nabla_1 C_{\ell\delta R}$$

Aircraft Thrust Derivatives:

$$C_{T\bar{X}} = C^{E}_{T\bar{X}\delta T}\,\Delta^{T}_{1}$$

$$C_{T\bar{X}V_X} = C^{I}_{T\bar{X}V_X}$$

$$C_{T\bar{X}\alpha} = C^{I}_{T\bar{X}\alpha}$$

$$C_{T\bar{X}\dot{\alpha}} = C^{I}_{T\bar{X}\dot{\alpha}}$$

$$C_{T\bar{X}\omega_Y} = C^{I}_{T\bar{X}\omega_Y}$$

$$C_{T\bar{X}\delta T} = C^{E}_{T\bar{X}\delta T}$$

$$C_{T\bar{Z}} = C^{E}_{T\bar{Z}\delta T}\,\Delta^{T}_{1}$$

$$C_{T\bar{Z}V_X} = C^{I}_{T\bar{Z}V_X}$$

$$C_{T\bar{Z}\alpha} = C^{I}_{T\bar{Z}\alpha}$$

$$C_{T\bar{Z}\dot{\alpha}} = C^{I}_{T\bar{Z}\dot{\alpha}}$$

$$C_{T\bar{Z}\omega_Y} = C^{I}_{T\bar{Z}\omega_Y}$$

$$C_{T\bar{Z}\delta T} = C^{E}_{T\bar{Z}\delta T}$$

$$K_{T\bar{Y}} = K^{E}_{T\bar{Y}\delta T}\,\Delta^{T}_{1}$$

$$K_{T\bar{Y}V_X} = K^{I}_{T\bar{Y}V_X}$$

$$K_{T\bar{Y}\alpha} = K^{I}_{T\bar{Y}\alpha}$$

$$K_{T\bar{Y}\dot{\alpha}} = K^{I}_{T\bar{Y}\dot{\alpha}}$$

$$K_{T\bar{Y}\omega_Y} = K^{I}_{T\bar{Y}\omega_Y}$$

$$K_{T\bar{Y}\delta T} = K^{E}_{T\bar{Y}\delta T}$$

$$C_{T\bar{Y}} = 0$$

$$C_{T\bar{Y}\beta} = C^{I}_{T\bar{Y}\beta}$$

$$C_{T\bar{Y}\dot{\beta}} = C^{I}_{T\bar{Y}\dot{\beta}}$$

$$C_{T\bar{Y}\omega_X} = C^{I}_{T\bar{Y}\omega_X}$$

$$C_{T\bar{Y}\omega_Z} = C^{I}_{T\bar{Y}\omega_Z}$$

$$K_{T\bar{X}} = 0$$

$$K_{T\bar{X}\beta} = K^{I}_{T\bar{X}\beta}$$

$$K_{T\bar{x}\beta} = K^{I}_{T\bar{x}\beta}$$

$$K_{T\bar{x}\omega_x} = K^{I}_{T\bar{x}\omega_x}$$

$$K_{T\bar{x}\omega_z} = K^{I}_{T\bar{x}\omega_z}$$

$$K_{T\bar{z}} = 0$$

$$K_{T\bar{z}\beta} = K^{I}_{T\bar{z}\beta}$$

$$K_{T\bar{z}\dot{\beta}} = K^{I}_{T\bar{z}\dot{\beta}}$$

$$K_{T\bar{z}\omega_x} = K^{I}_{T\bar{z}\omega_x}$$

$$K_{T\bar{z}\omega_z} = K^{I}_{T\bar{z}\omega_z}$$

Thrust Derivative Transformations:

$$C_{T_x} = C_{T_{\bar{x}}} + \bar{V}_1 C_{T_{\bar{z}}}$$

$$C_{T_{x v_x}} = C_{T_{\bar{x} v_x}} + \bar{V}_1 C_{T_{\bar{z} v_x}}$$

$$C_{T_{x\alpha}} = C_{T_{\bar{x}\alpha}} + \bar{V}_1 C_{T_{\bar{z}\alpha}}$$

$$C_{T_{x\dot{\alpha}}} = C_{T_{\bar{x}\dot{\alpha}}} + \bar{V}_1 C_{T_{\bar{z}\dot{\alpha}}}$$

$$C_{T_{x\omega_y}} = C_{T_{\bar{x}\omega_y}} + \bar{V}_1 C_{T_{\bar{z}}}\omega_y$$

$$C_{T_{x\delta_T}} = C_{T_{\bar{x}\delta_T}} + \bar{V}_1 C_{T_{\bar{z}\delta_T}}$$

$$C_{T_z} = C_{T_{\bar{z}}} - \bar{V}_1 C_{T_{\bar{x}}}$$

$$C_{T_{z v_x}} = C_{T_{\bar{z} v_x}} - \bar{V}_1 C_{T_{\bar{x} v_x}}$$

$$C_{T_{z\alpha}} = C_{T_{\bar{z}\alpha}} - \bar{V}_1 C_{T_{\bar{x}\alpha}}$$

$$C_{T_{z\dot{\alpha}}} = C_{T_{\bar{z}\dot{\alpha}}} - \bar{V}_1 C_{T_{\bar{x}\dot{\alpha}}}$$

$$C_{T_{z\omega_y}} = C_{T_{\bar{z}}}\omega_y - \bar{V}_1 C_{T_{\bar{x}\omega_y}}$$

$$C_{T_{z\delta_T}} = C_{T_{\bar{z}\delta_T}} - \bar{V}_1 C_{T_{\bar{x}\delta_T}}$$

$$K_{T_y} = K_{T_{\bar{y}}}$$

$$K_{T_{y v_x}} = K_{T_{\bar{y} v_x}}$$

$$K_{T_{y\alpha}} = K_{T_{\bar{y}\alpha}}$$

$$K_{T_{y\dot{\alpha}}} = K_{T_{\bar{y}\dot{\alpha}}}$$

$$K_{T_{y\omega_y}} = K_{T_{\bar{y}}}\omega_y$$

$$K_{T_{y\delta_T}} = K_{T_{\bar{y}\delta_T}}$$

$$C_{T_y} = C_{T_{\bar{y}}}$$

$$C_{T_{y\beta}} = C_{T_{\bar{y}\beta}}$$

$$C_{T_{y\dot{\beta}}} = C_{T_{\bar{y}\dot{\beta}}}$$

$$C_{T_{y\omega_x}} = C_{T_{\bar{y}\omega_x}}$$

$$C_{T_{y\omega_z}} = C_{T_{\bar{y}\omega_z}}$$

$$K_{T_x} = K_{T_{\bar{x}}} + \bar{V}_1 K_{T_{\bar{z}}}$$

$$K_{T_{x\beta}} = K_{T_{\bar{x}\beta}} + \bar{V}_1 K_{T_{\bar{z}\beta}}$$

$$K_{T\dot{x}\dot{\beta}} = K_{T\bar{x}\dot{\beta}} + \bar{\nabla}_1 K_{T\bar{z}\dot{\beta}}$$

$$K_{T\dot{x}\omega_x} = K_{T\bar{x}\omega_x} + \bar{\nabla}_1 K_{T\bar{z}\omega_x}$$

$$K_{T\dot{x}\omega_z} = K_{T\bar{x}\omega_z} + \bar{\nabla}_1 K_{T\bar{z}\omega_z}$$

$$K_{Tz} = K_{T\bar{z}} - \bar{\nabla}_1 K_{T\bar{x}}$$

$$K_{Tz\beta} = K_{T\bar{z}\beta} - \bar{\nabla}_1 K_{T\bar{x}\beta}$$

$$K_{Tz\dot{\beta}} = K_{T\bar{z}\dot{\beta}} - \bar{\nabla}_1 K_{T\bar{x}\dot{\beta}}$$

$$K_{Tz\omega_x} = K_{T\bar{z}\omega_x} - \bar{\nabla}_1 K_{T\bar{x}\omega_x}$$

$$K_{Tz\omega_z} = K_{T\bar{z}\omega_z} - \bar{\nabla}_1 K_{T\bar{x}\omega_z}$$

APPENDIX C

ELEMENT STABILITY AND CONTROL DERIVATIVES

The element stability and control derivatives as mentioned in Chapter IV are contained in this appendix. The notation of W, H, B and V before each equation indicates the equation is applicable to the corresponding element. Some derivatives are obtained from graphs contained in reference (11) rather than a closed form expression. For these derivatives, the notation "see reference (11)" is used. The element aerodynamic derivatives are divided into a subsonic and supersonic category. If an element aerodynamic derivative does not appear in the supersonic category, the supersonic expression is identical to the subsonic expression.

Element Aerodynamic Subsonic Derivatives:

$$C_D^W = C_{D_o}^W + C_{D_\alpha}^W (\nabla_1 - \alpha_o^W + I^W - \varepsilon_1^W)$$

$$C_D^H = C_{D_o}^H + C_{D_\alpha}^H (\nabla_1 - \alpha_o^H + I^H)$$

$$C_D^B = C_{D_o}^B + C_{D_\alpha}^B (\nabla_1)$$

$$C_D^V = C_{D_o}^V$$

W, H, B, V $\quad C_{D_o}$ = see reference (11)

W, H, B, V $\quad C_{D_{V_X}} = \dfrac{M_1 C_D}{V_S (1 - M_1^2)}$

W, H $\quad C_{D_\alpha} = \dfrac{2 C_L C_{L_\alpha}}{\pi A e}$

$$C_{D_\alpha}^B = 0$$

$$C_{D_{\dot\alpha}}^W = \frac{2 C_L^W C_{L_{\dot\alpha}}^W}{\pi A e}$$

W, H, B $\quad C_{D_{\omega_Y}} = -\dfrac{\bar X_{AC}}{V_{X_1}} C_{D_\alpha} + \bar Z_{AC} C_{D_{V_X}}$

$$C_{D_{\omega_Y}}^V = \bar Z_{AC}^V C_{D_{V_X}}^V$$

$$C_{D_{\delta F}}^W = \text{see reference (11)}$$

$$C_{D_{\delta E}}^H = \text{see reference (11)}$$

$$C_L^W = C_{L_\alpha}^W (\nabla_1 - \alpha_o^W + I^W - \varepsilon_1^W)$$

$$C_L^H = C_{L_\alpha}^H (\nabla_1 - \alpha_o^H + I^H)$$

$$C_L^B = C_{L_\alpha}^B (\nabla_1)$$

W, H, B $\quad C_{L_{V_X}} = \dfrac{M_1 C_L}{V_S (1 - M_1^2)}$

$$C_{L_\alpha}^W = \frac{2\pi A^W}{2 + \left[\frac{A^{W2}\beta^2}{\kappa^{W2}}\left(1 + \frac{\tan^2 \Lambda^W_{c/2}}{\beta^2}\right) + 4\right]^{1/2}} \left(1 - \frac{d\varepsilon^W}{d\alpha}\right)$$

$$C_{L_\alpha}^H = \frac{2\pi A^H}{2 + \left[\frac{A^{H2}\beta^2}{\kappa^{H2}}\left(1 + \frac{\tan^2 \Lambda^H_{c/2}}{\beta^2}\right) + 4\right]^{1/2}}$$

$$C_{L_\alpha}^B = \frac{2(K_2 - K_1) S_o}{S^B}, \quad S_o, (K_2 - K_1) = \text{see reference (11)}$$

$$C_{L_{\dot\alpha}}^W = \frac{C_{L_\alpha}^W \frac{d\varepsilon^W}{d\alpha} + \varepsilon}{\left(1 - \frac{d\varepsilon^W}{d\alpha}\right)}$$

W, H, B $\quad C_{L_{\omega_Y}} = -\dfrac{\bar X_{AC}}{V_{X_1}} C_{L_\alpha} + \bar Z_{AC} C_{L_{V_X}}$

$C_{L_{\delta F}}^{W}$ = see reference (11)

$C_{L_{\delta E}}^{H}$ = see reference (11)

$C_m^W = C_{m_o}^W + C_{m_\alpha}^W (\nabla_1 - \alpha_o^W + I^W - \varepsilon_1^W)$

$C_m^H = C_{m_o}^H + C_{m_\alpha}^H (\nabla_1 - \alpha_o^H + I^H)$

$C_m^B = C_{m_o}^B + C_{m_\alpha}^B (\nabla_1)$

W, H $\quad C_{m_o} = \dfrac{A \cos^2 \Lambda_{c/4}}{A + 2\cos \Lambda_{c/4}} C_{m_o}$

$C_{m_o}^B = 0$

W, H, B $\quad C_{m_{V_X}} = \dfrac{M_1 C_m}{V_S (1 - M_1^2)}$

W, H, B $\quad C_{m_\alpha} = 0$

$\bar{\bar{X}}_{AC}^B = \dfrac{V^B}{S^B} - \ell^B$

$C_{m_{\dot{\alpha}}}^W = C_{m_\alpha}^W \dfrac{d\varepsilon^W}{d\alpha} t^\varepsilon$

W, H, B $\quad C_{m_{\omega_Y}} = - \dfrac{\bar{X}_{AC}}{V_{X_1}} C_{m_\alpha} + \bar{Z}_{AC} C_{m_{V_X}}$

$C_{m_{\delta F}}^W$ = see reference (11)

$C_{m_{\delta E}}^H$ = see reference (11)

V, B $\quad C_Y = 0$

$$C_{Y_\beta}^V = - \frac{2\pi A^V}{2 + \left[\frac{A^{V^2} \beta^2}{\kappa^{V^2}} \left(1 + \frac{\tan^2 \Lambda^V_{c/2}}{\beta^2} \right) + 4 \right]^{1/2}} \left(1 - \frac{d\sigma^V}{d\beta} \right)$$

$C_{Y_\beta}^B = - C_{L_\alpha}^B$

$C_{Y_{\dot{\beta}}}^V = \dfrac{C_{Y_\beta}^B \dfrac{d\sigma^V}{d\beta} t^\sigma}{\left(1 - \dfrac{d\sigma^V}{d\beta} \right)}$

V, B $\quad C_{Y_{\omega_X}} = - \dfrac{\bar{Z}_{AC}}{V_{X_1}} C_{Y_\beta}$

V, B $\quad C_{Y_{\omega_Z}} = \dfrac{\bar{X}_{AC}}{V_{X_1}} C_{Y_\beta}$

$C_{Y_{\delta R}}^V$ = see reference (11)

W, H, B $\quad C_\ell = 0$

W, H, B $C_{l_\beta} = 0$

W, H $C_{l_{\omega_X}} = -\frac{\bar{y}_{AC_R}}{b^W}\frac{\bar{y}_{AC_R}}{V_{X_1}} C_{L_\alpha}$

$C^B_{l_{\omega_X}} = -\frac{\bar{z}^B_{AC}}{V_{X_1}} C^B_{l_\beta}$

W, H $C_{l_{\omega_Z}} = \frac{\bar{y}_{AC_R}}{b^W}\bar{y}_{AC_R} C_{L_{V_X}}$

$C^B_{l_{\omega_Z}} = \frac{\bar{x}^B_{AC}}{V_{X_1}} C^B_{l_\beta}$

$C^W_{l_{\delta A}}$ = see reference (11)

W, H, B, V $C_n = 0$

W, H, B, V $C_{n_\beta} = 0$

$C^V_{n_{\dot\beta}} = C^V_{n_\beta}\frac{d\sigma^V}{d\beta} t^\sigma$

W, H $C_{n_{\omega_X}} = \frac{\bar{y}_{AC_R}}{b^W}\frac{\bar{y}_{AC_R}}{V_{X_1}} C_{D_\alpha}$

$C^V_{n_{\omega_X}} = -\frac{\bar{z}^V_{AC}}{V_{X_1}} C^V_{n_\beta}$

$C^B_{n_{\omega_X}} = -\frac{\bar{z}^B_{AC}}{V_{X_1}} C^B_{n_\beta}$

W, H $C_{n_{\omega_Z}} = -\frac{\bar{y}_{AC_B}}{b^W}\bar{y}_{AC_R} C_{D_{V_X}}$

$C^V_{n_{\omega_Z}} = \frac{\bar{x}^V_{AC}}{V_{X_1}} C^V_{n_\beta}$

$C^B_{n_{\omega_Z}} = \frac{\bar{x}^B_{AC}}{V_{X_1}} C^B_{n_\beta}$

$C^W_{n_{\delta A}}$ = see reference (11)

$C^V_{n_{\delta R}}$ = see reference (11)

Element Aerodynamic Supersonic Derivatives:

W,H,B,V C_{D_o} = see reference (11)

W,H C_{D_α} = see reference (11)

$C_{D_{\delta F}}^{W}$ = see reference (11)

$C_{D_{\delta E}}^{H}$ = see reference (11)

W,H,B C_{L_α} = see reference (11)

$C_{L_{\delta F}}^{W}$ = see reference (11)

$C_{L_{\delta E}}^{H}$ = see reference (11)

W,H,B C_{m_o} = see reference (11)

$\bar{x}_{AC}^{B}$ = see reference (11)

$C_{m_{\delta F}}^{W}$ = see reference (11)

$C_{m_{\delta E}}^{H}$ = see reference (11)

$C_{y_\beta}^{V}$ = see reference (11)

$C_{y_{\delta R}}^{V}$ = see reference (11)

$C_{\ell_{\delta A}}^{W}$ = see reference (11)

$C_{n_{\delta A}}^{W}$ = see reference (11)

$C_{n_{\delta R}}^{V}$ = see reference (11)

Element Thrust Derivatives:

$$C_{T_{\bar{x}v_x}}^{I} = -\frac{\rho A^I V_{x_1}}{q_1 S^w}$$

$$C_{T_{\bar{x}\alpha}}^{I} = 0$$

$$C_{T_{\bar{x}\dot{\alpha}}}^{I} = 0$$

$$C_{T_{\bar{x}\omega_y}}^{I} = -\frac{\rho A^I V_{x_1} \bar{z}^I}{q_1 S^w}$$

$$C_{T_{\bar{x}\delta T}}^{E} = \frac{T_{max}^{E}}{q_1 S^w}$$

$$C_{T_{\bar{z}v_x}}^{I} = 0$$

$$C_{T_{\bar{z}\alpha}}^{I} = -\frac{\rho A^I V_{x_1}^2}{q_1 S^w}$$

$$C_{T_{\bar{z}\dot{\alpha}}}^{I} = 0$$

$$C_{T_{\bar{z}\omega_y}}^{I} = \frac{\rho A^I V_{x_1} \bar{x}^I}{q_1 S^w}$$

$$C_{T_{\bar{z}\delta T}}^{E} = 0$$

$$K_{T_{\bar{y}v_x}}^{I} = -\frac{\rho A^I V_{x_1} \bar{z}^I}{q_1 S^w \bar{c}^w}$$

$$K_{T_{\bar{y}\alpha}}^{I} = \frac{\rho A^I V_{x_1}^2 \bar{x}_I}{q_1 S^w \bar{c}^w}$$

$$K_{T_{\bar{y}\dot{\alpha}}}^{I} = 0$$

$$K_{T_{\bar{y}\omega_y}}^{I} = -\frac{\rho A^I V_{x_1} (\bar{x}^{I^2} + \bar{z}^{I^2})}{q_1 S^w \bar{c}^w}$$

$$K_{T_{\bar{y}\delta T}}^{E} = \frac{\bar{z}^E T_{max}^{E}}{q_1 S^w \bar{c}^w}$$

$$C_{T_{\bar{y}\beta}}^{I} = -\frac{\rho A^I V_{x_1}^2}{q_1 S^w}$$

$$C_{T_{\bar{y}\dot{\beta}}}^{I} = 0$$

$$C^{I}_{T\bar{Y}\omega_X} = \frac{\rho A^I V_{X_1} \bar{Z}^I}{q_1 S^w}$$

$$C^{I}_{T\bar{Y}\omega_Z} = -\frac{\rho A^I V_{X_1} \bar{X}^I}{q_1 S^w}$$

$$K^{I}_{T\bar{X}\beta} = \frac{\rho A^I V_{X_1}^2 \bar{Z}^I}{q_1 S^w b^w}$$

$$K^{I}_{T\bar{X}\dot{\beta}} = 0$$

$$K^{I}_{T\bar{X}\omega_X} = -\frac{\rho A^I V_{X_1} \bar{Z}^{I^2}}{q_1 S^w b^w}$$

$$K^{I}_{T\bar{X}\omega_Z} = \frac{\rho A^I V_{X_1} \bar{X}^I \bar{Z}^I}{q_1 S^w b^w}$$

$$K^{I}_{T\bar{Z}\beta} = -\frac{\rho A^I V_{X_1}^2 \bar{X}^I}{q_1 S^w b^w}$$

$$K^{I}_{T\bar{Z}\dot{\beta}} = 0$$

$$K^{I}_{T\bar{Z}\omega_X} = \frac{\rho A^I V_{X_1} \bar{X}^I \bar{Z}^I}{q_1 S^w b^w}$$

$$K^{I}_{T\bar{Z}\omega_Z} = -\frac{\rho A^I V_{X_1} \bar{X}^{I^2}}{q_1 S^w b^w}$$

APPENDIX D

GRAPHICAL RESULTS

The aerodynamic center and center of gravity location, root locus, mode shape and time response graphs for the various flight conditions mentioned in Chapter V are contained in this appendix. Each figure describes which variables are being graphed and the corresponding flight condition.

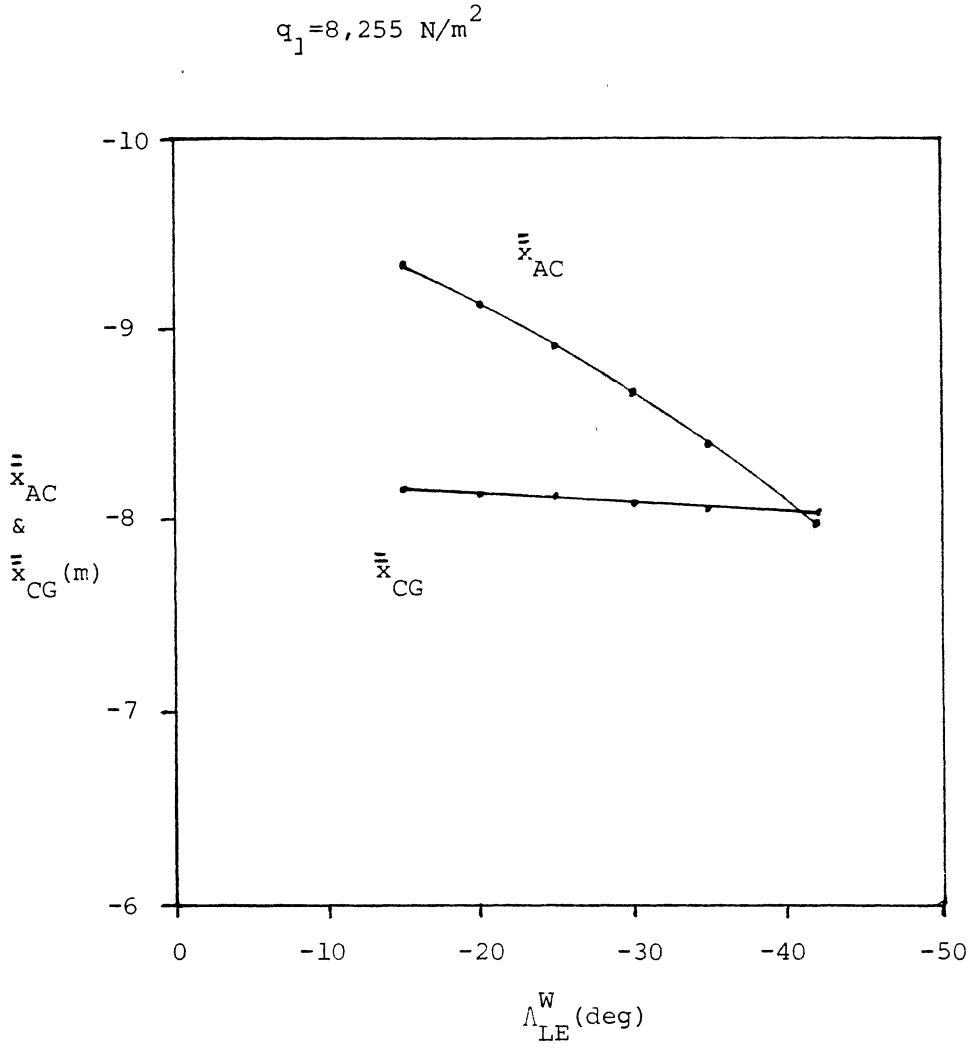

Aerodynamic center and center of gravity location vs. sweep angle

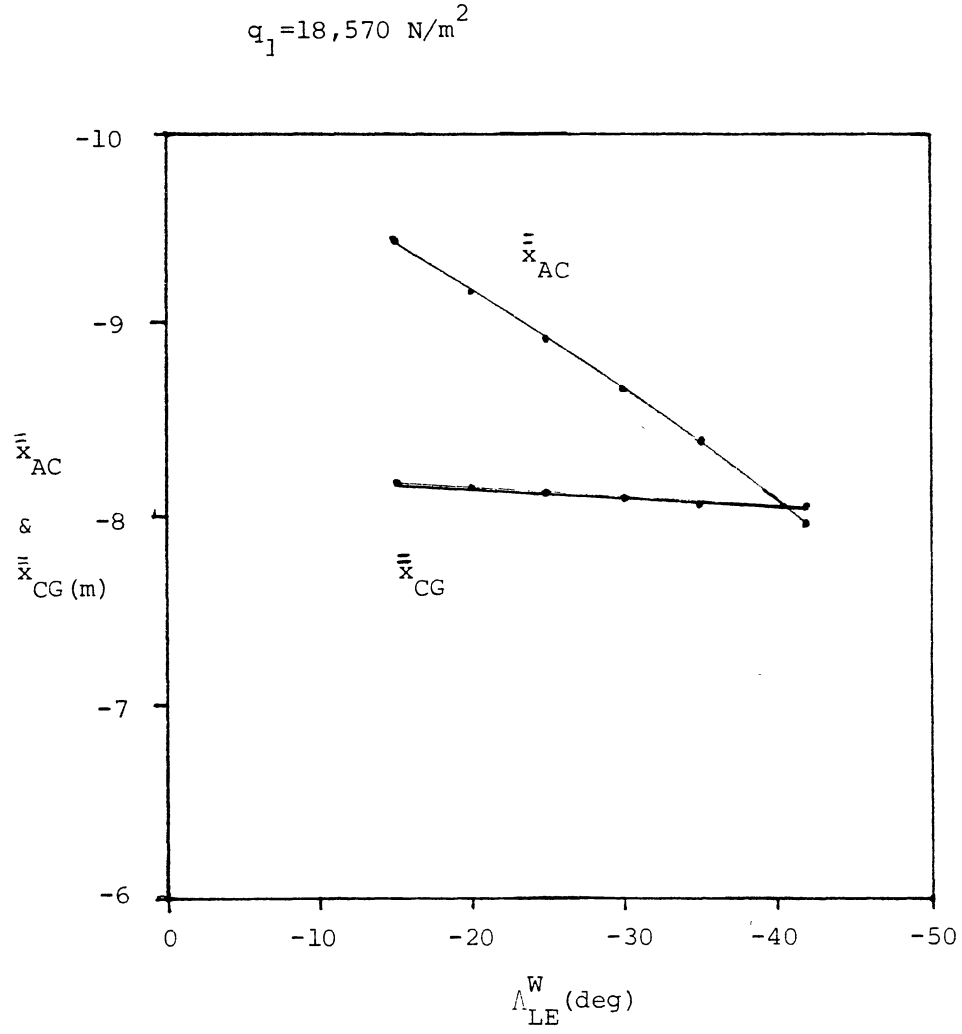

Aerodynamic center and center of gravity
location vs. sweep angle

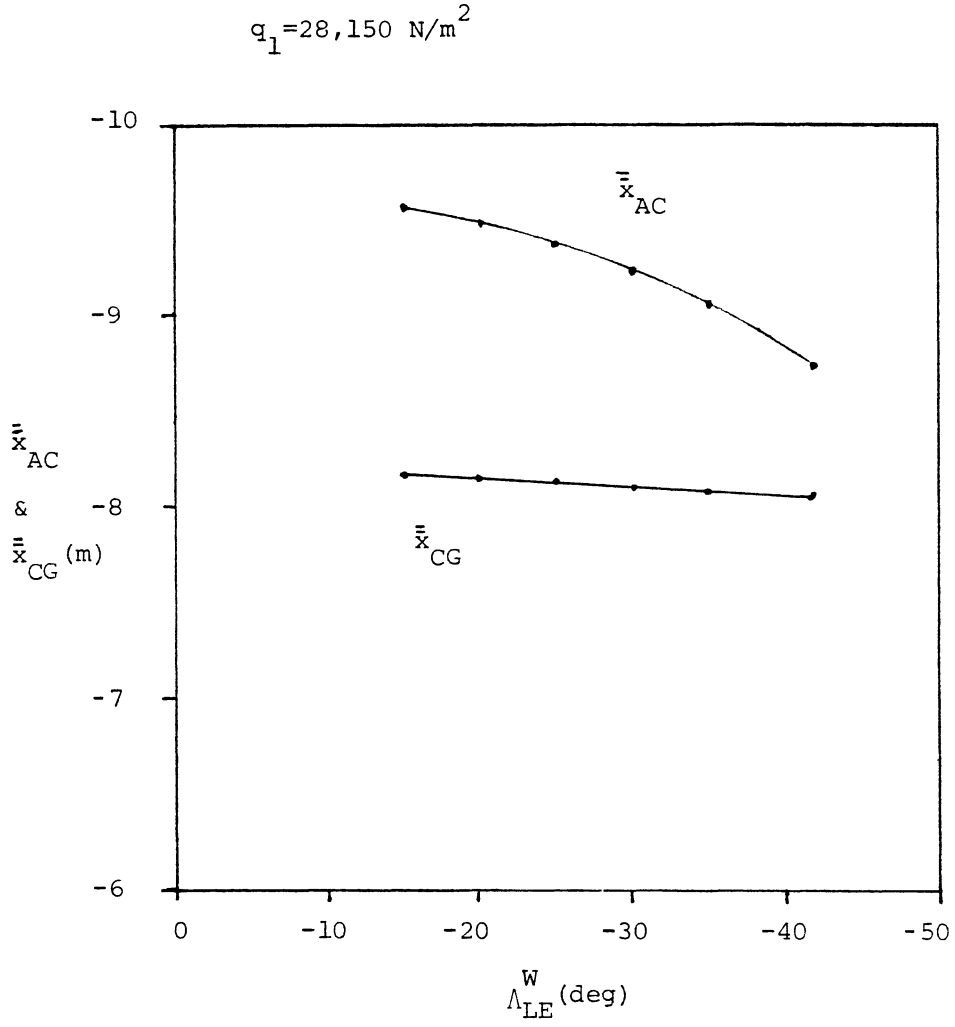

Aerodynamic center and center of gravity
location vs. sweep angle

q_1=8,255 N/m^2

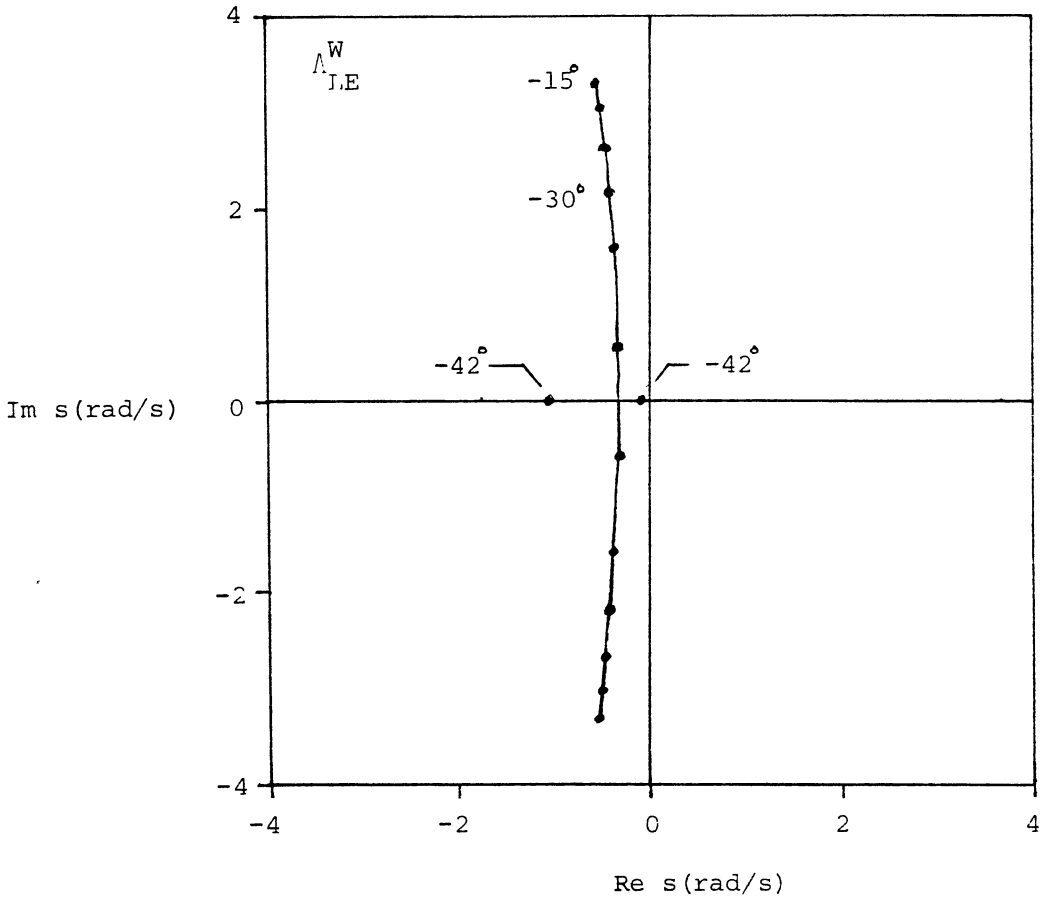

Short period root locus
with varying sweep

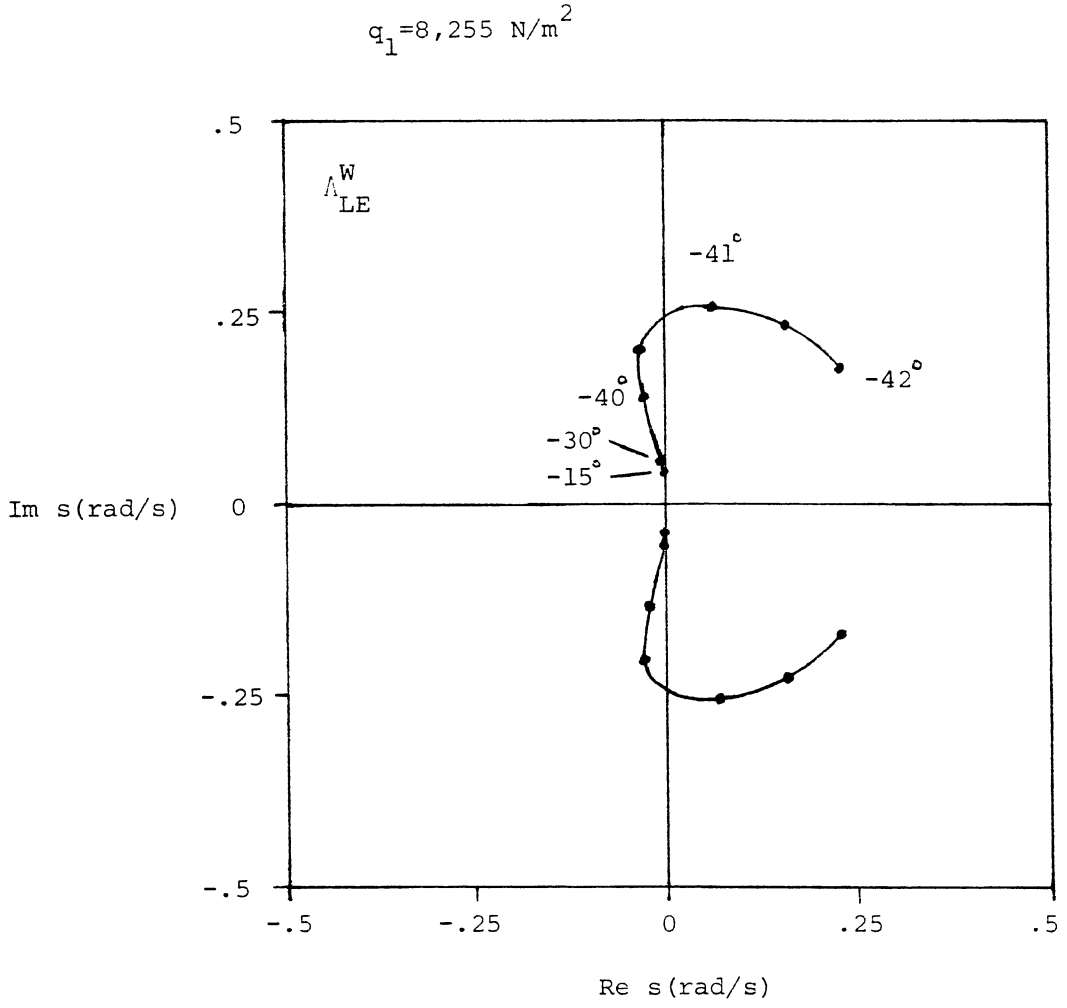

Phugoid root locus
with varying sweep

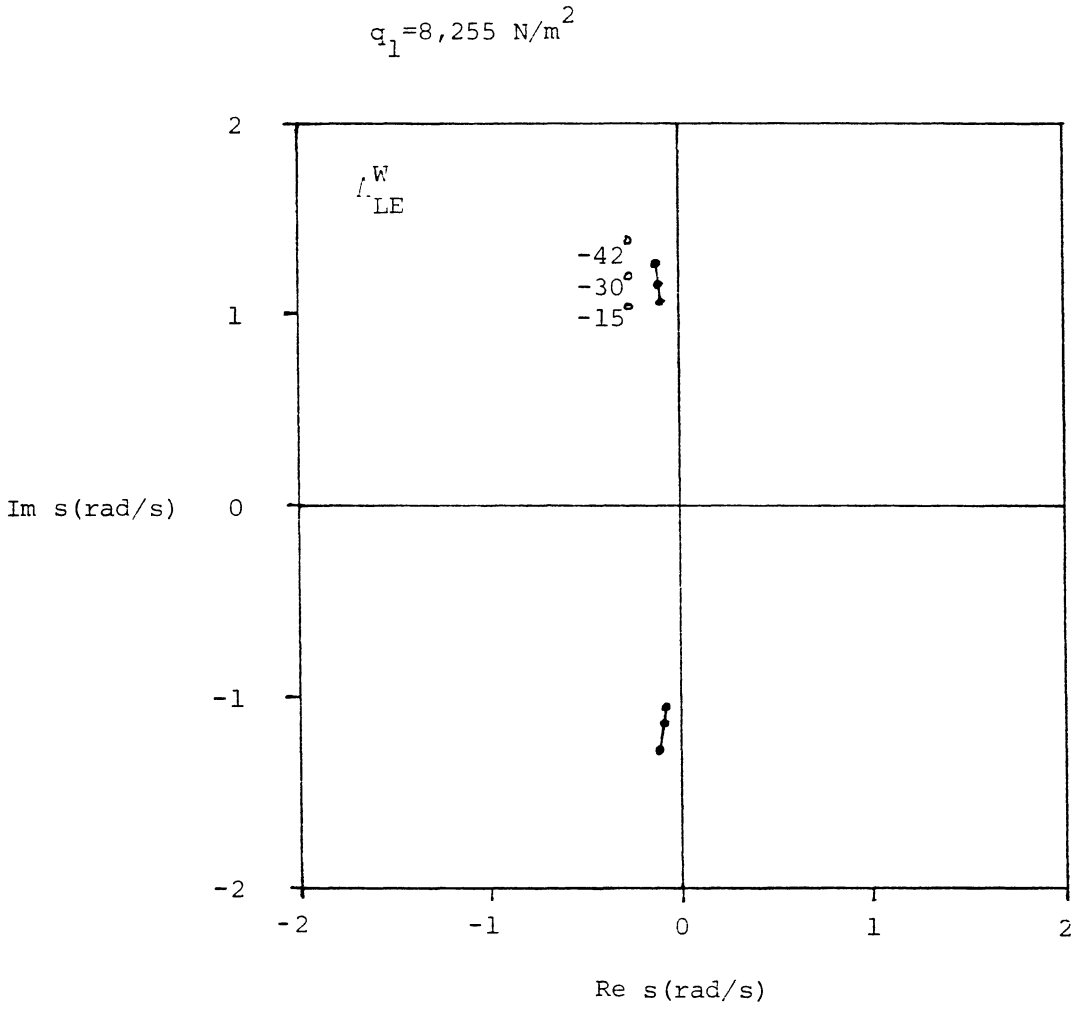

Dutch-roll root locus
with varying sweep

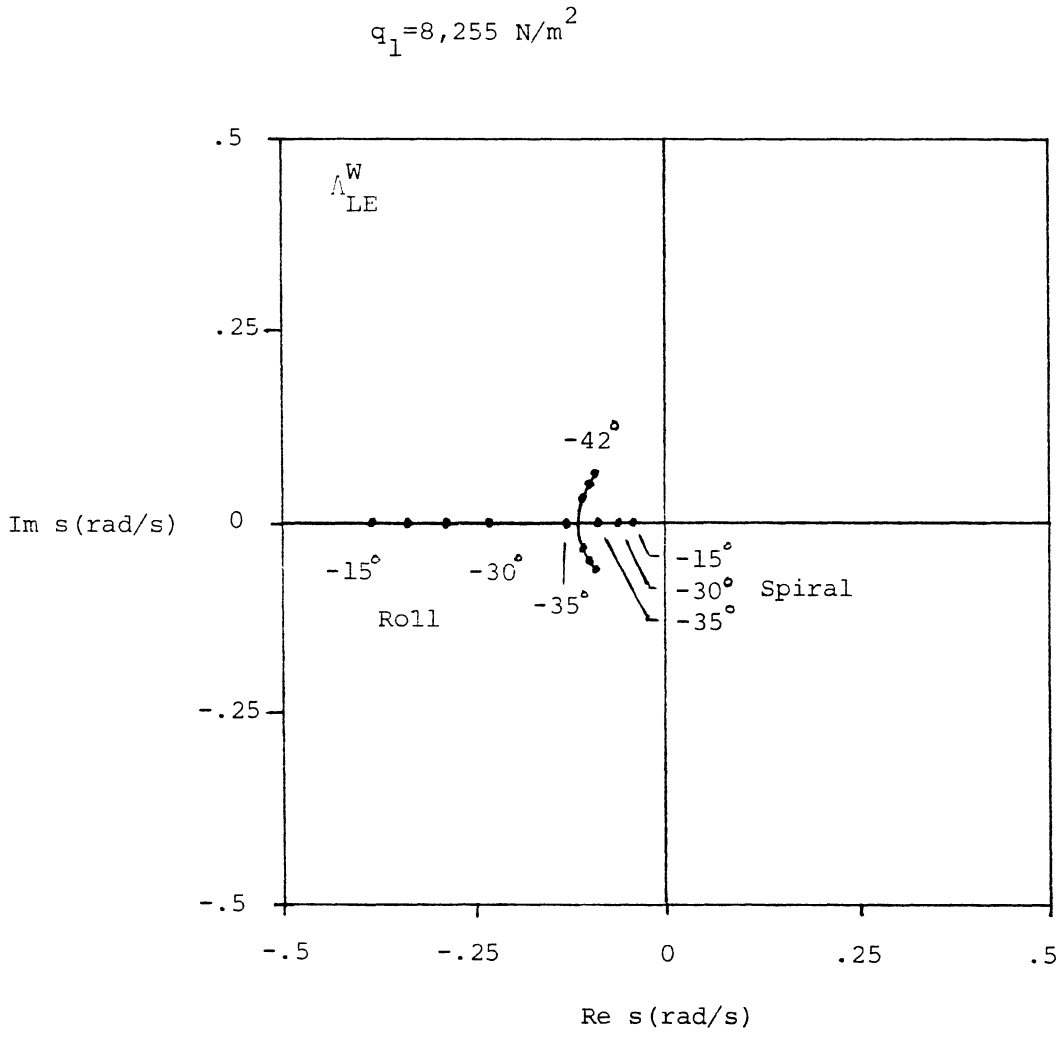

Roll and spiral root locus
with varying sweep

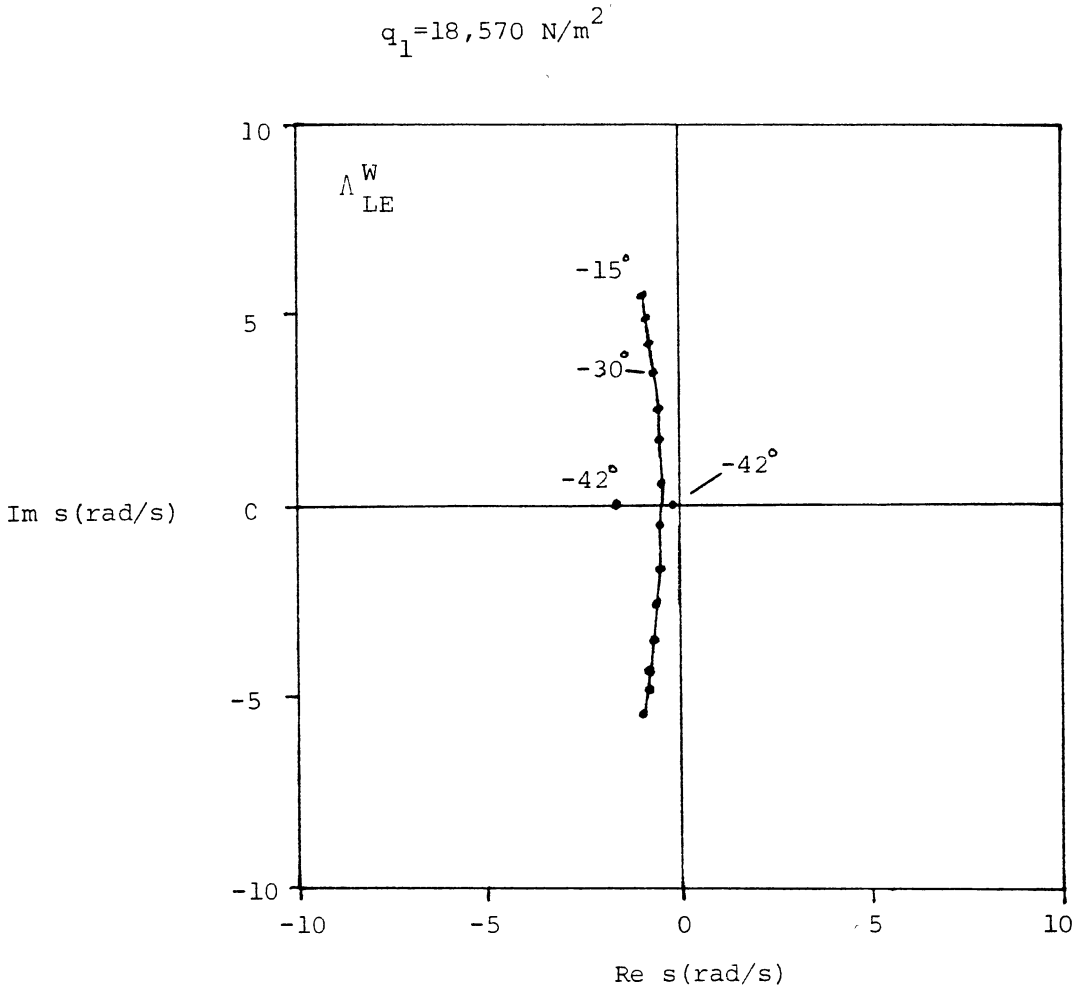

Short period root locus
with varying sweep

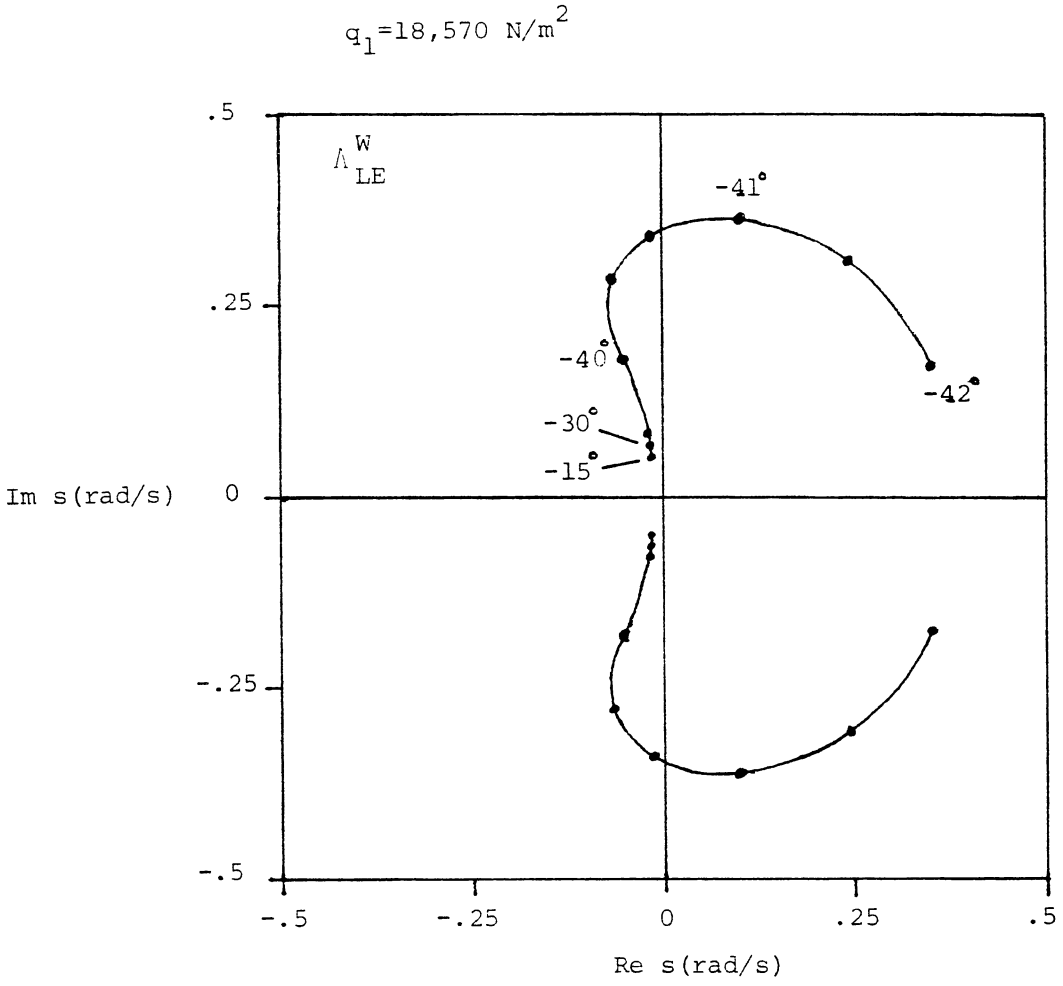

Phugoid root locus
with varying sweep

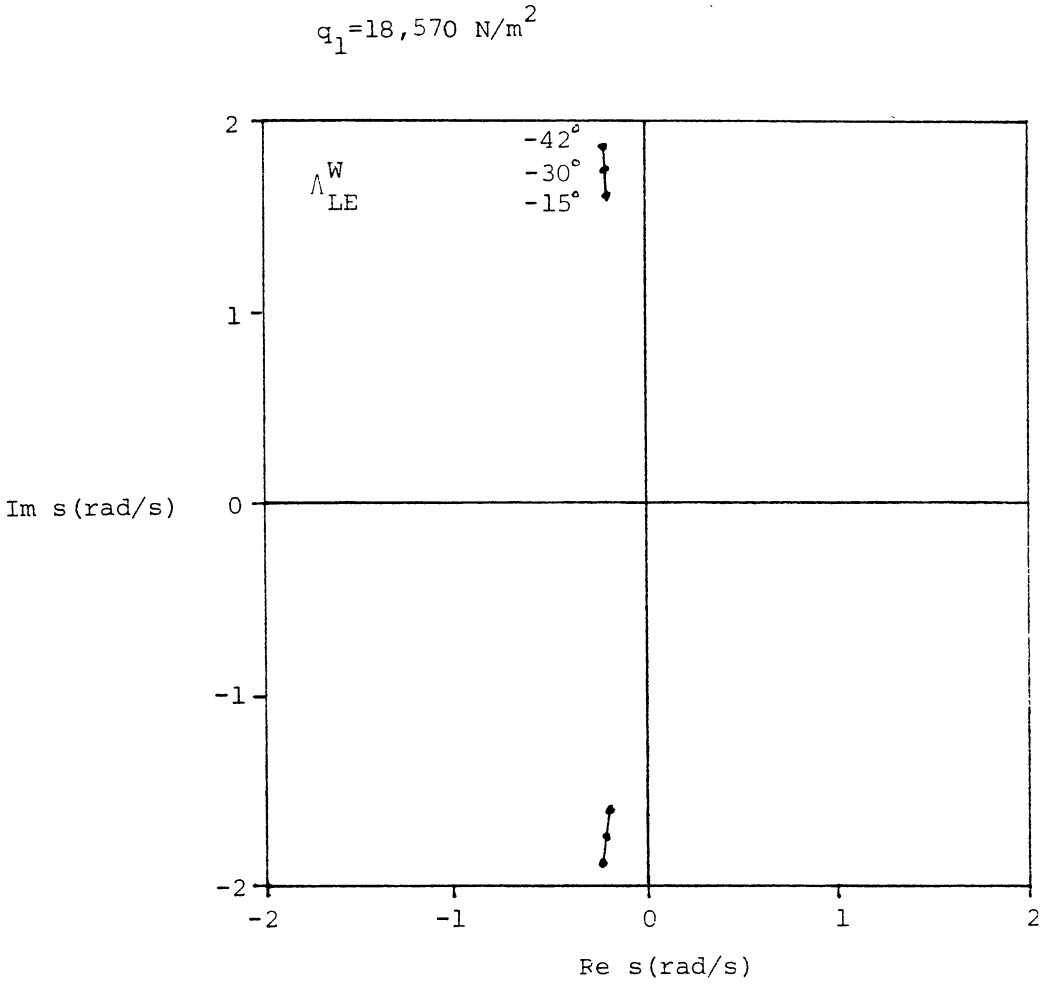

Dutch-roll root locus
with varying sweep

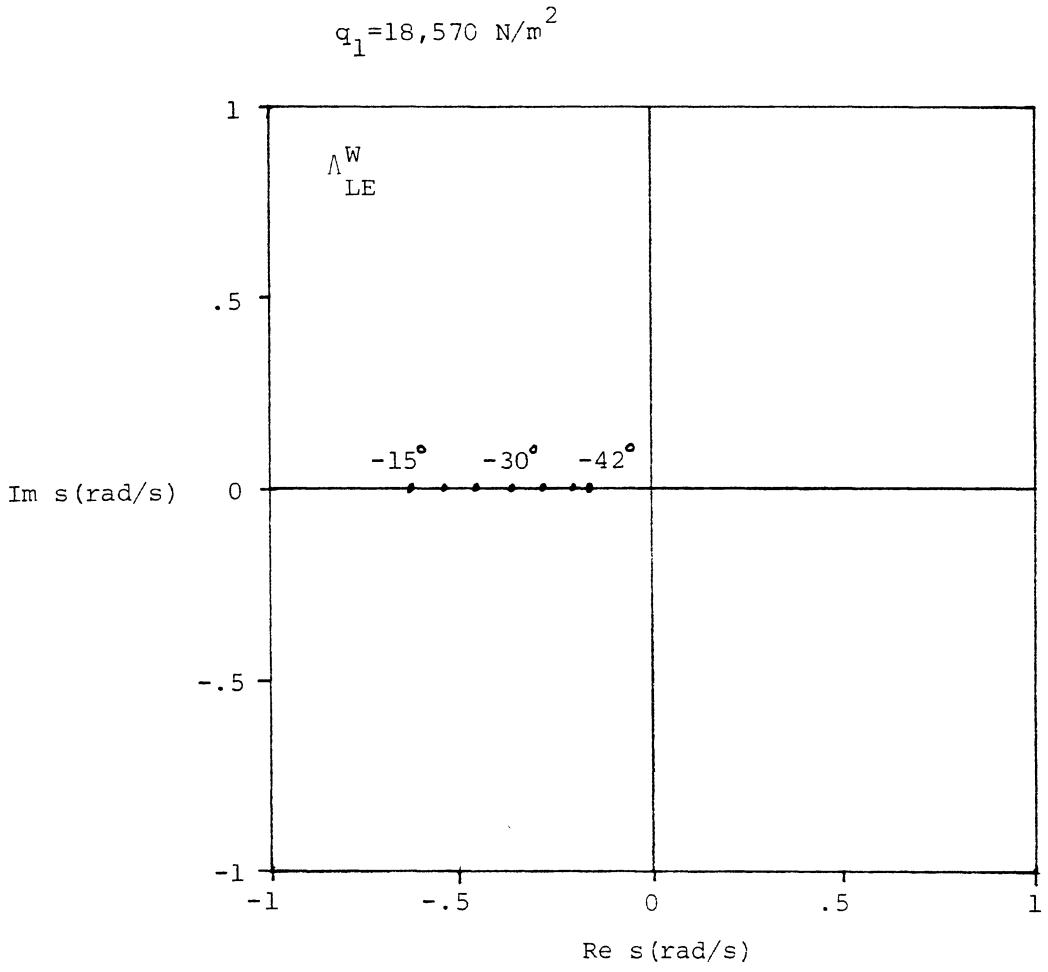

Roll root locus
with varying sweep

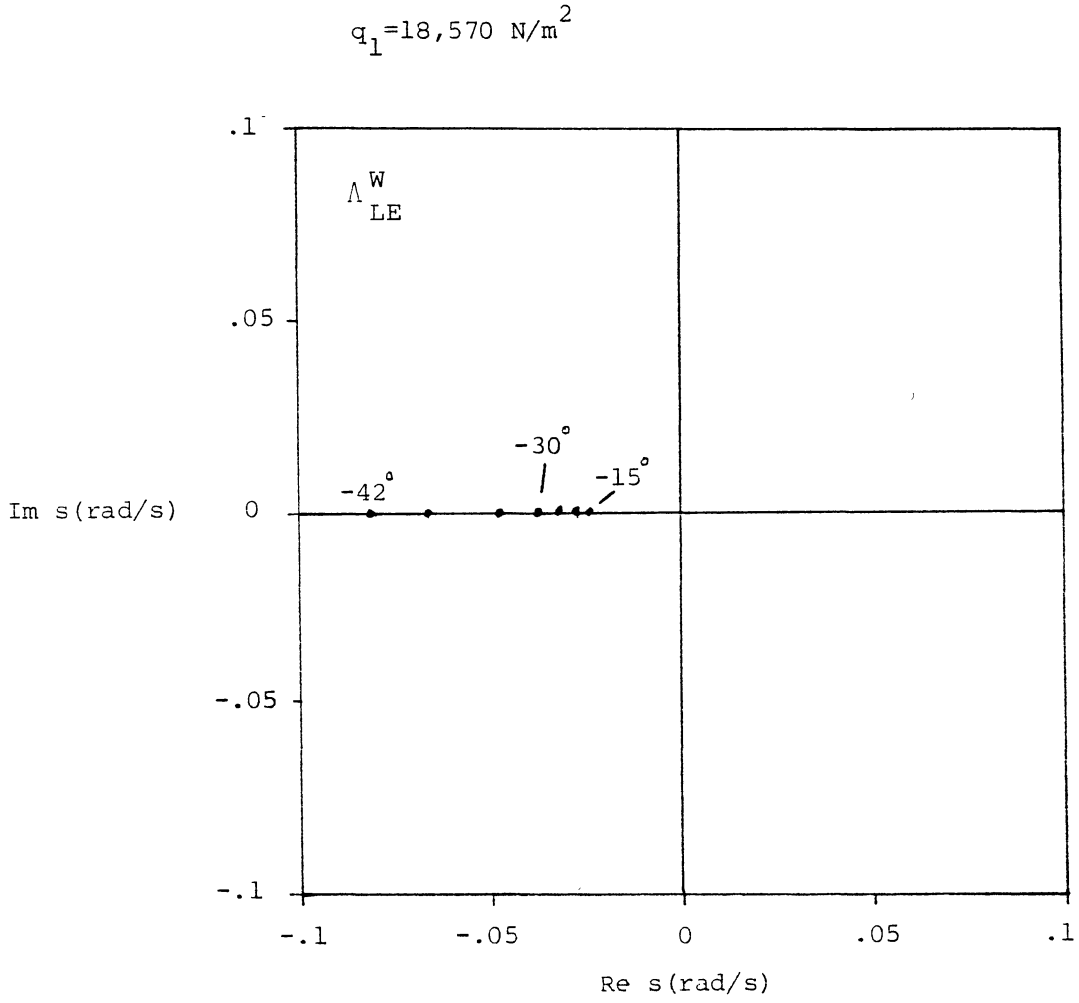

Spiral root locus
with varying sweep

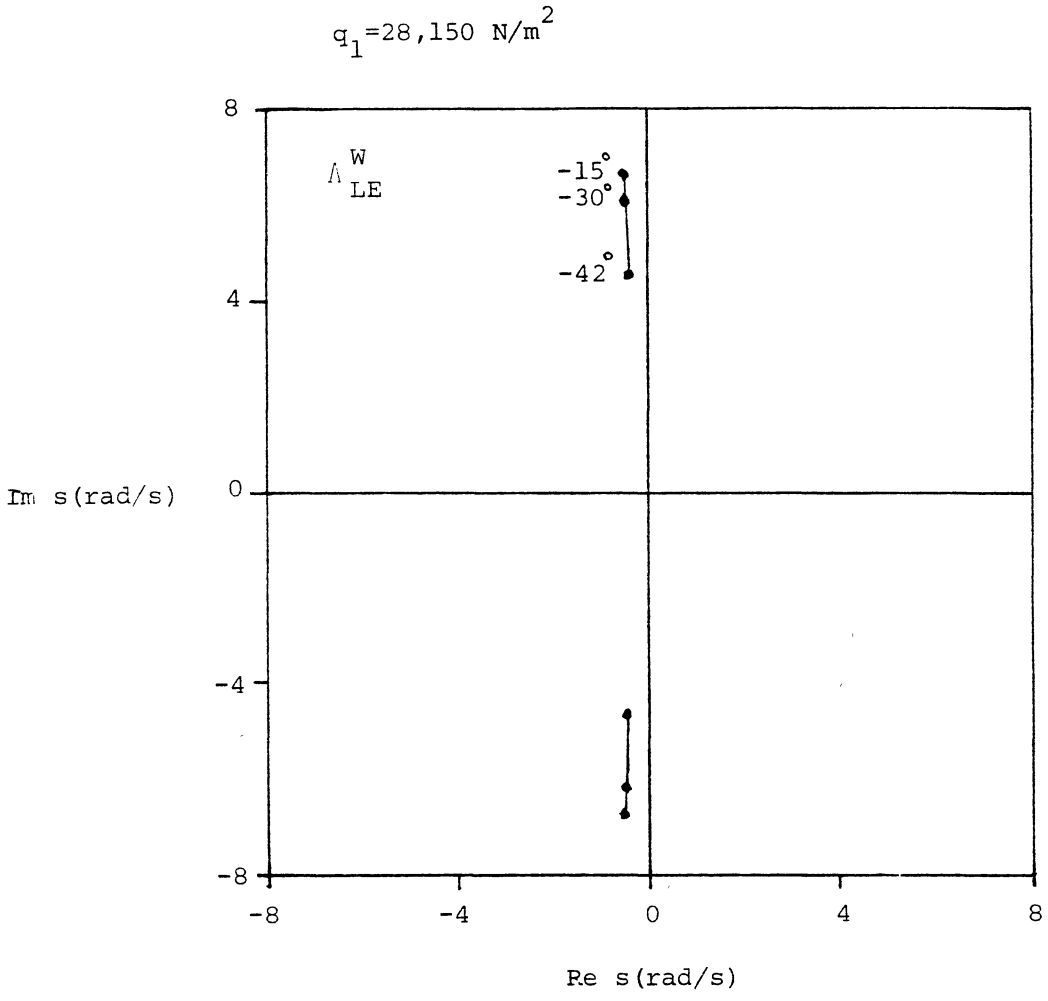

Short period root locus
with varying sweep

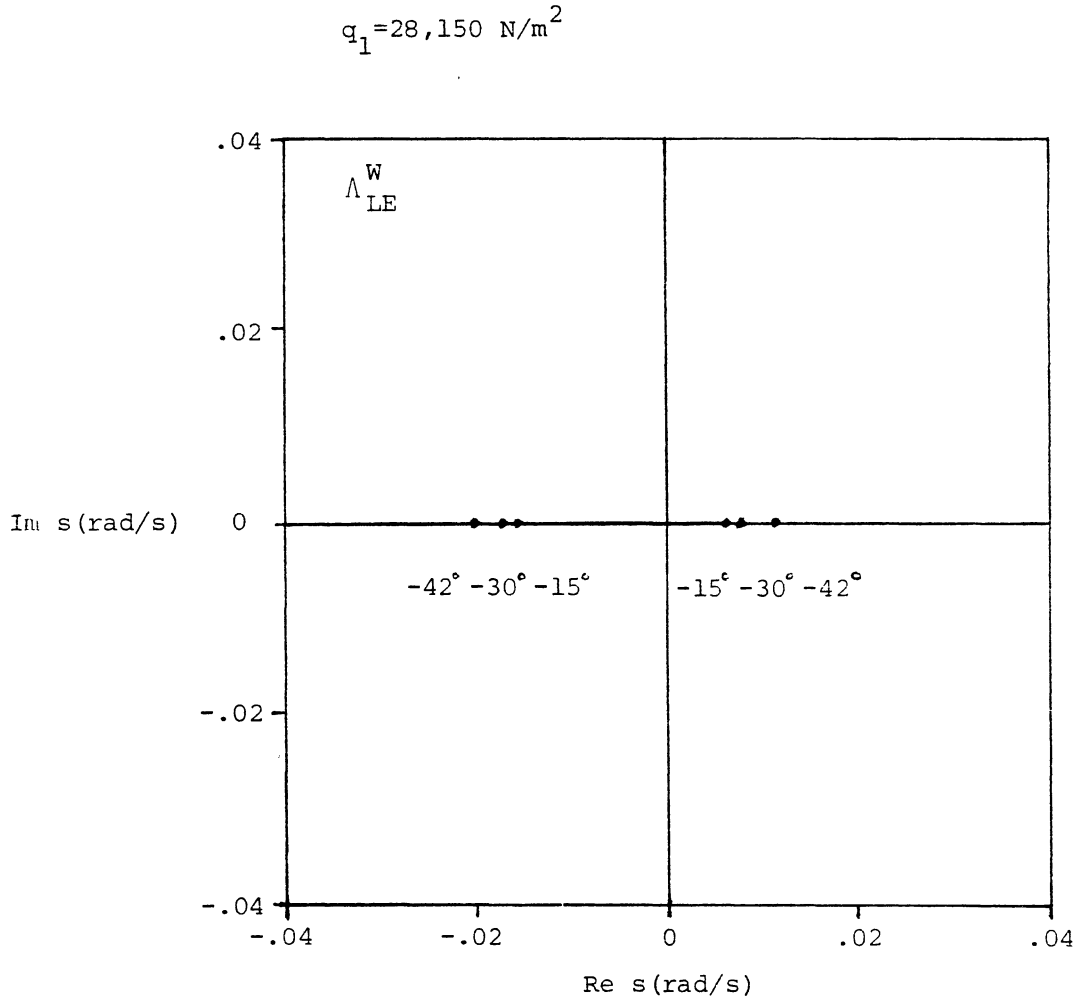

Phugoid root locus
with varying sweep

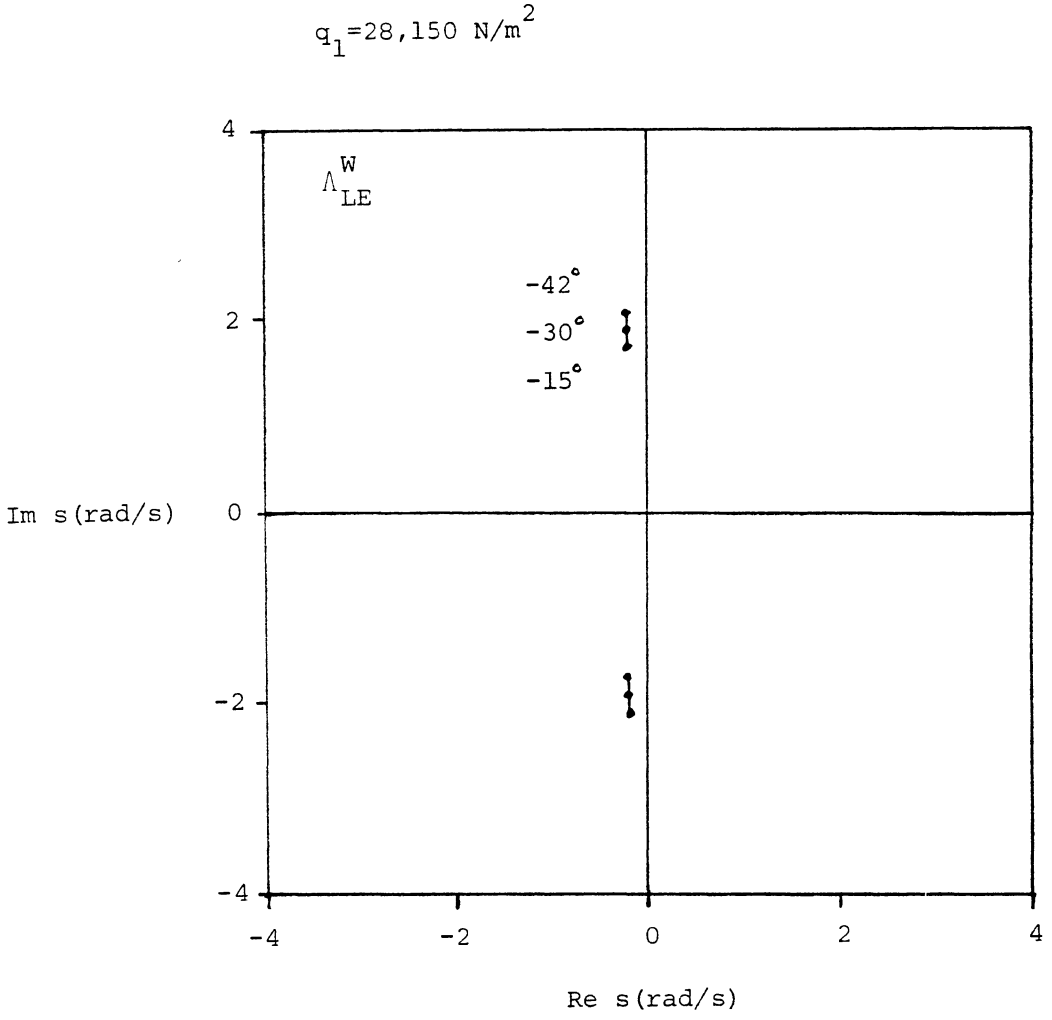

Dutch-roll root locus
with varying sweep

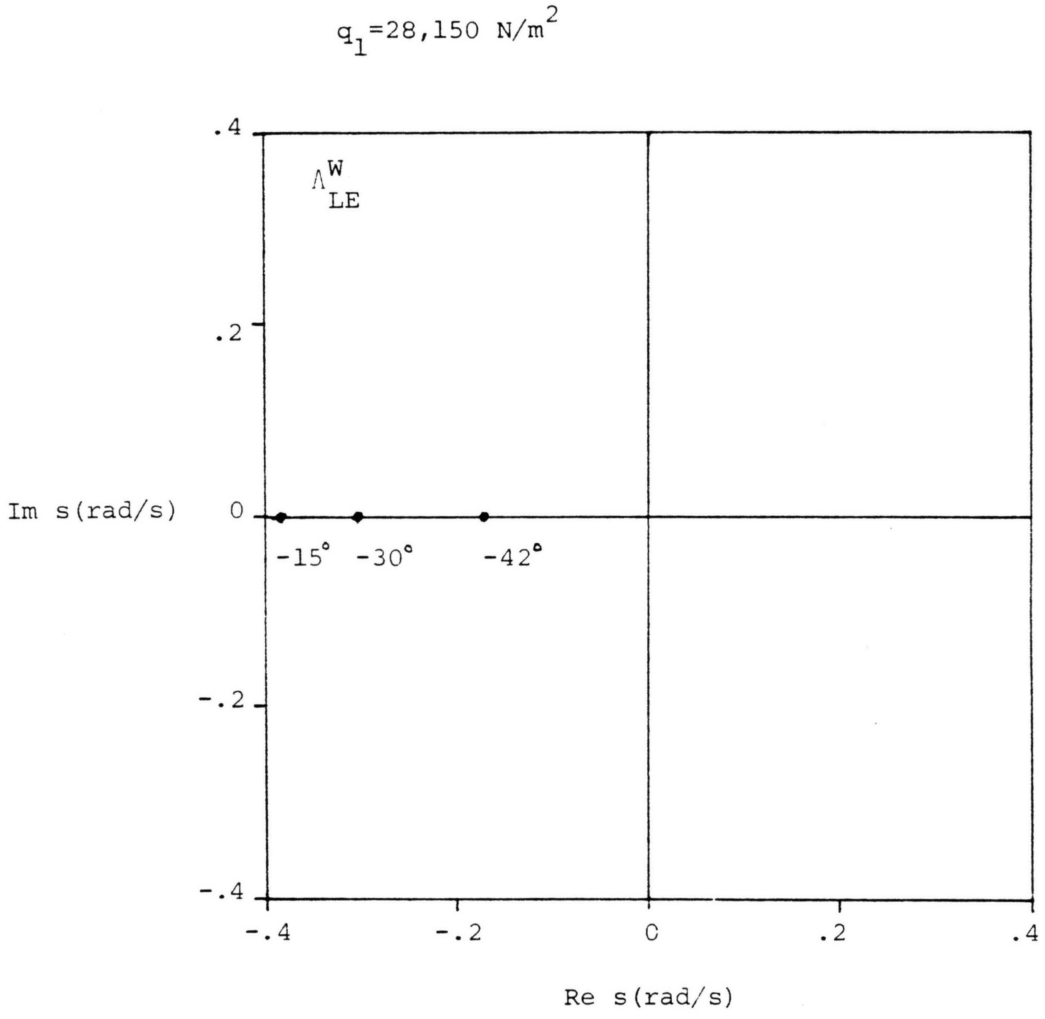

Roll root locus
with varying sweep

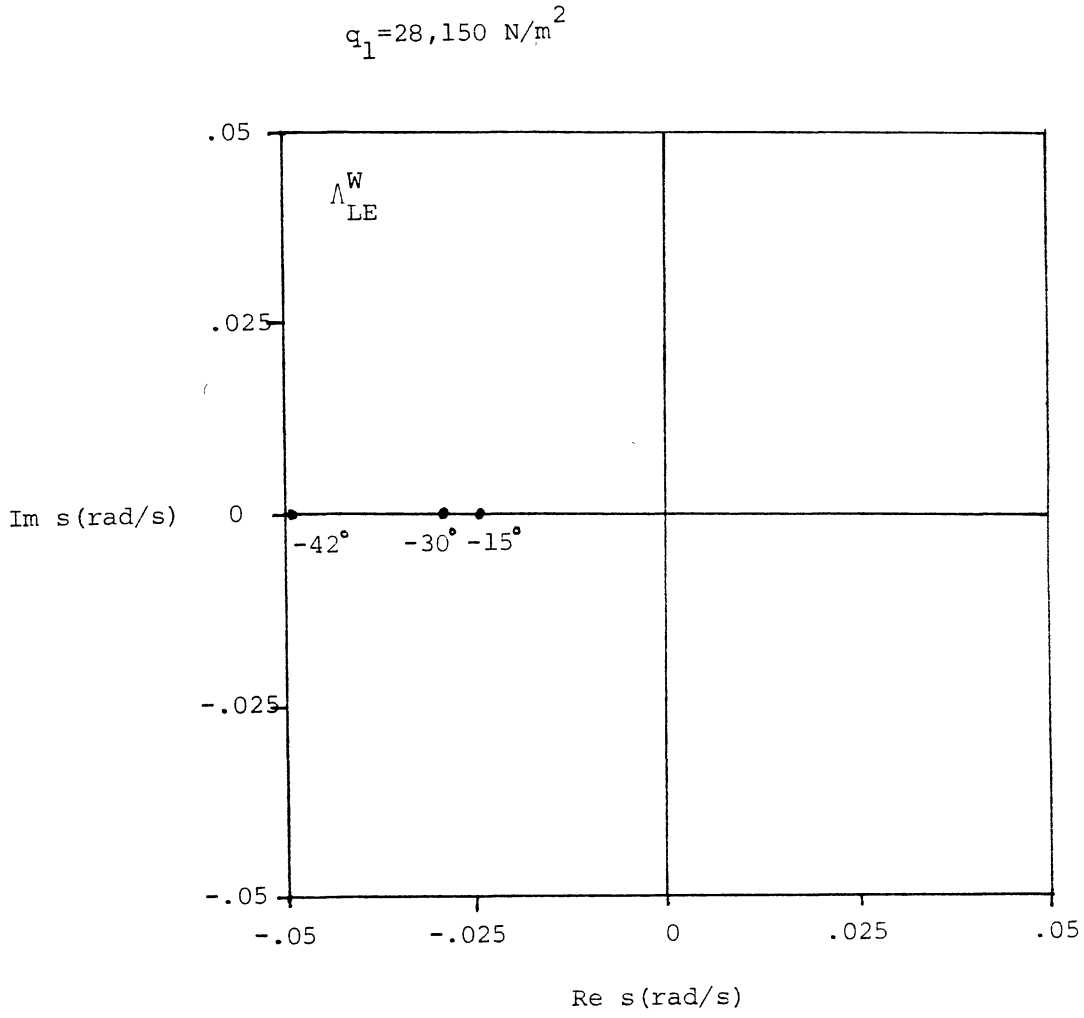

Spiral root locus
with varying sweep

q_1=8,255 N/m^2

θ=1$\angle$0°

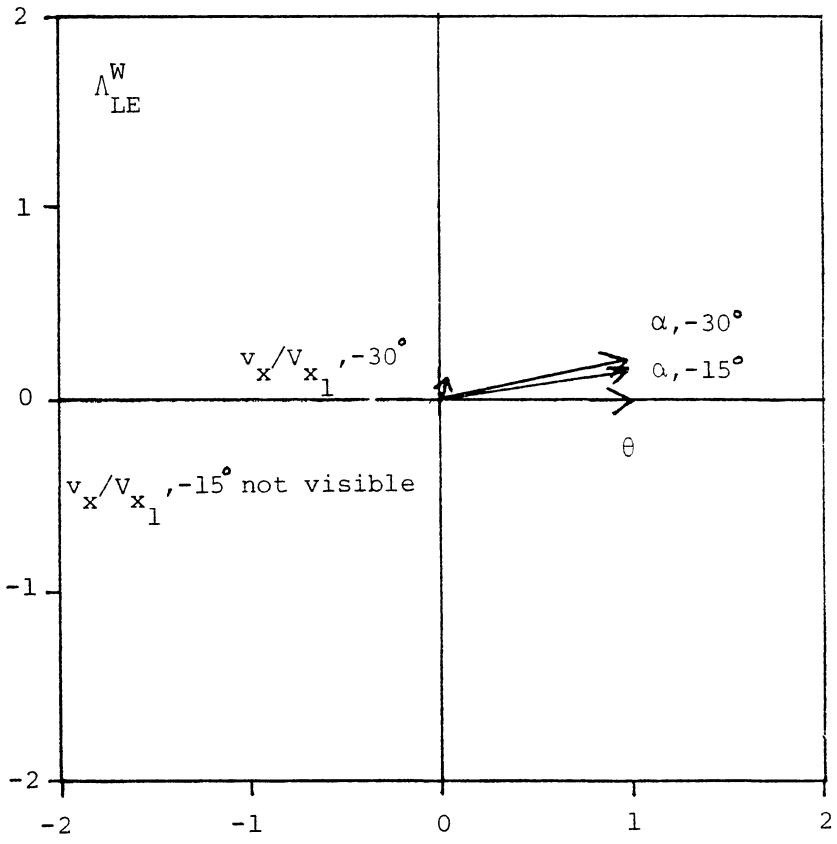

Short period mode shape
with varying sweep

q_1=8,255 N/m^2

θ=1$\angle$ 0°

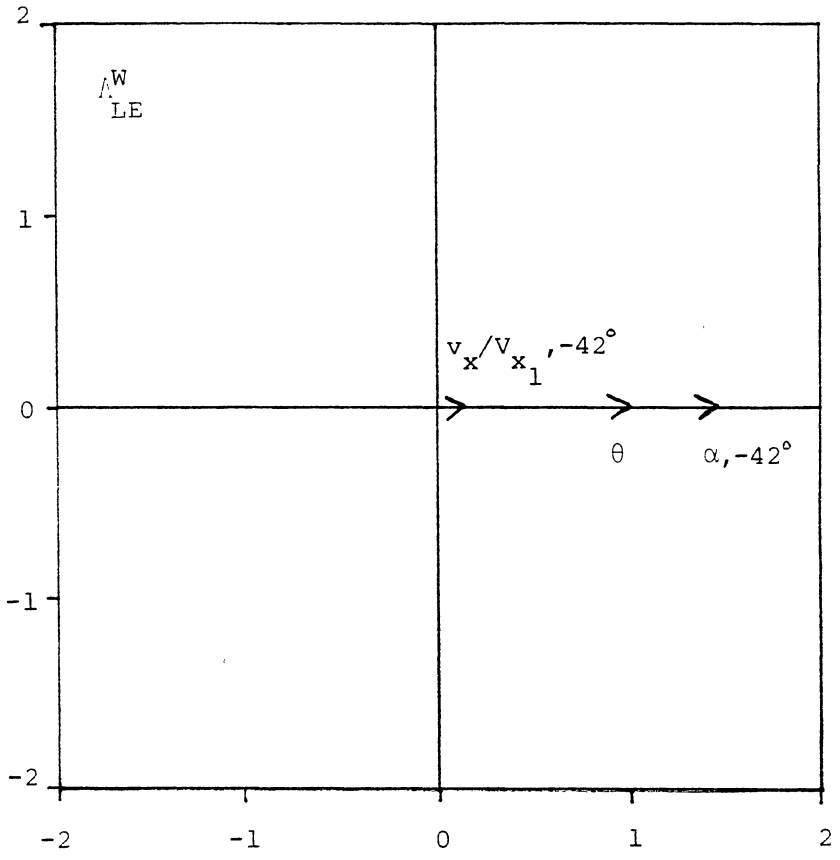

Short period(1) mode shape
with varying sweep

q_1=8,255 N/m^2

θ=1 $\angle$ 0°

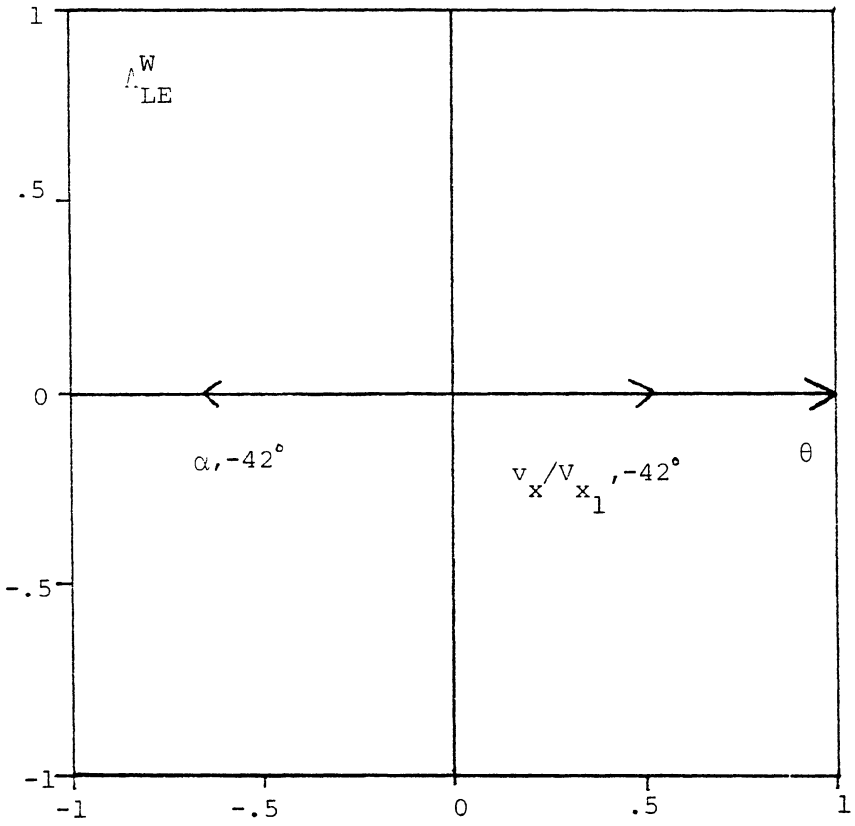

Short period(2) mode shape
with varying sweep

q_1=8,255 N/m^2

θ=1$\angle$0°

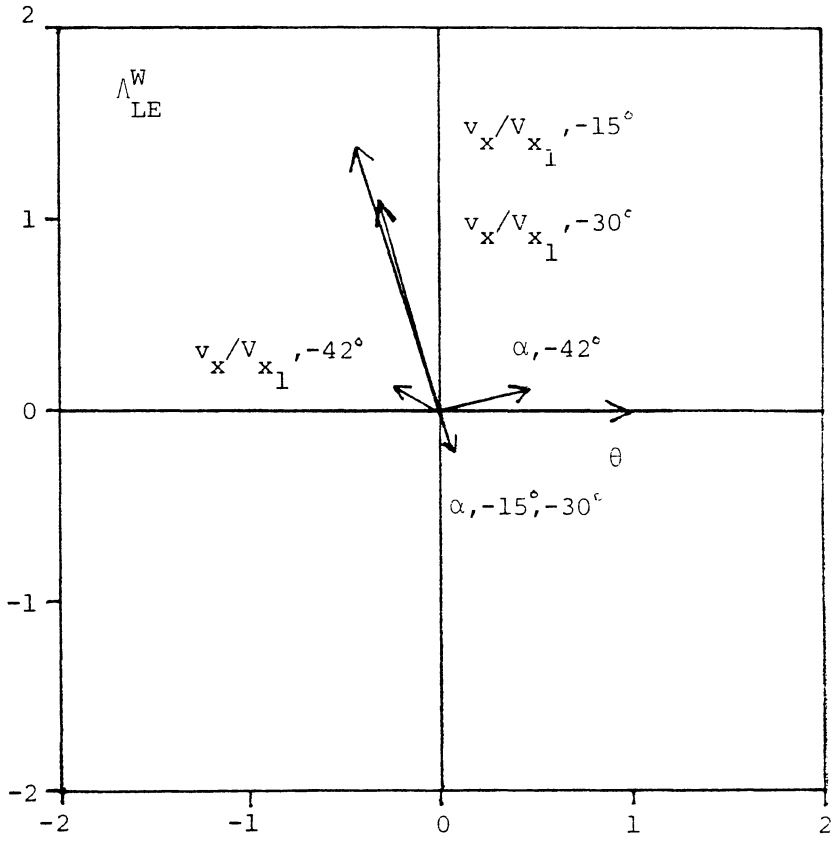

Phugoid mode shape
with varying sweep

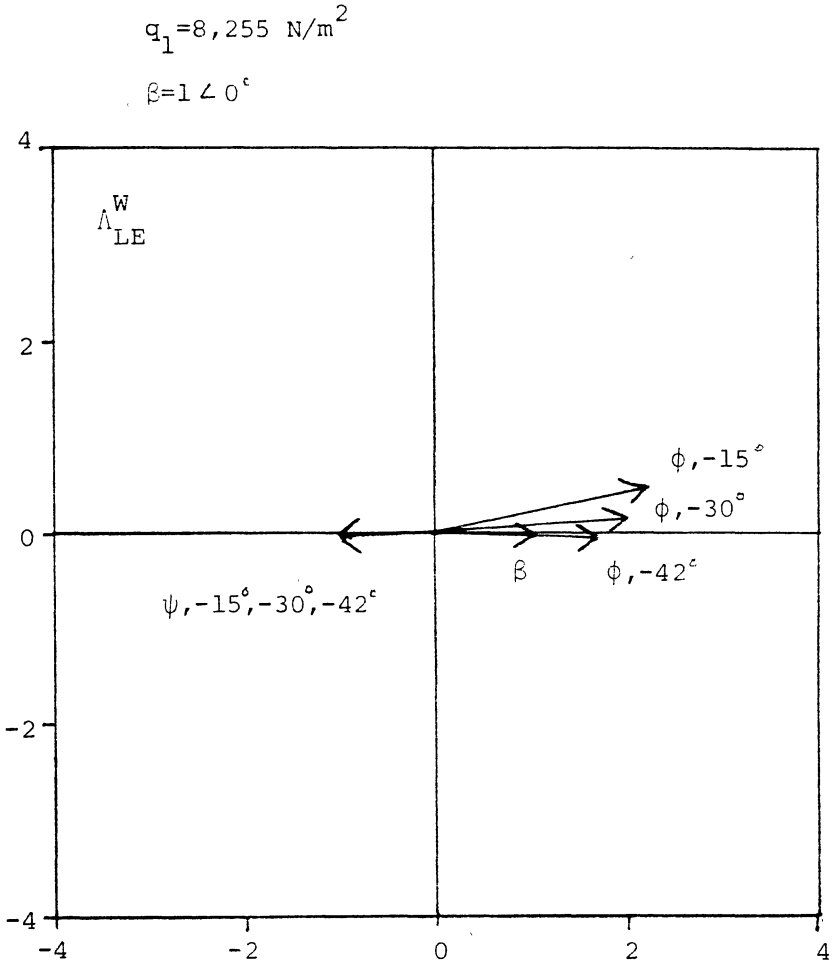

Dutch-roll mode shape
with varying sweep

q_1=8,255 N/m^2

β=1 $\angle$ 0^c

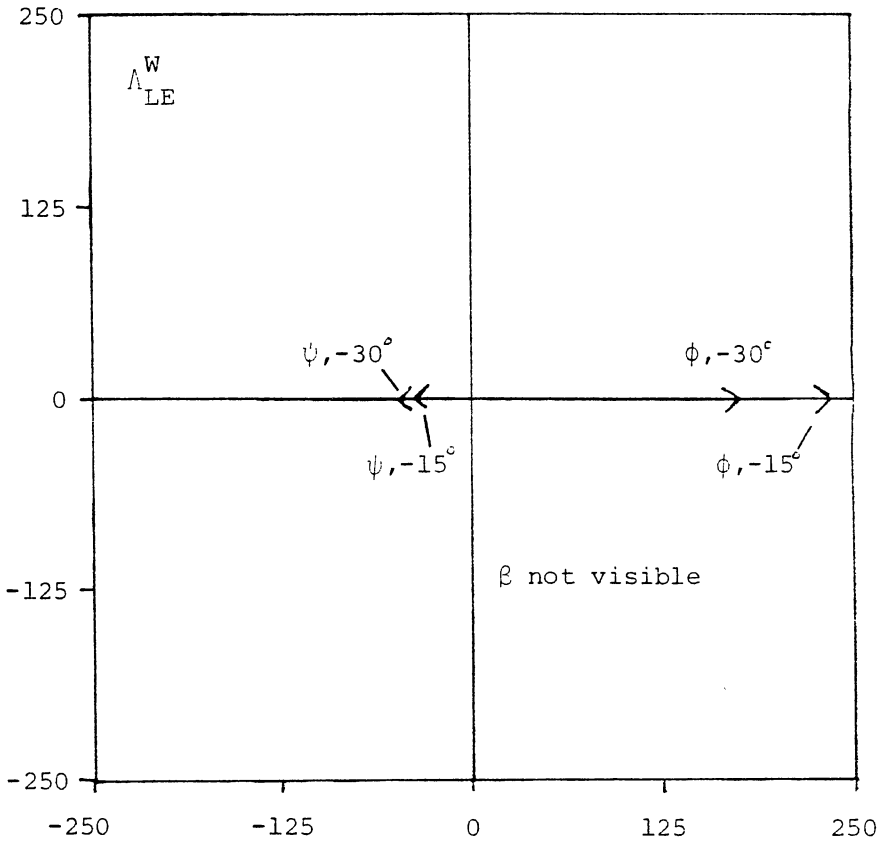

Roll mode shape
with varying sweep

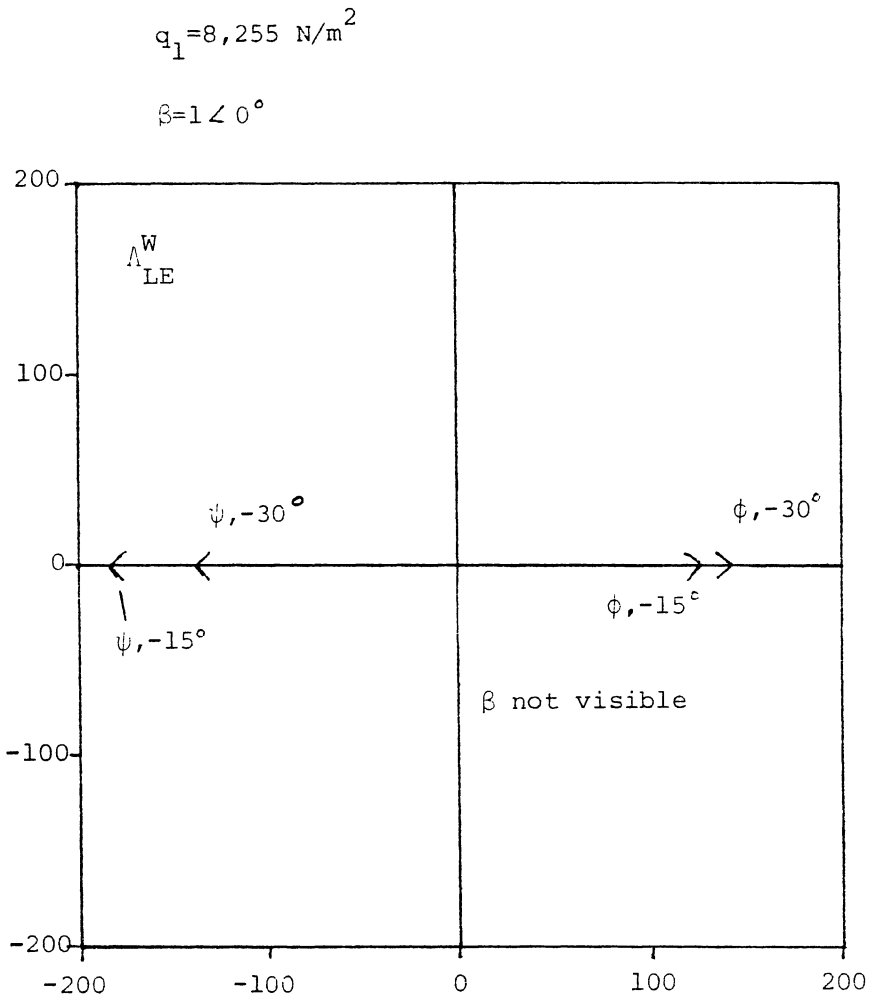

Spiral mode shape
with varying sweep

q_1=8,255 N/m^2

β=1 $\angle$ 0°

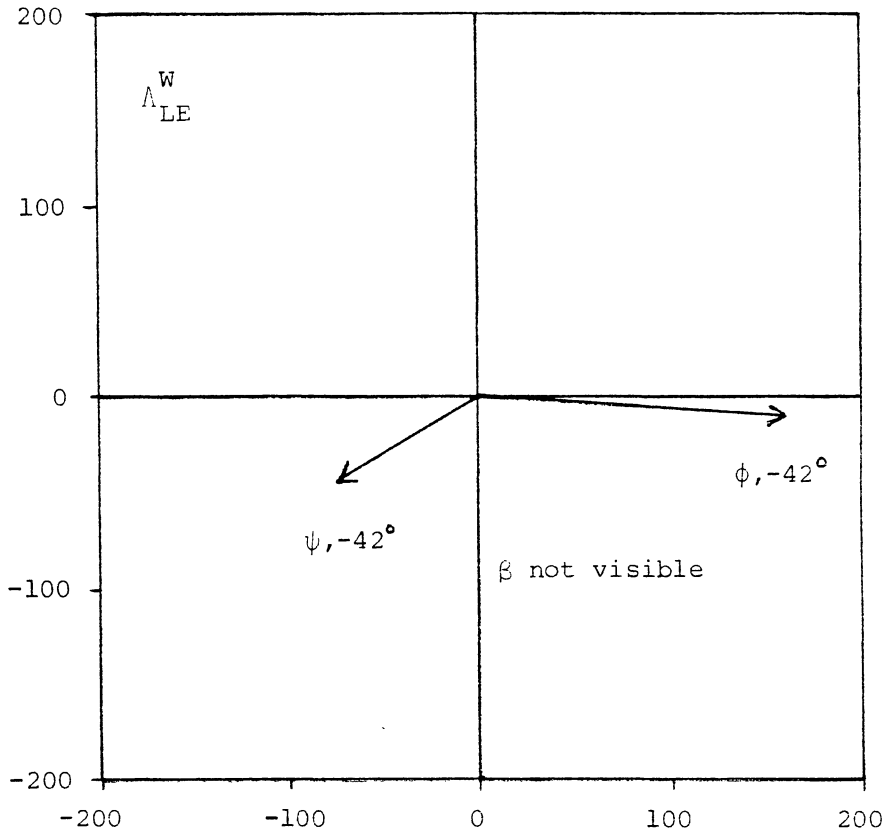

Roll and spiral mode shape
with varying sweep

q_1=18,570 N/m^2

θ=1 $\angle$ 0°

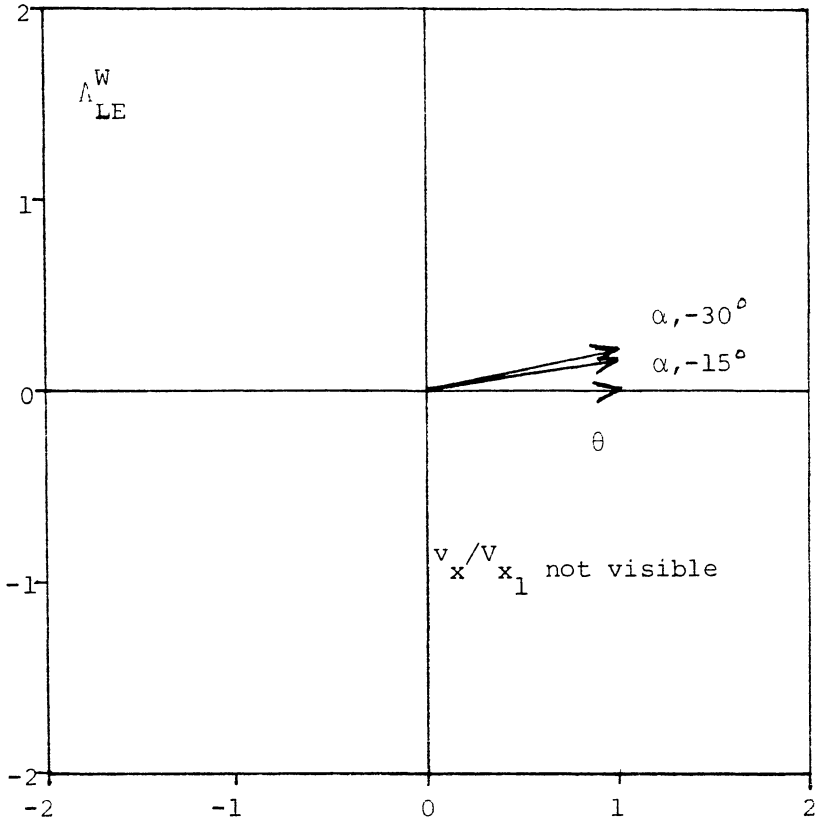

Short period mode shape
with varying sweep

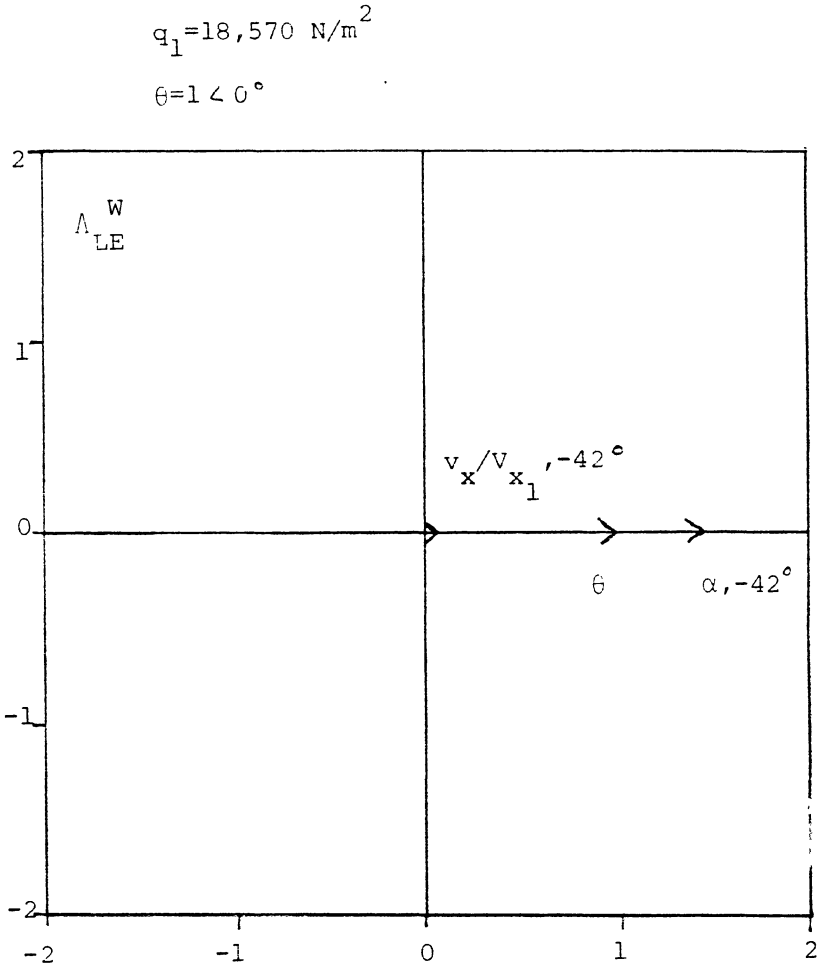

Short period(1) mode shape
with varying sweep

q_1=18,570 N/m^2

θ=1$\angle$0°

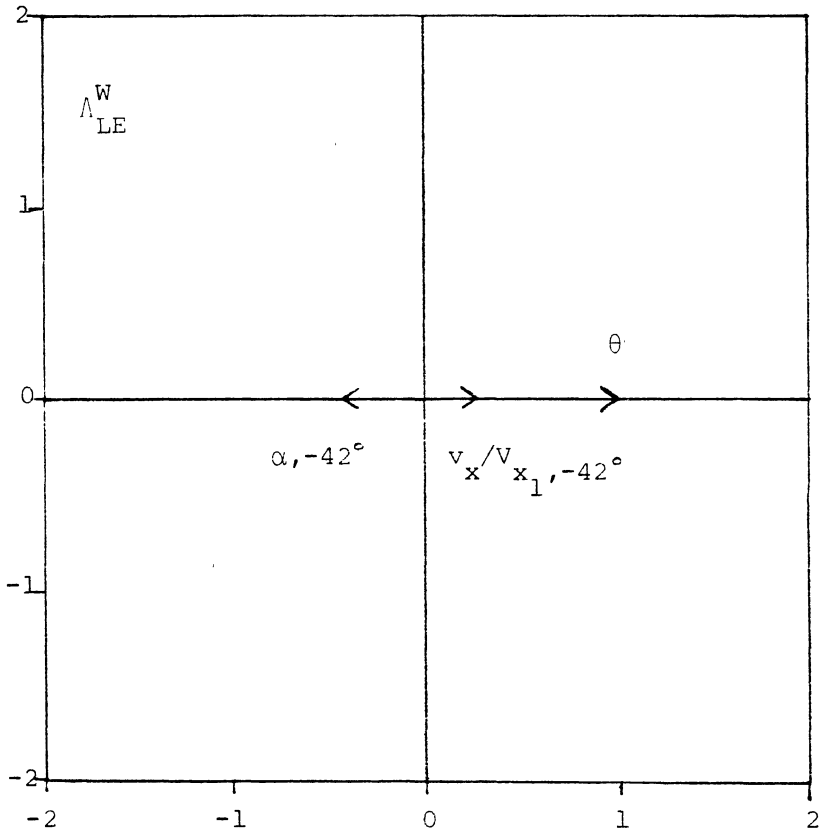

Short period(2) mode shape
with varying sweep

q_1=18,570 N/m^2

θ=1 $\angle$ 0°

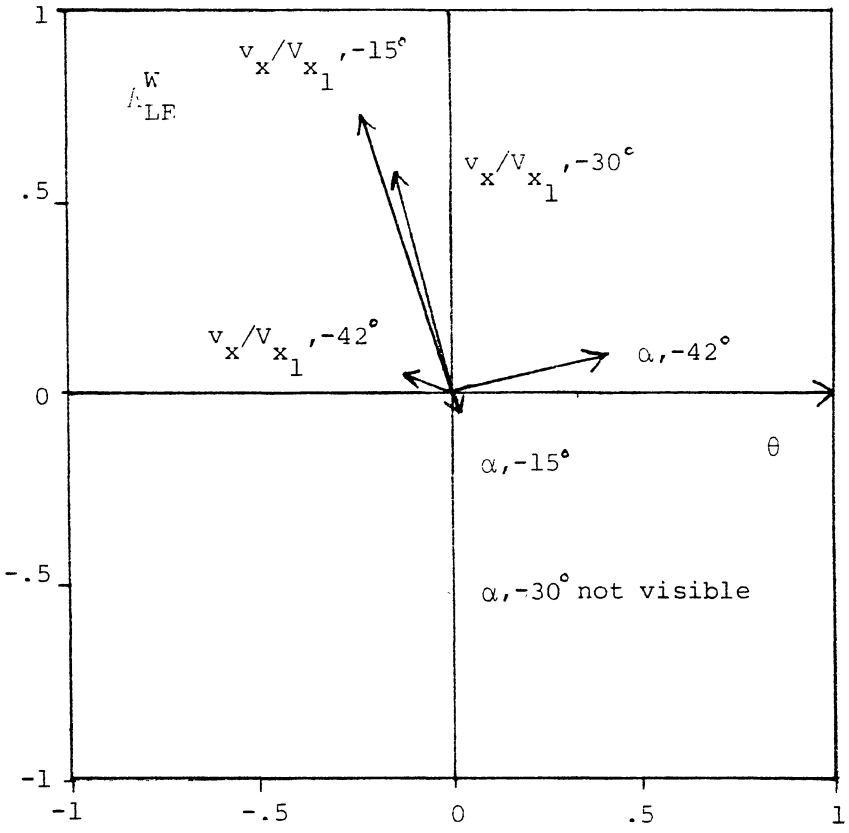

Phugoid mode shape
with varying sweep

q_1=18,570 N/m^2

β=1 $\angle$ 0°

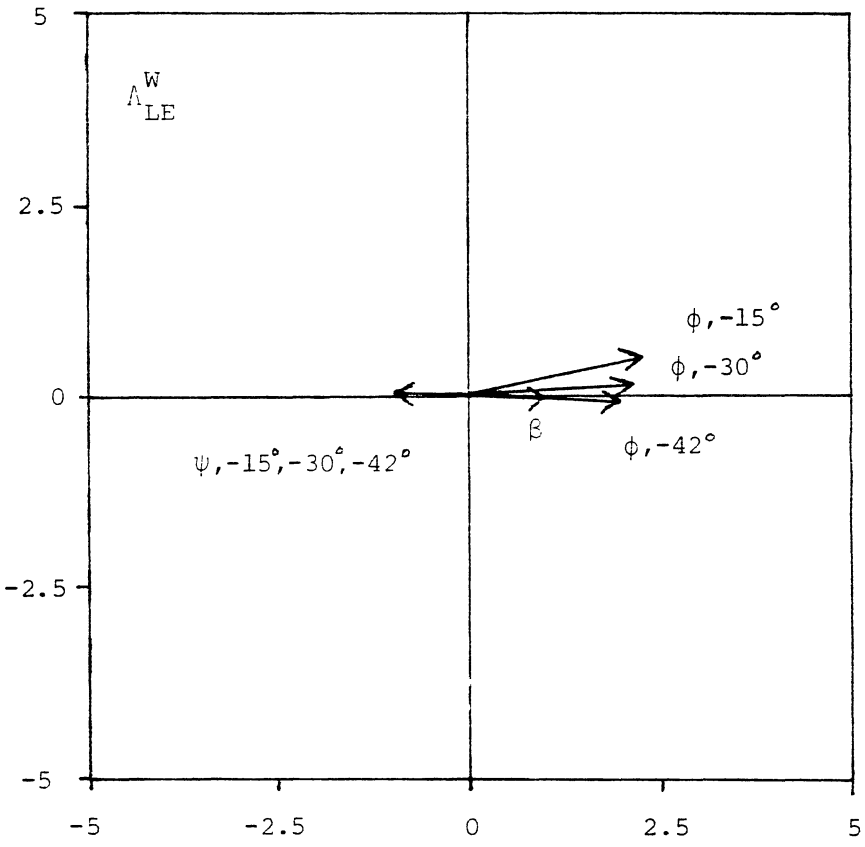

Dutch-roll mode shape
with varying sweep

q_1=18,570 N/m^2

β=1$\angle$ 0°

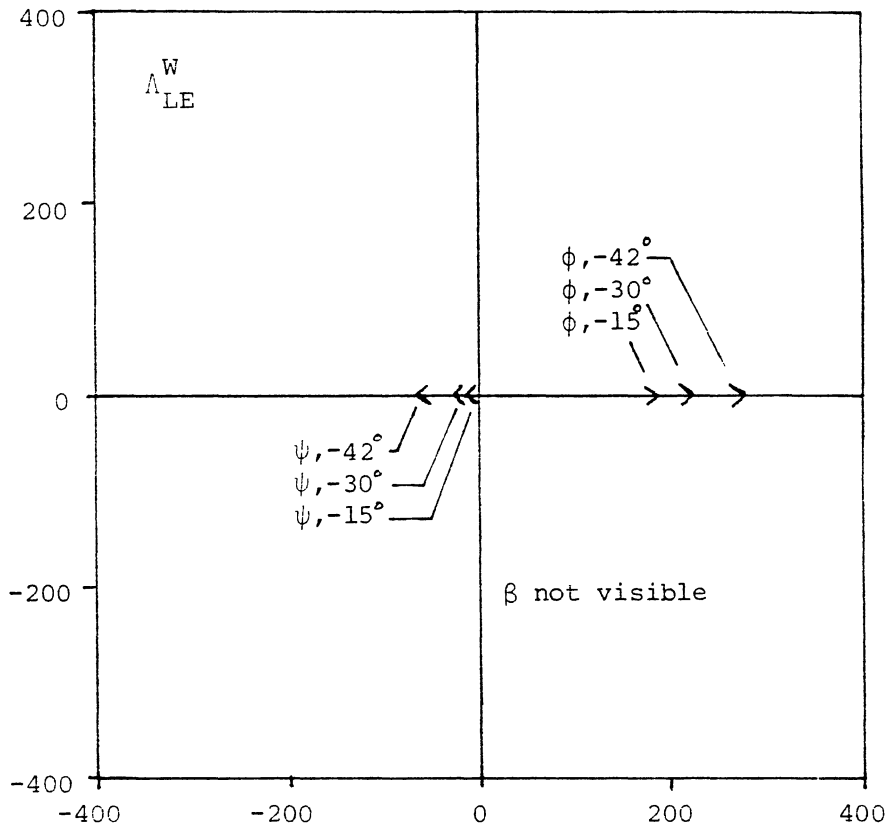

Roll mode shape
with varying sweep

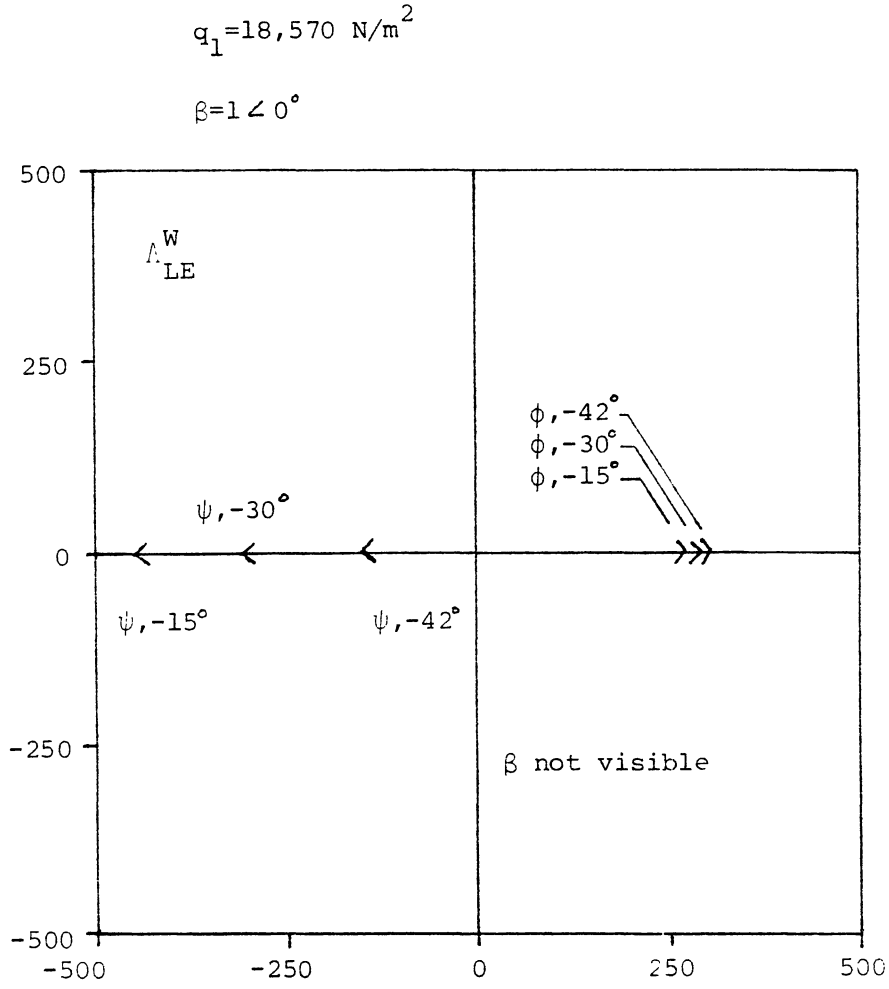

Spiral mode shape
with varying sweep

$q_1 = 28{,}150\ N/m^2$

$\theta = 1 \angle 0^\circ$

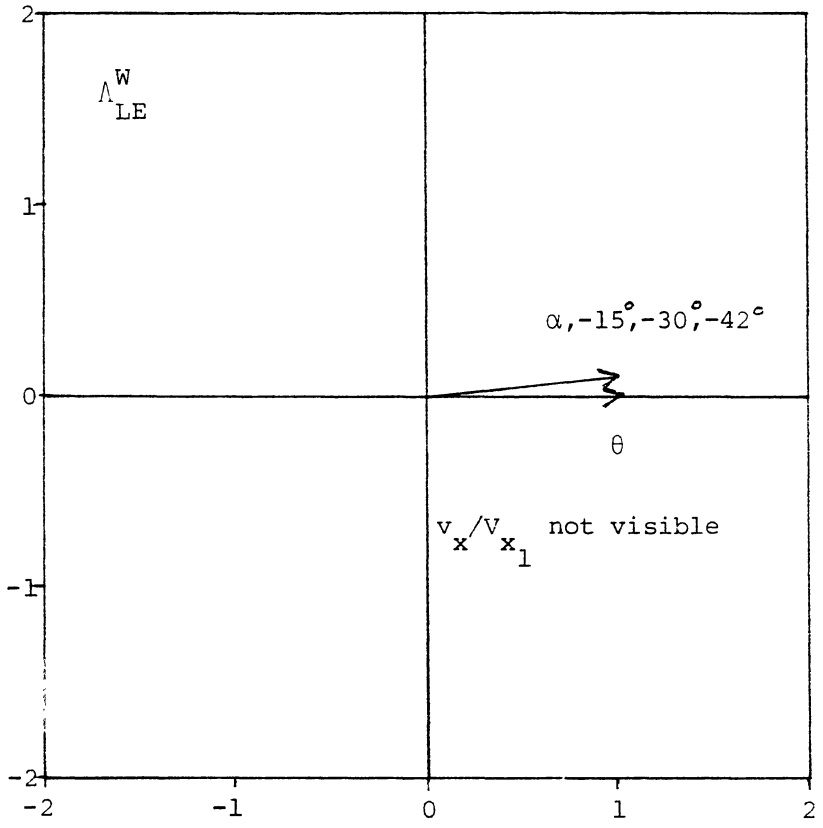

Short period mode shape
with varying sweep

$q_1 = 28{,}150\ N/m^2$

$\theta = 1 \angle 0^\circ$

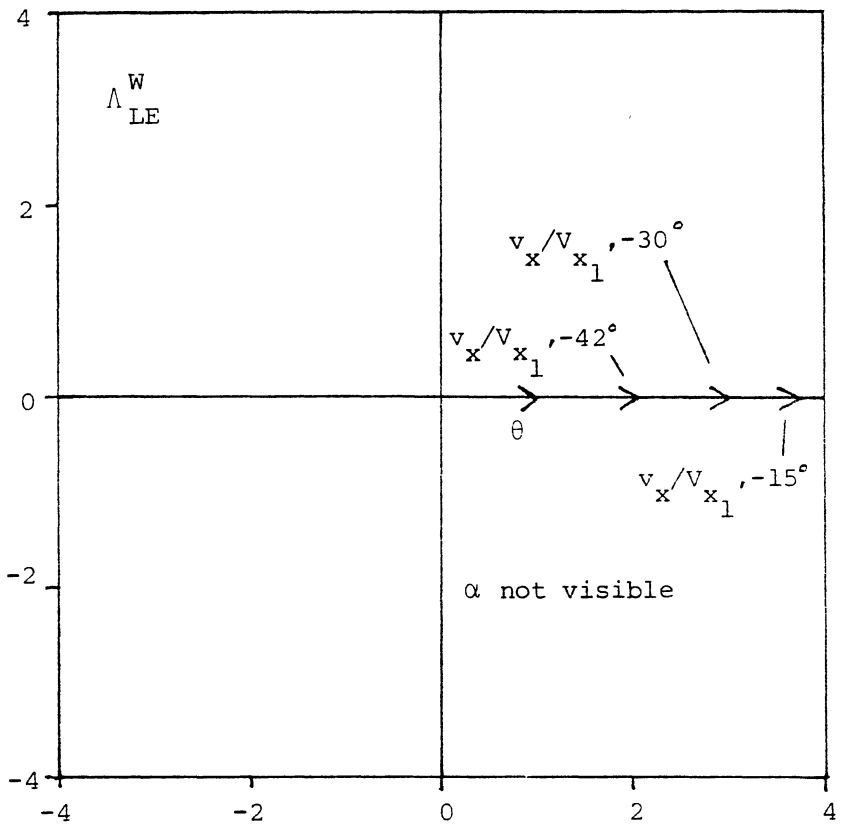

Phugoid(1) mode shape
with varying sweep

q_1=28,150 N/m^2

$\theta=1\angle 0^\circ$

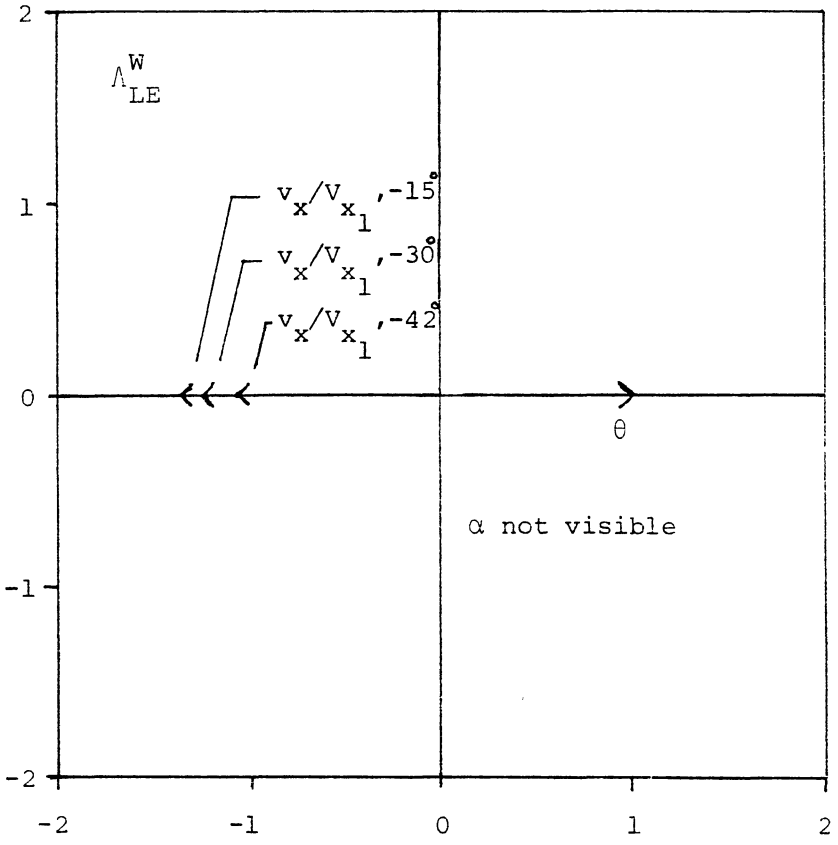

Phugoid(2) mode shape
with varying sweep

$q_1 = 28{,}150\ N/m^2$

$\beta = 1 \angle 0°$

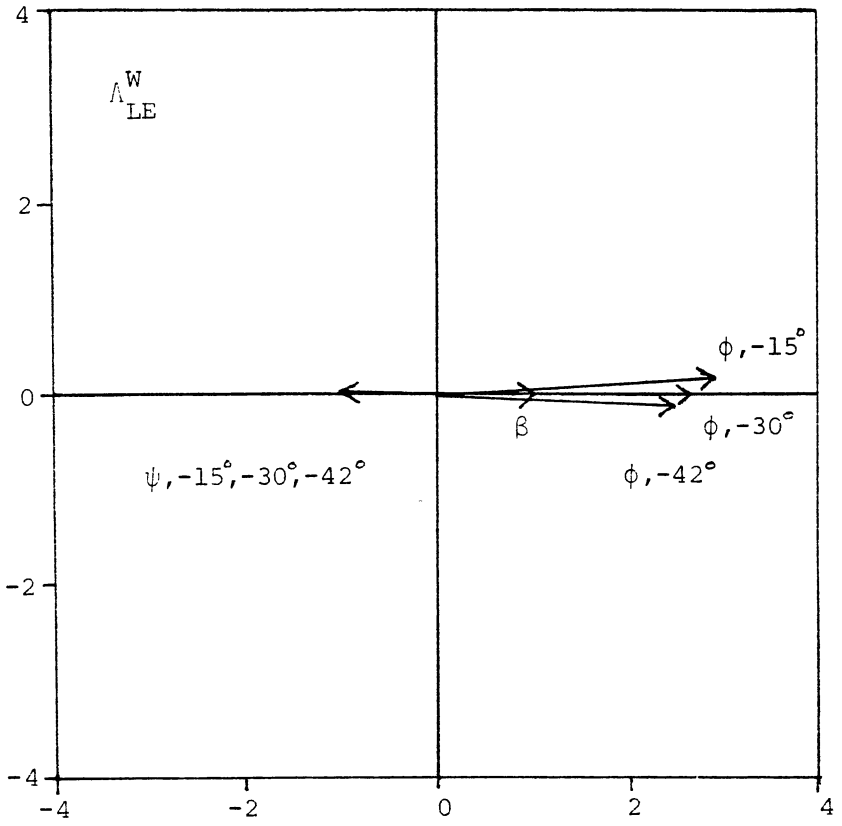

Dutch-roll mode shape
with varying sweep

q_1=28,150 N/m^2

β=1 $\angle$ 0°

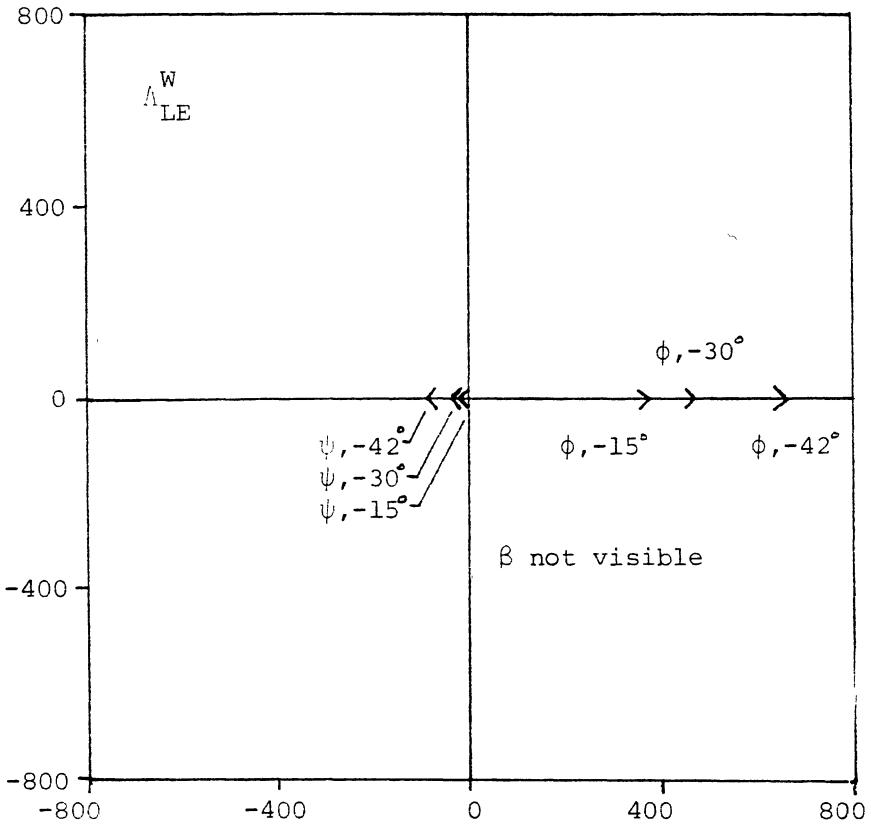

Roll mode shape
with varying sweep

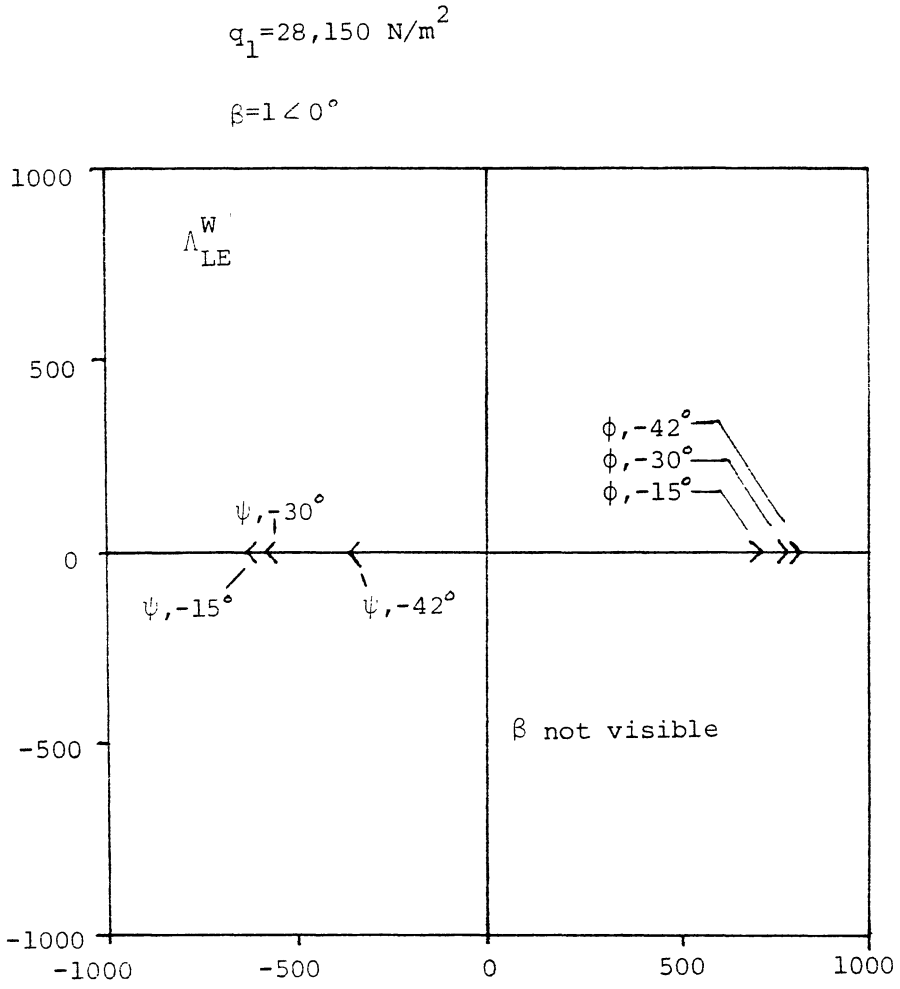

Spiral mode shape
with varying sweep

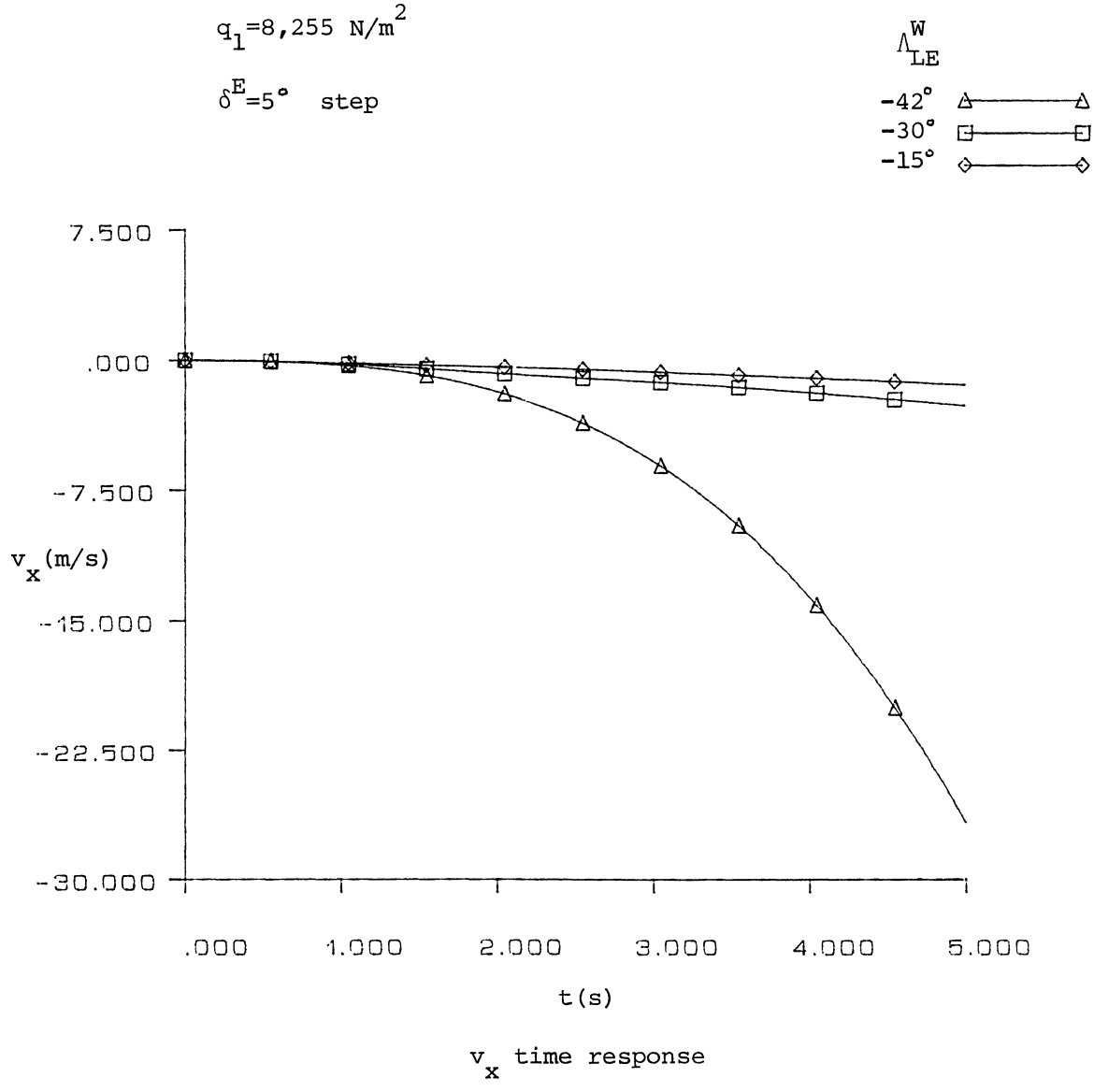

v_x time response

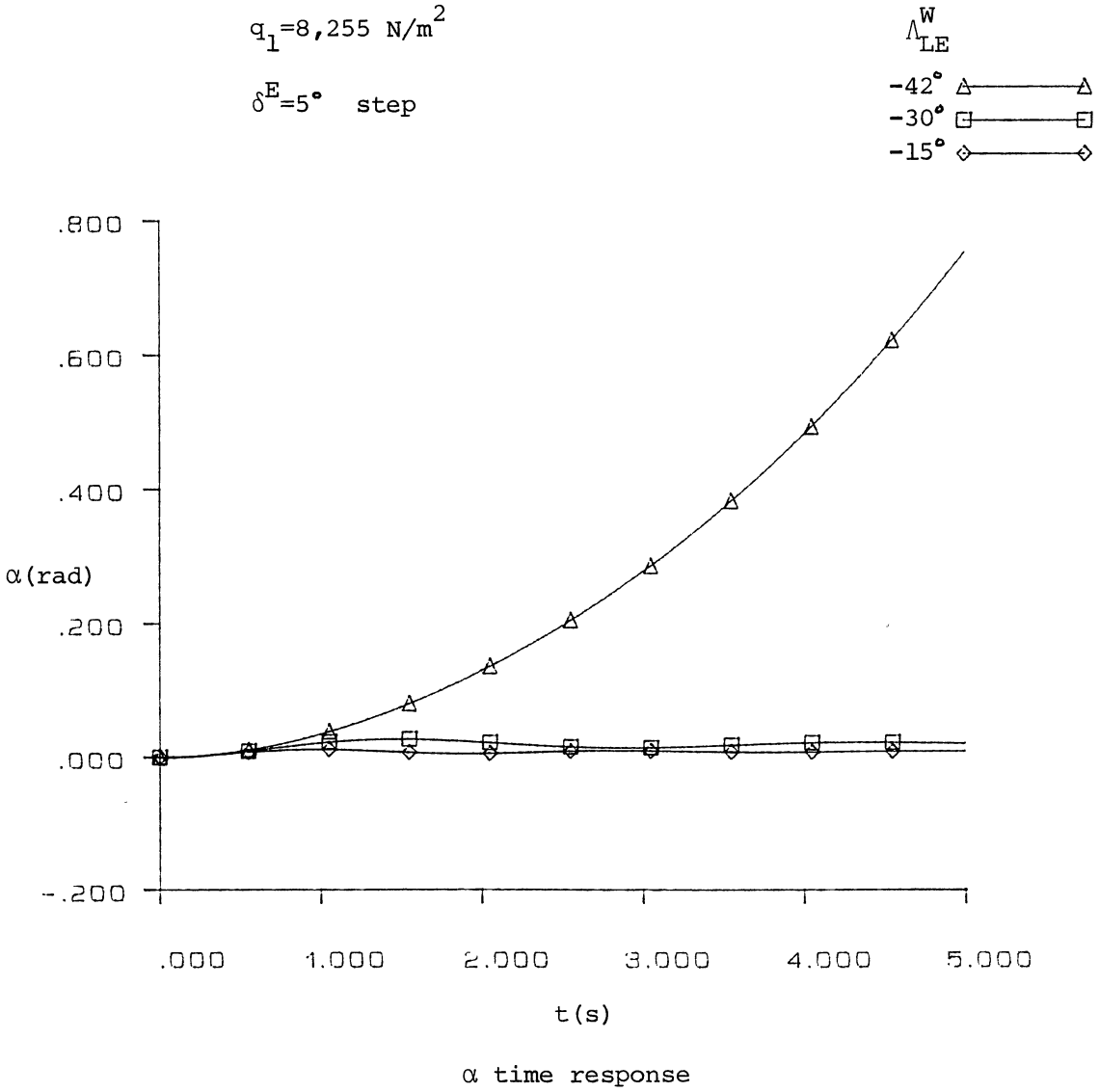

α time response

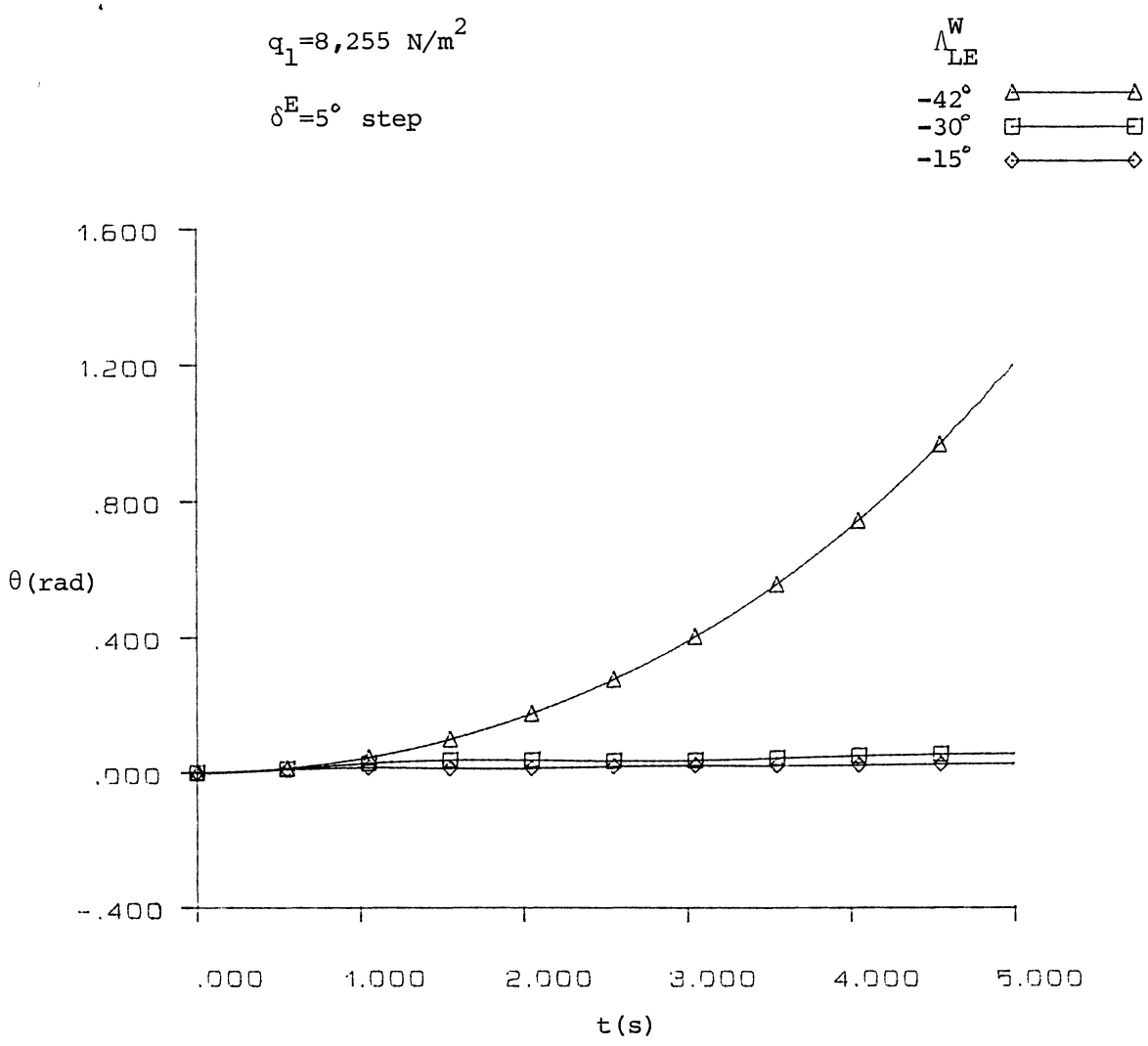

θ time response

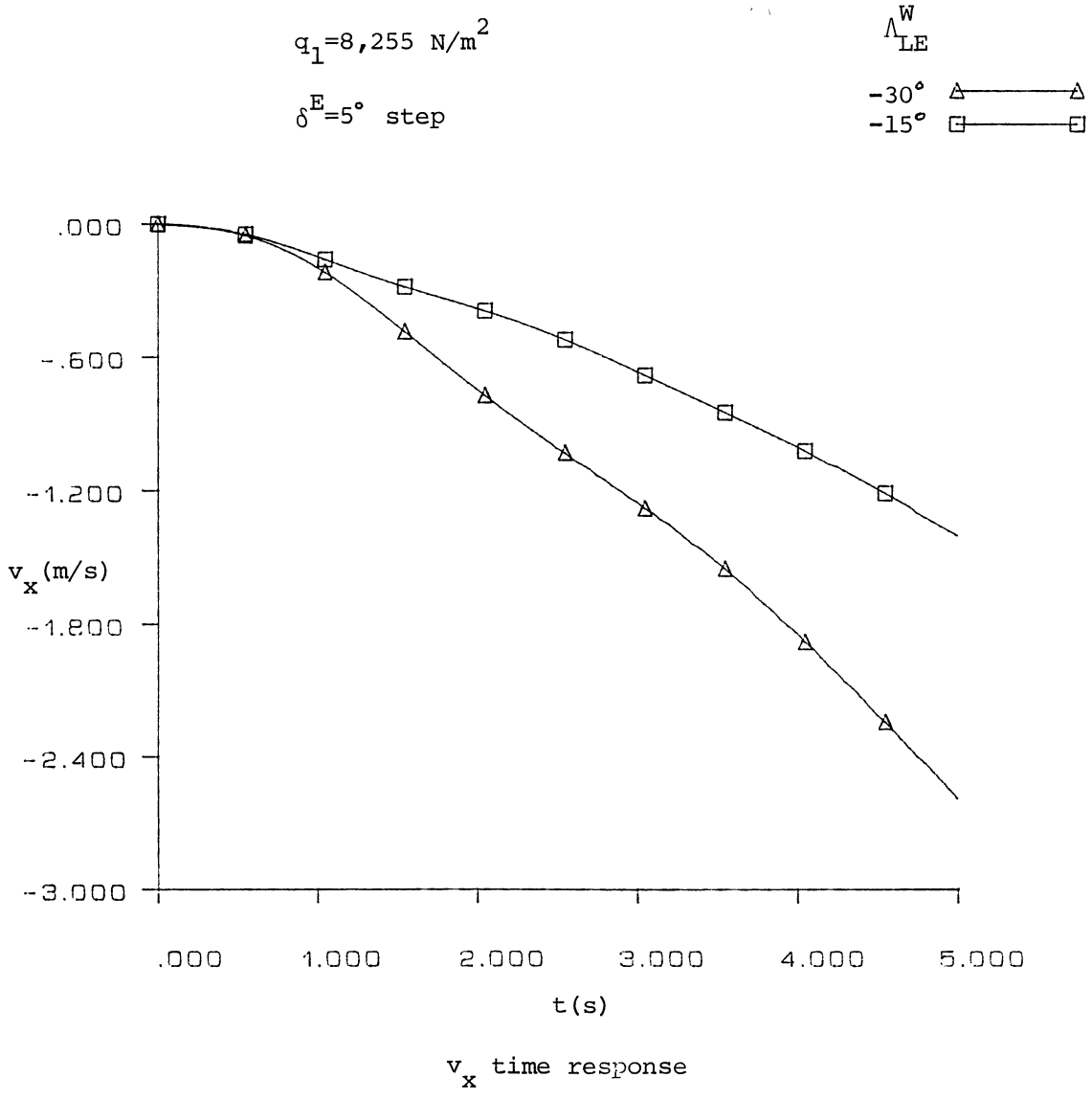

v_x time response

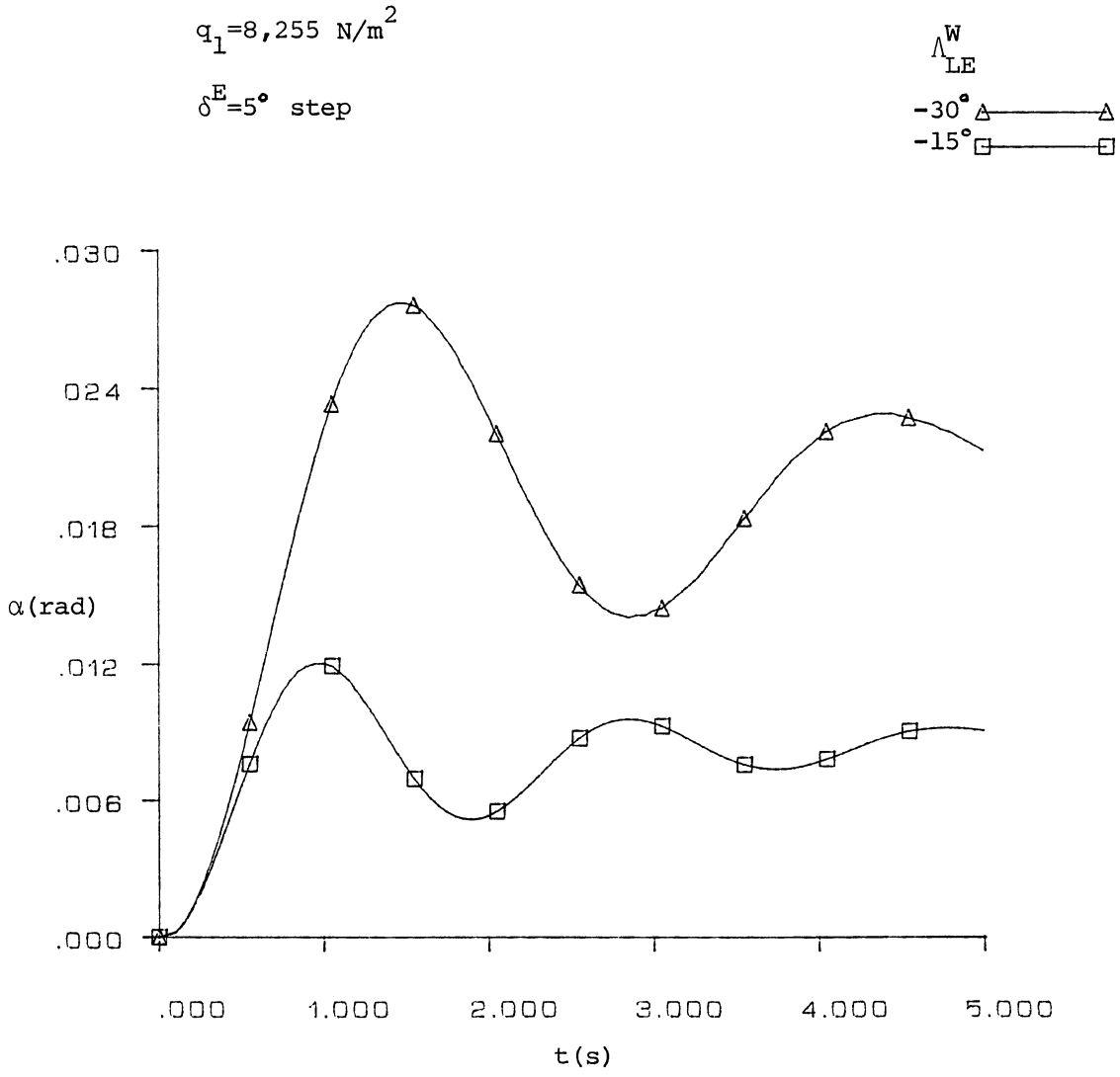

α time response

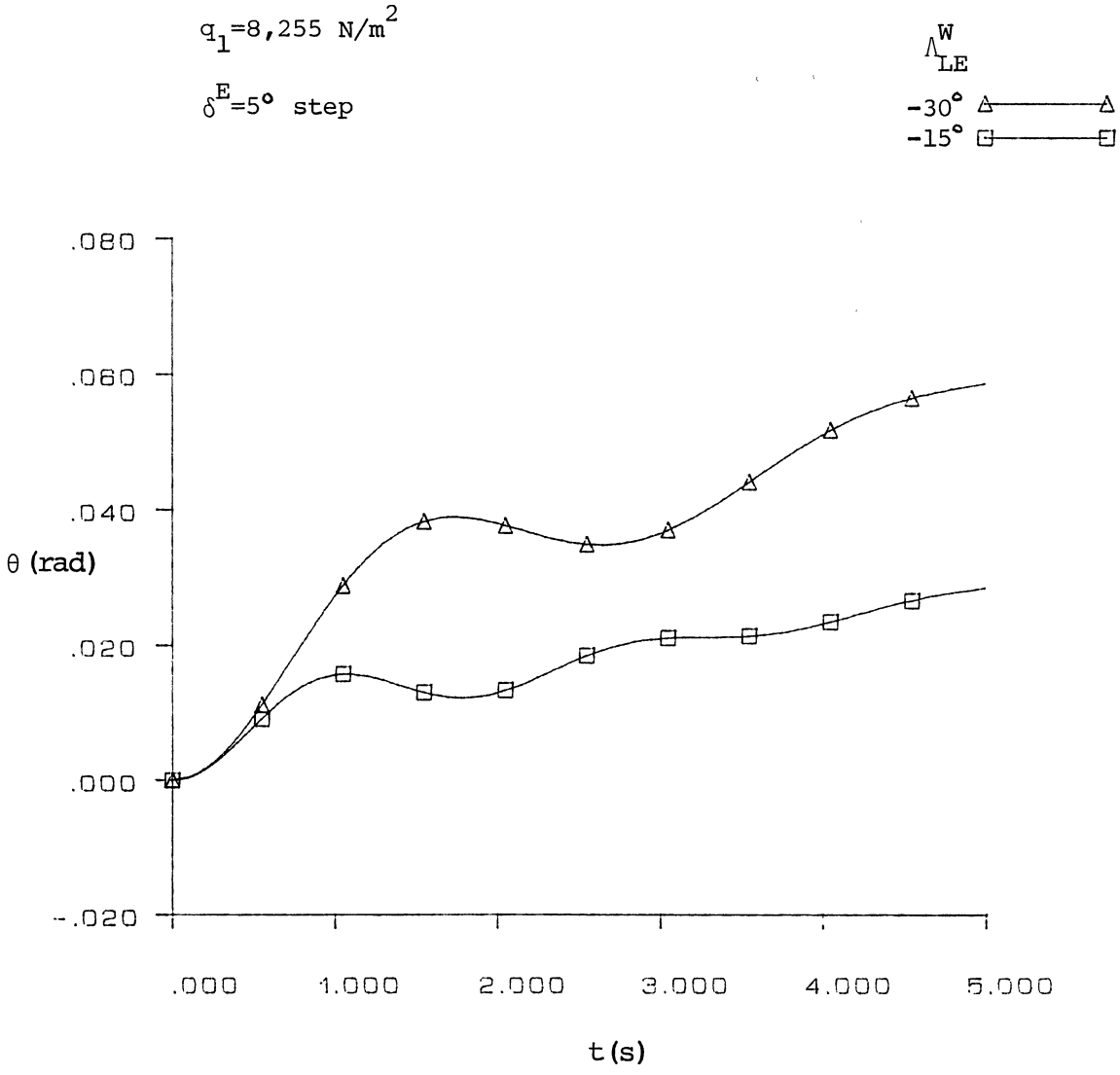

θ time response

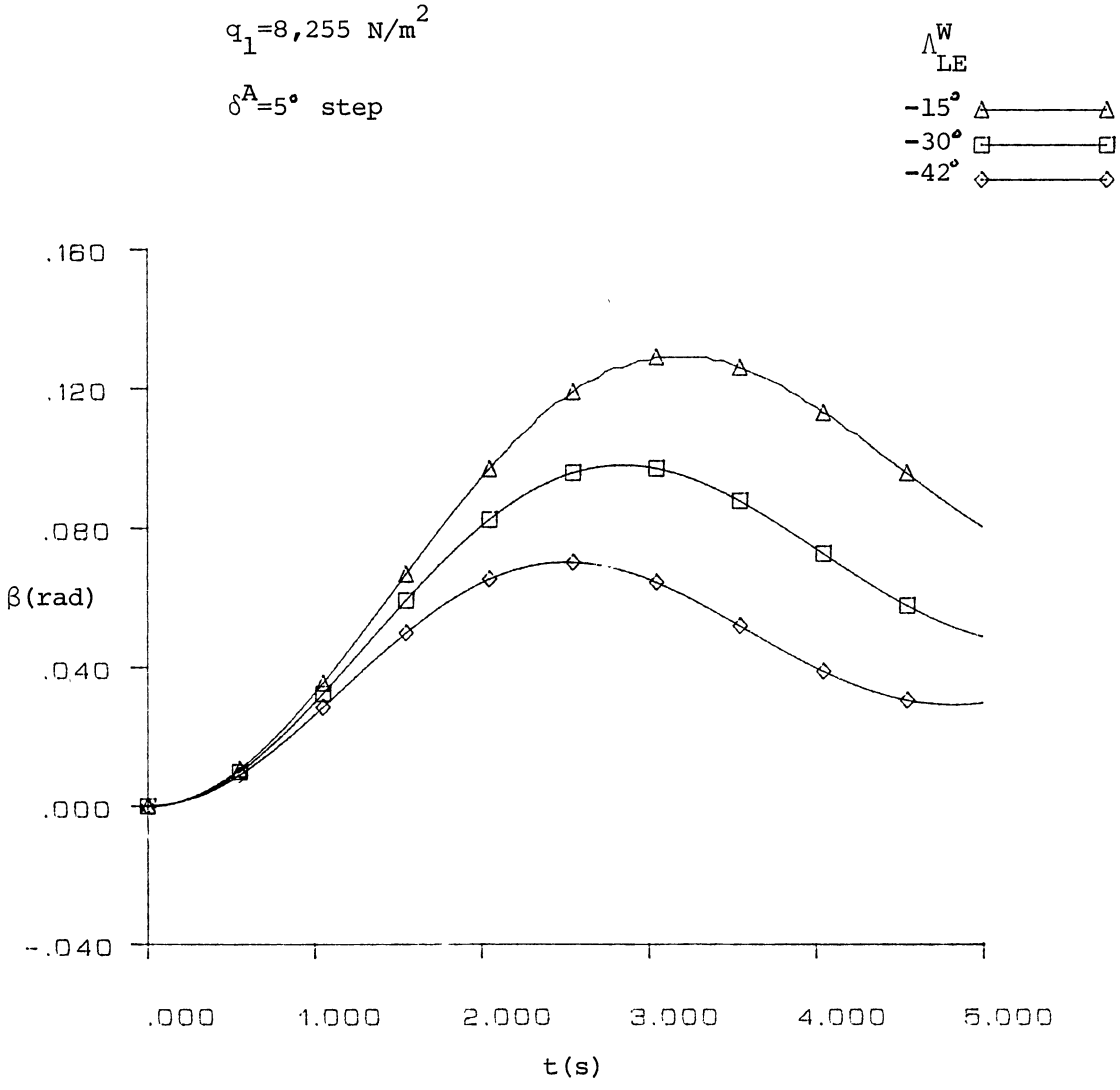

β time response

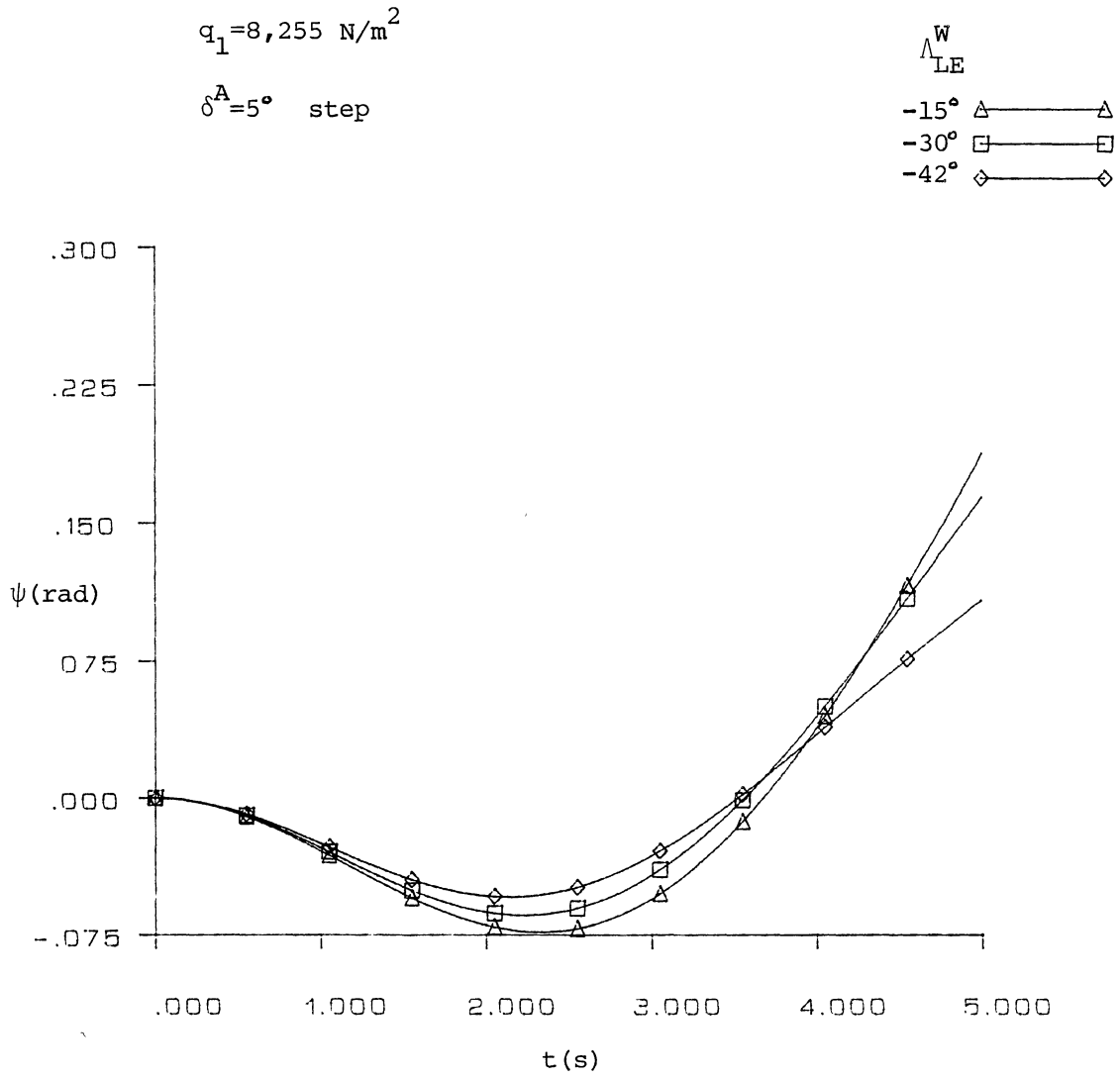

ψ time response

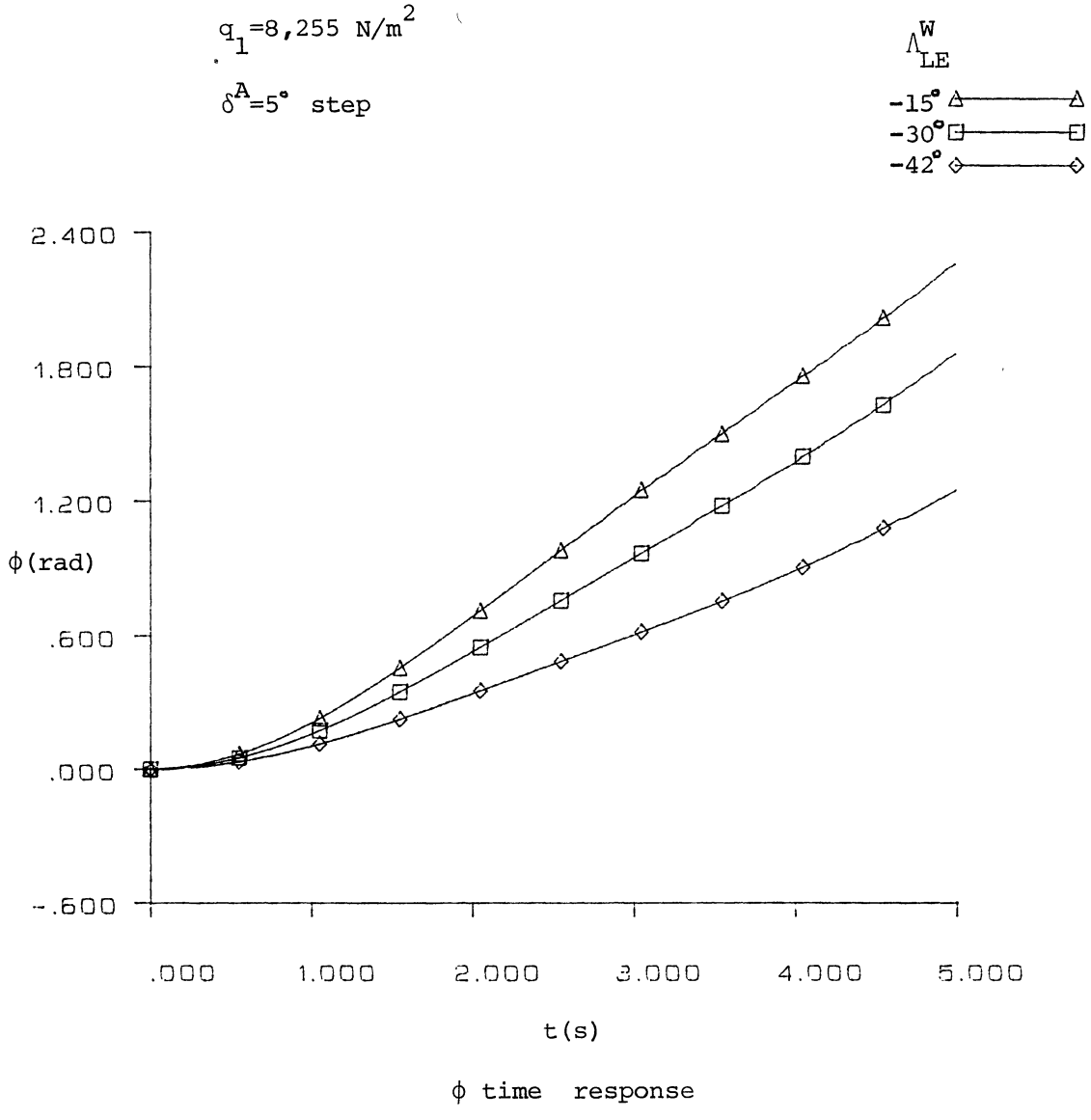

ϕ time response

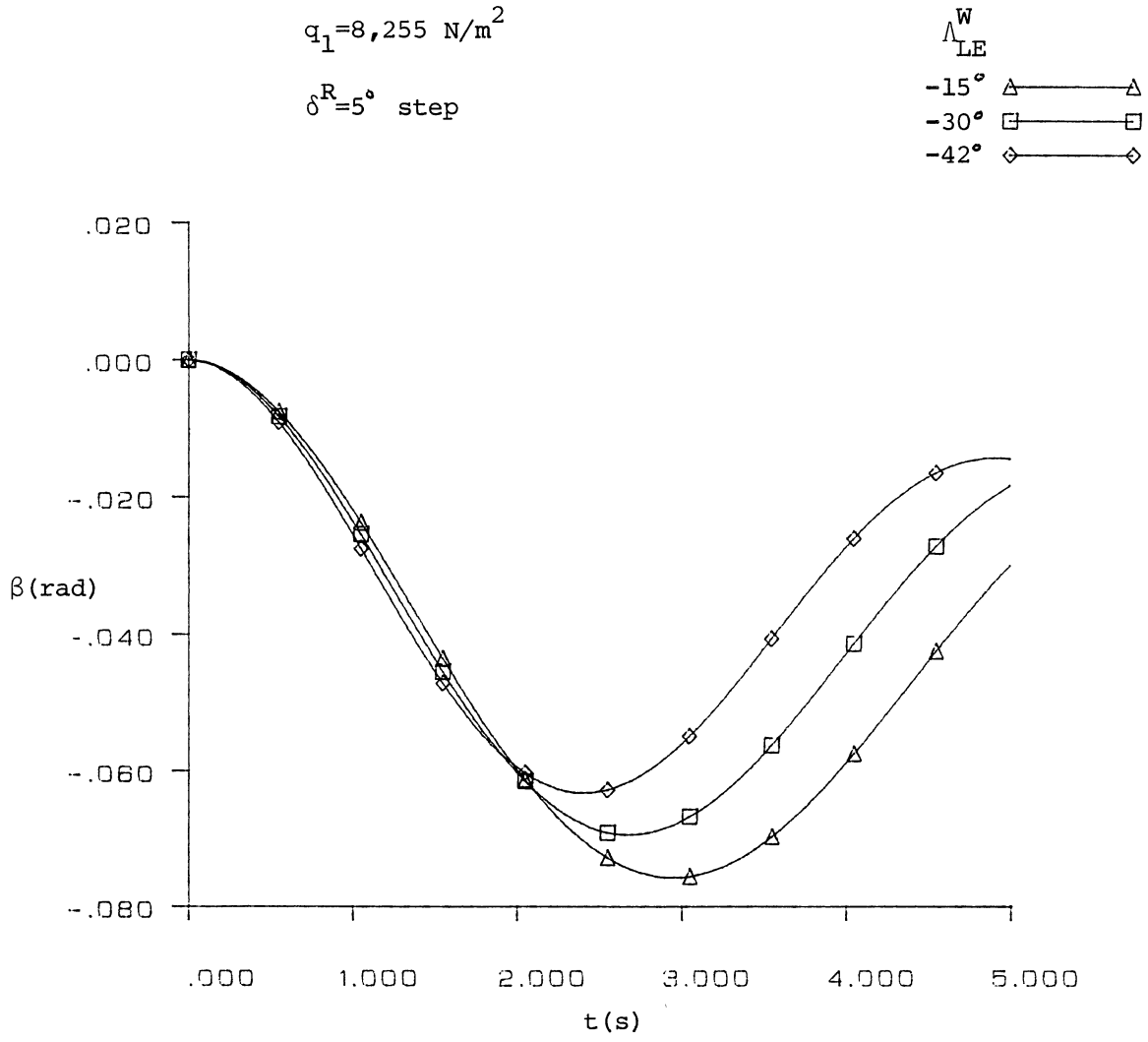

β time response

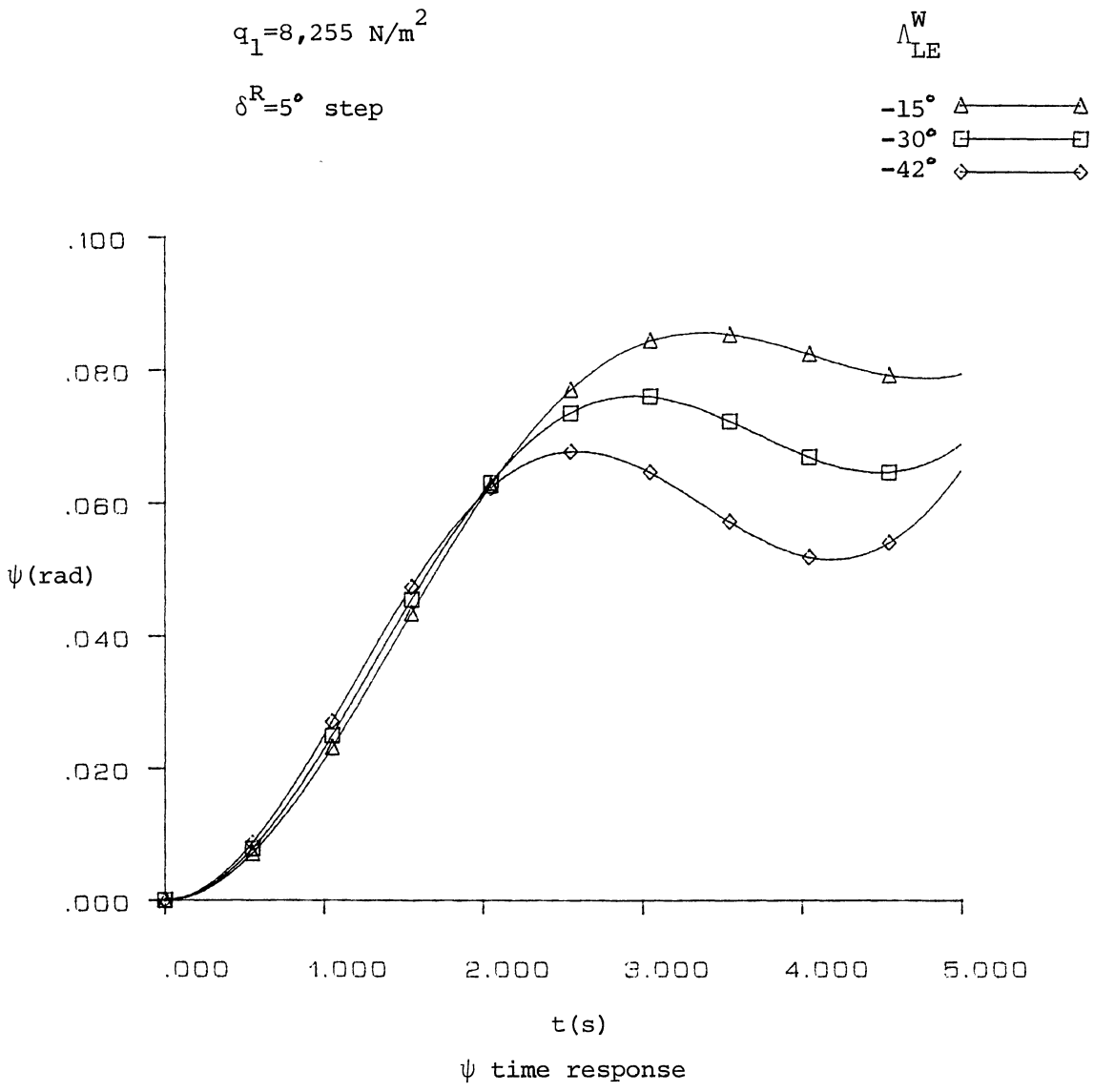

ψ time response

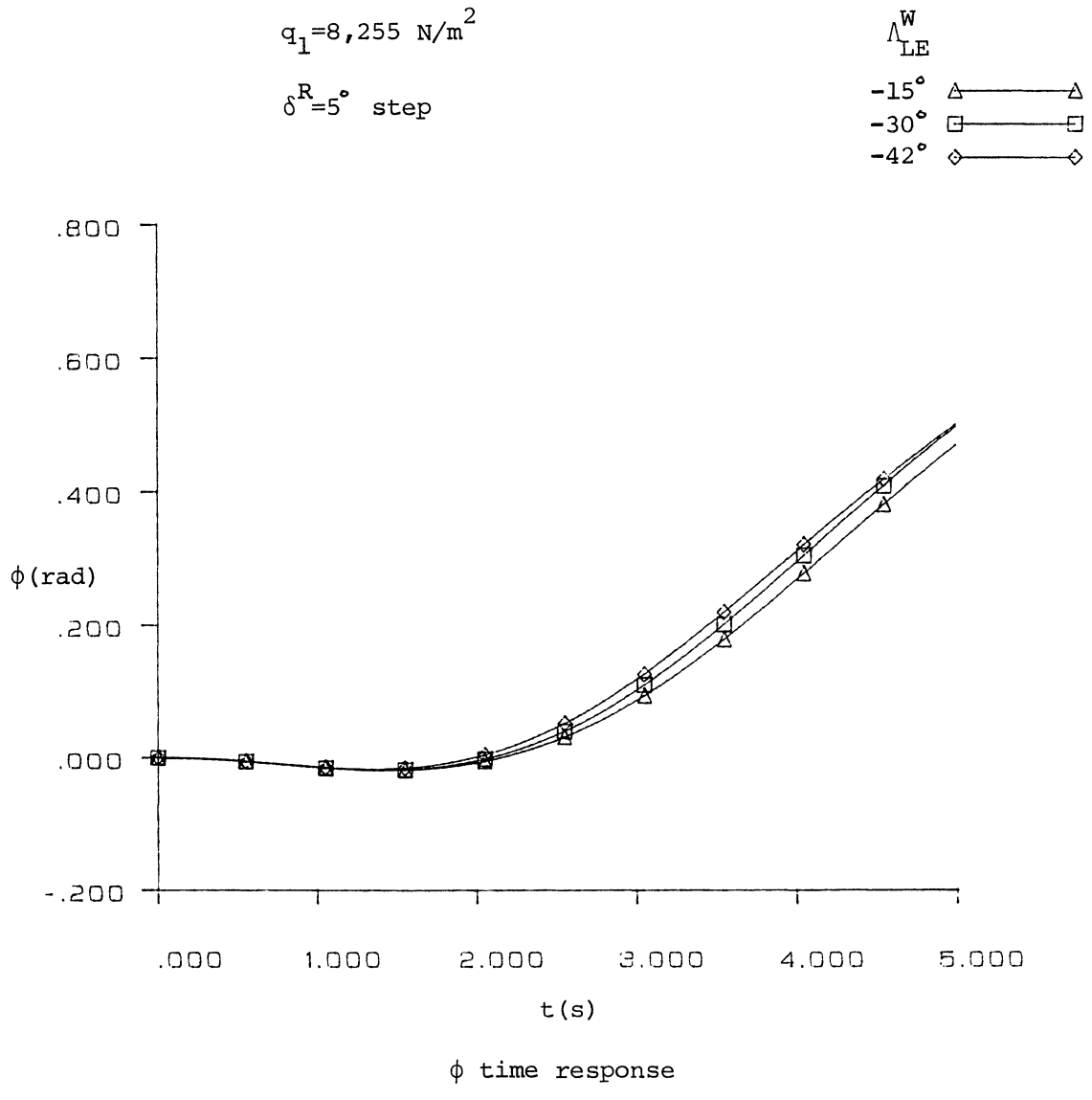

ϕ time response

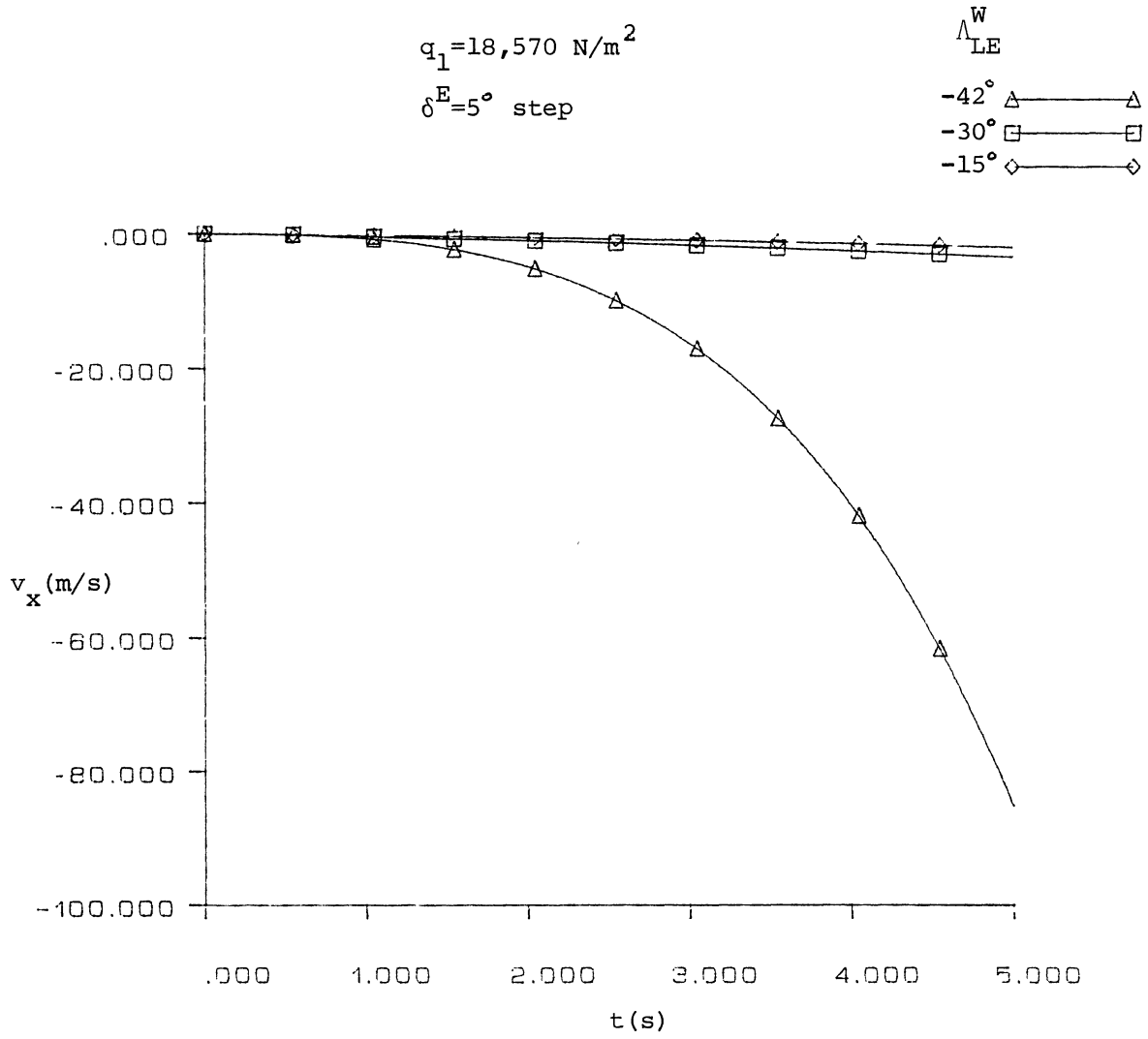

v_x time response

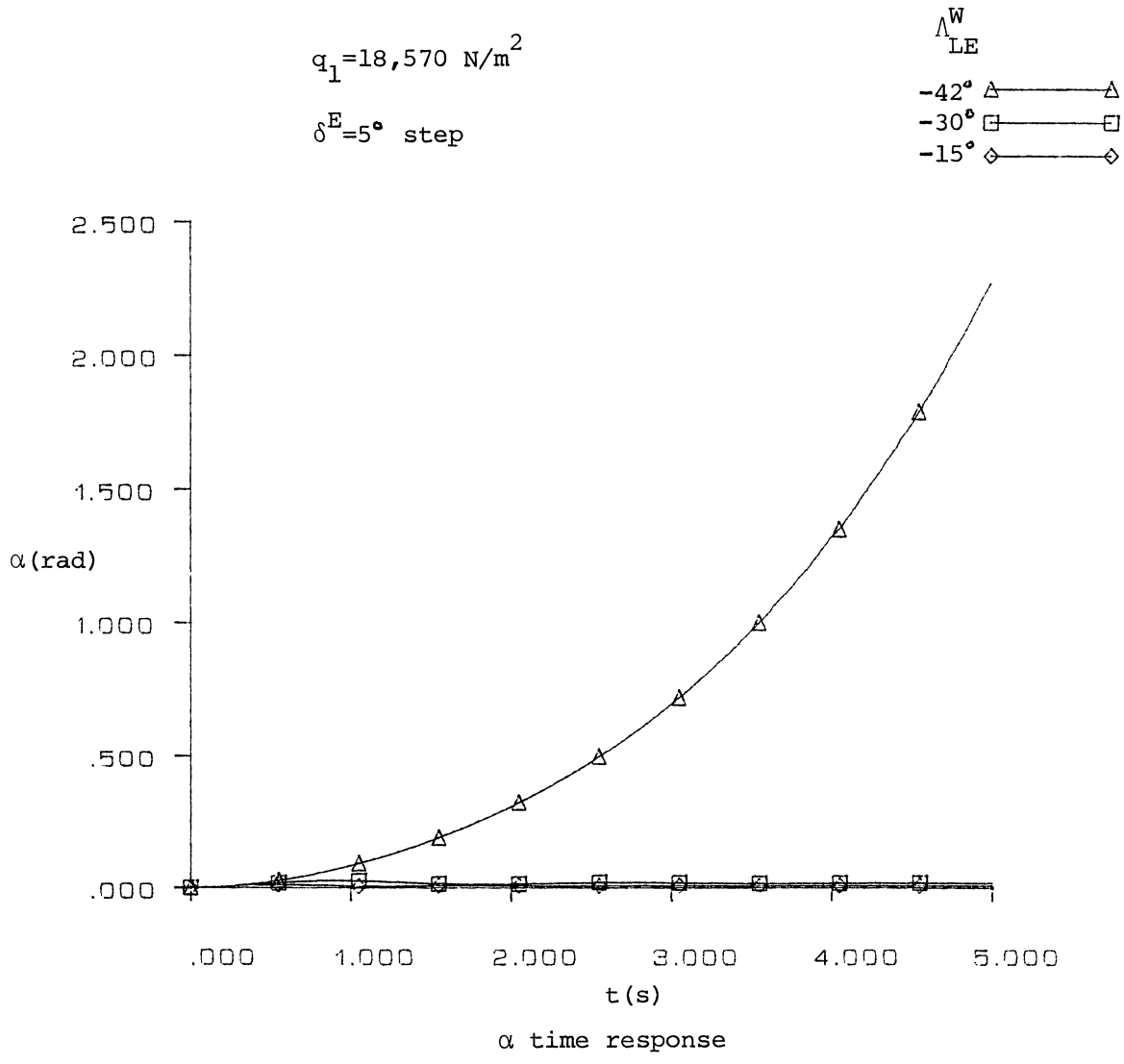

α time response

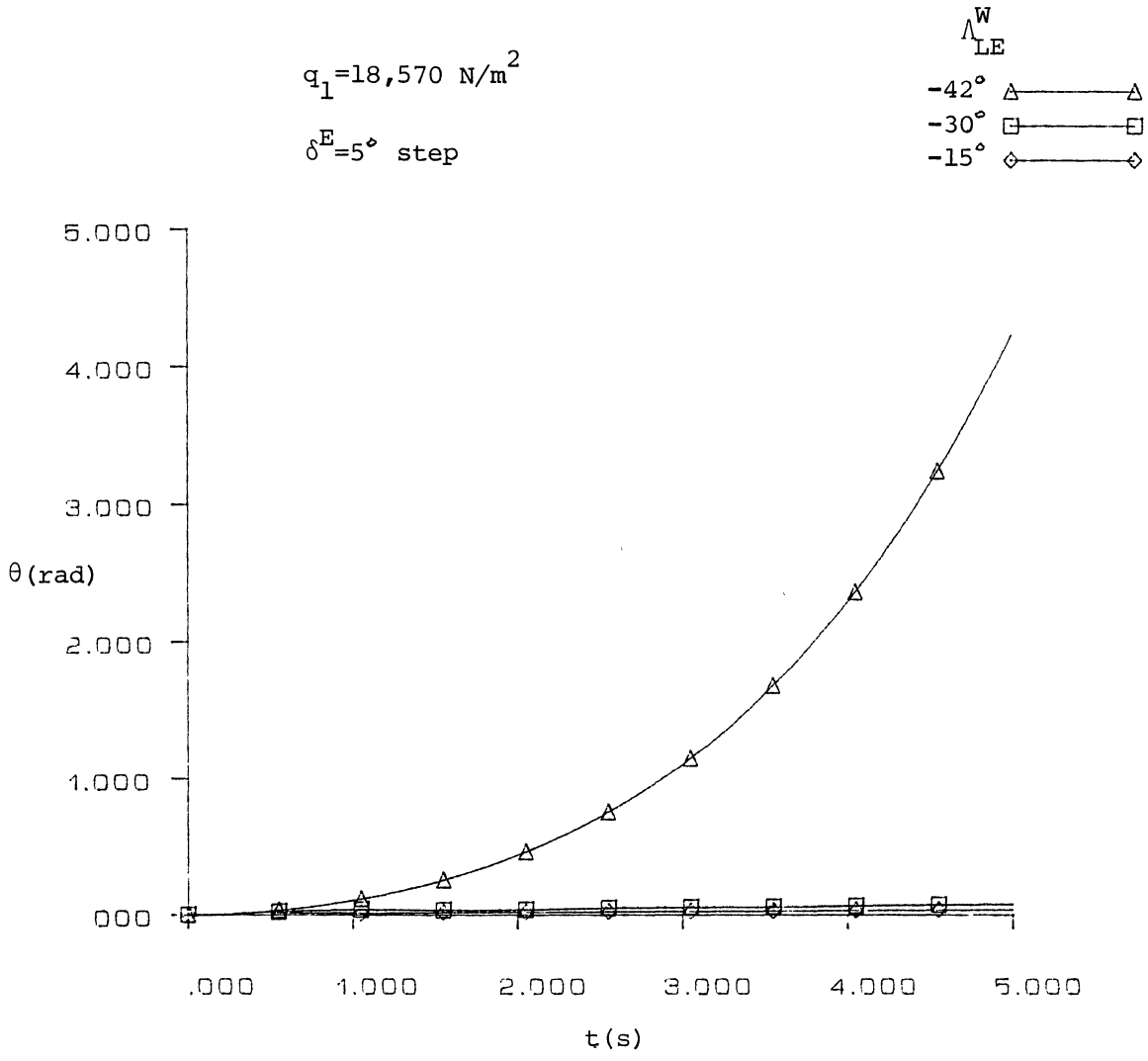

θ time response

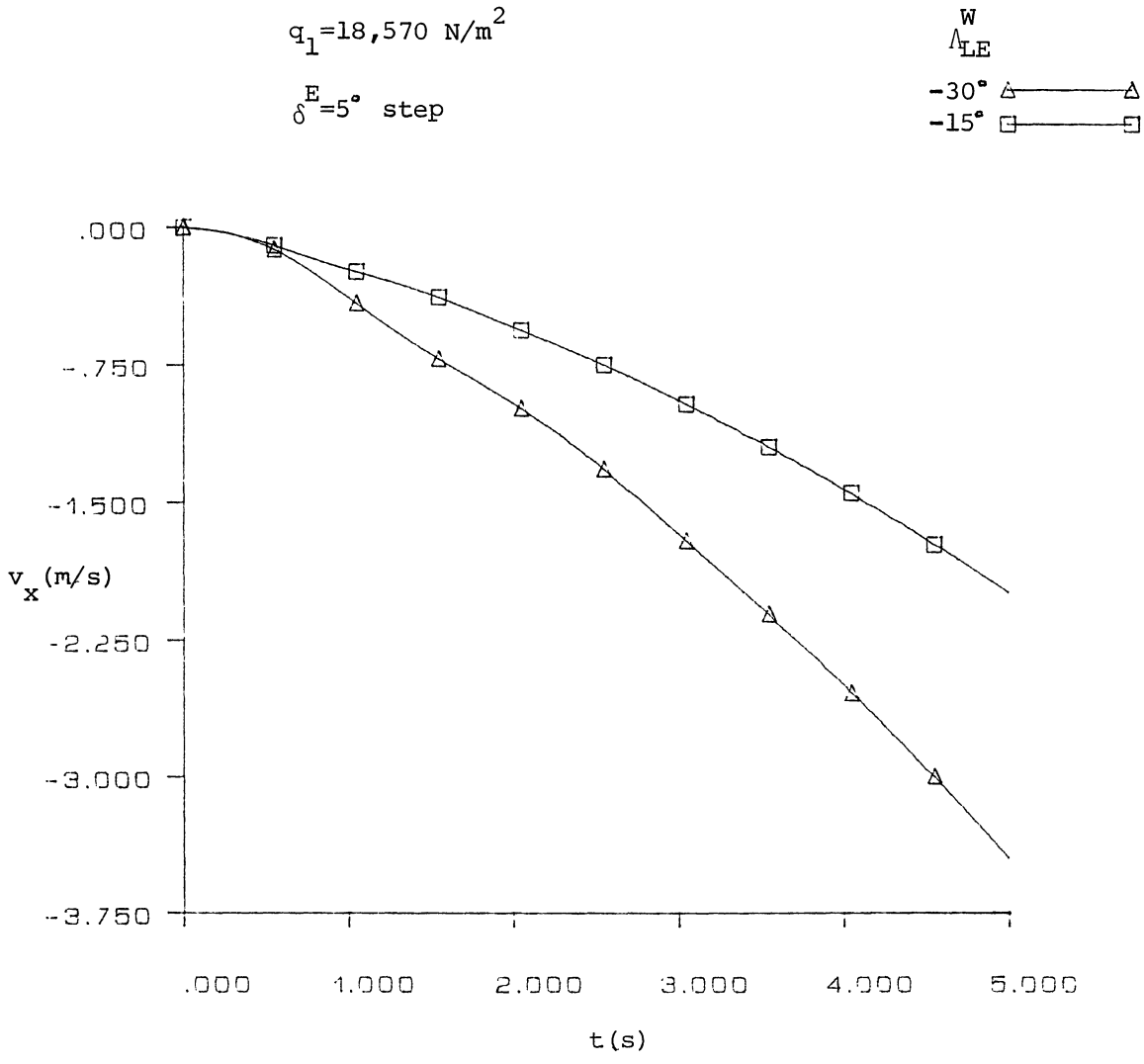

v_x time response

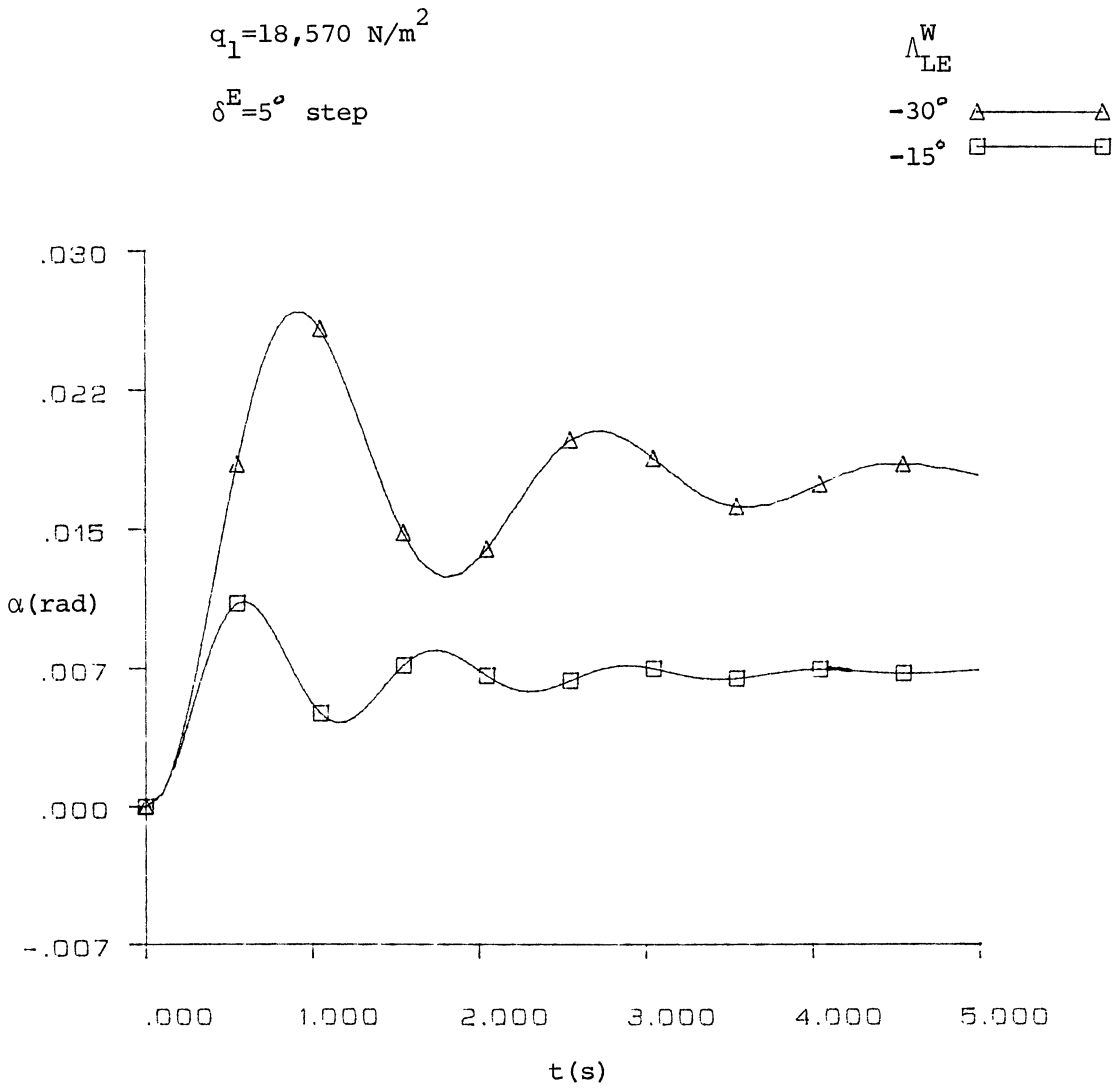

α time response

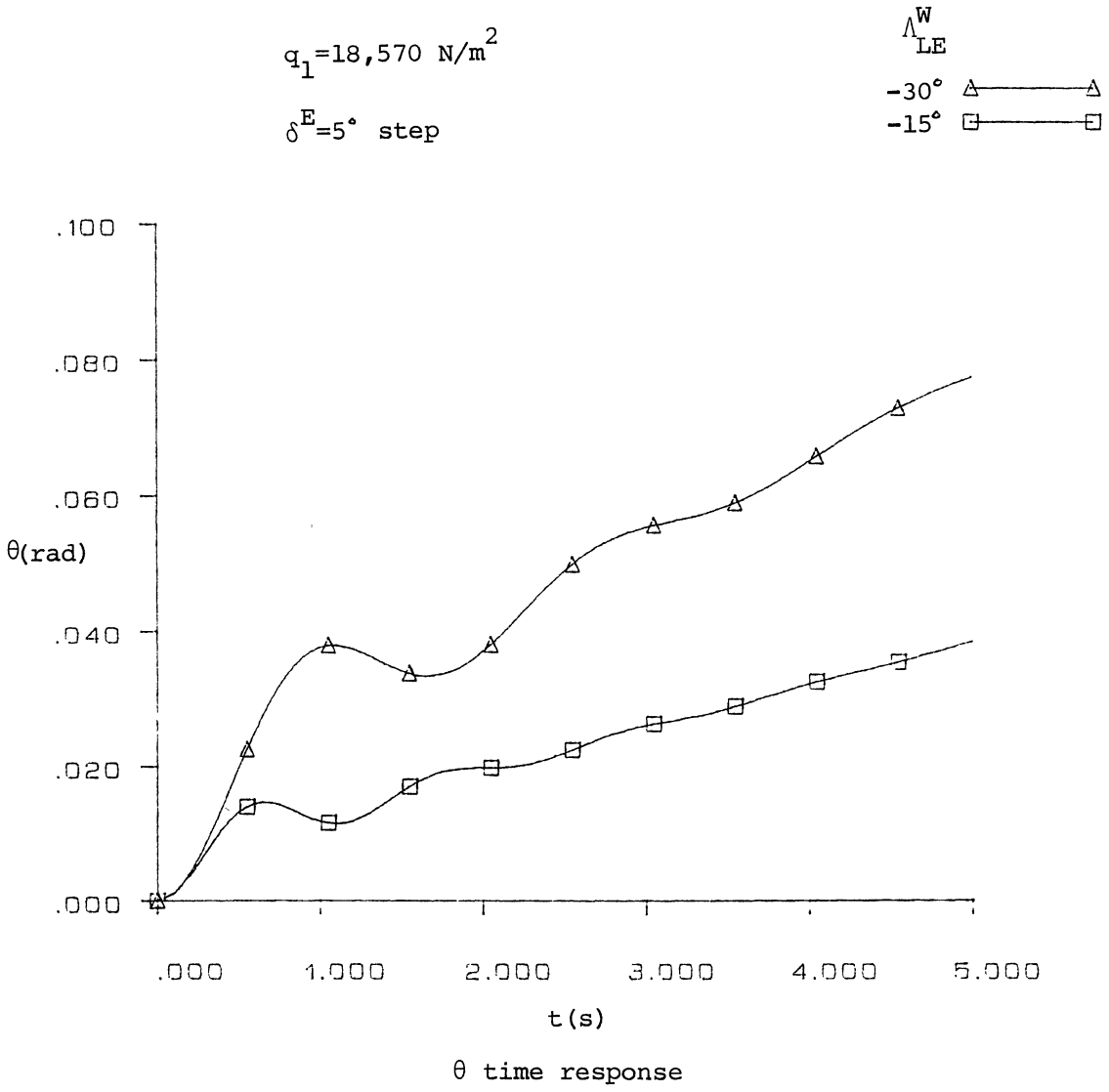

θ time response

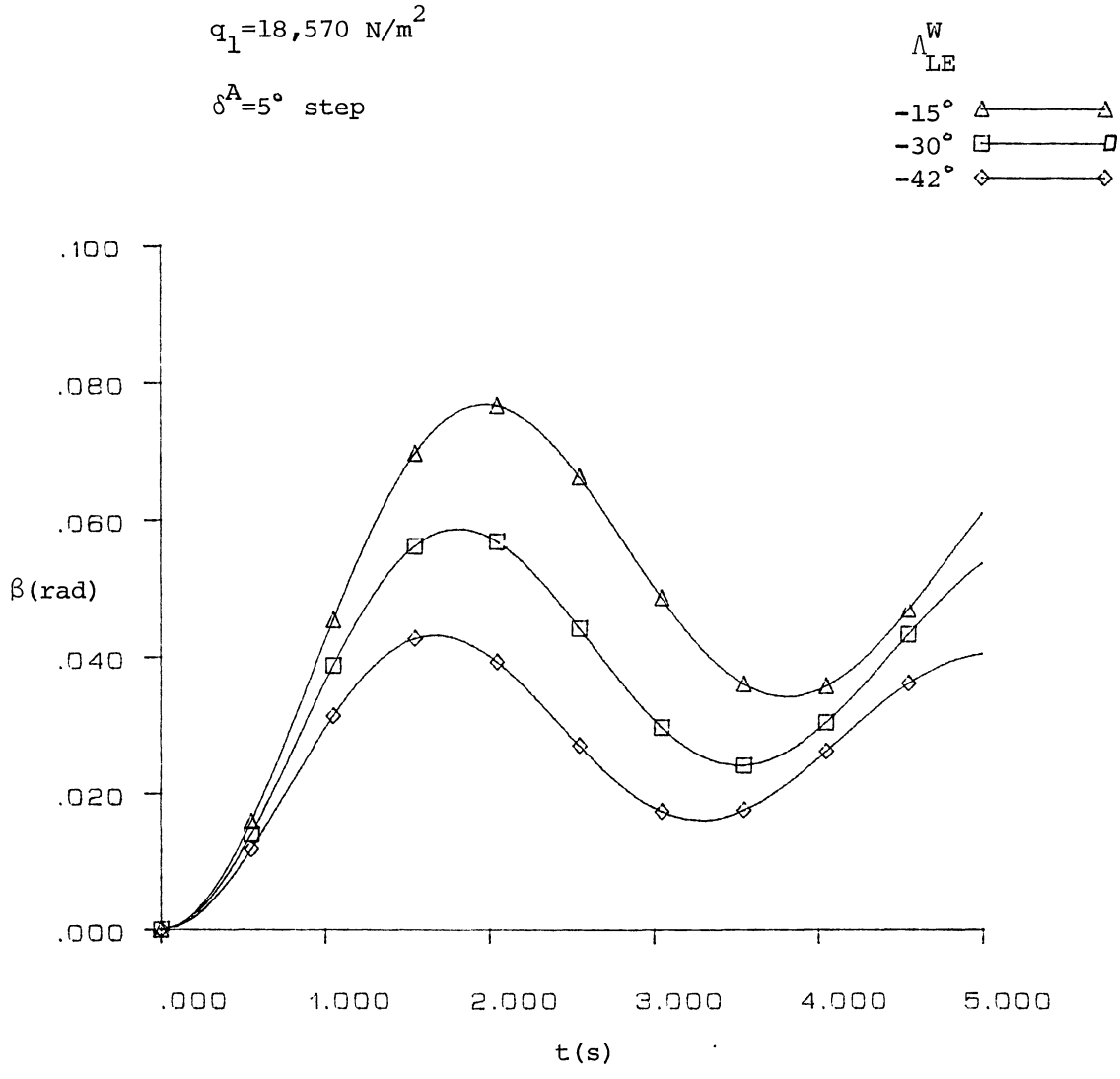

β time response

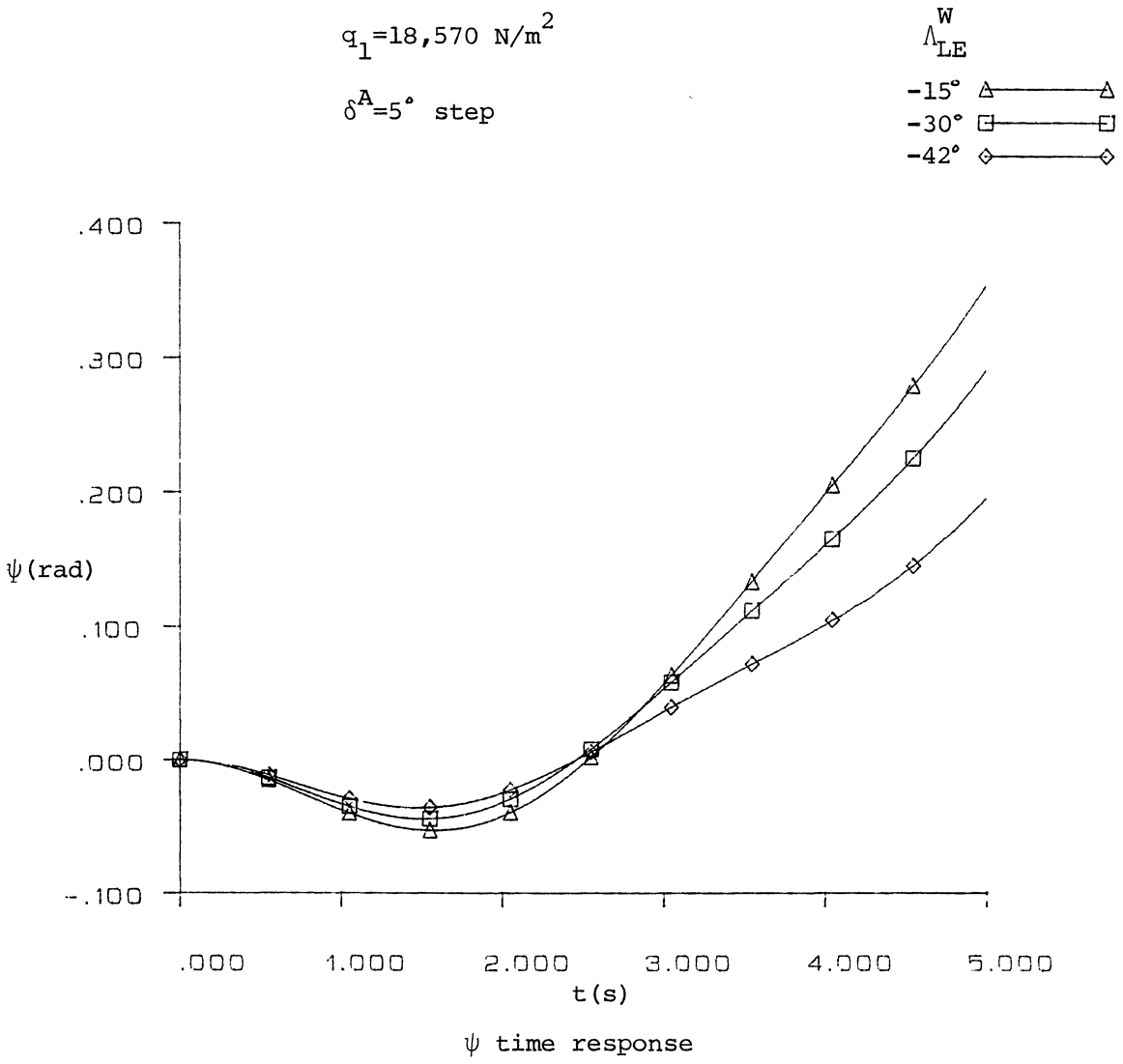

ψ time response

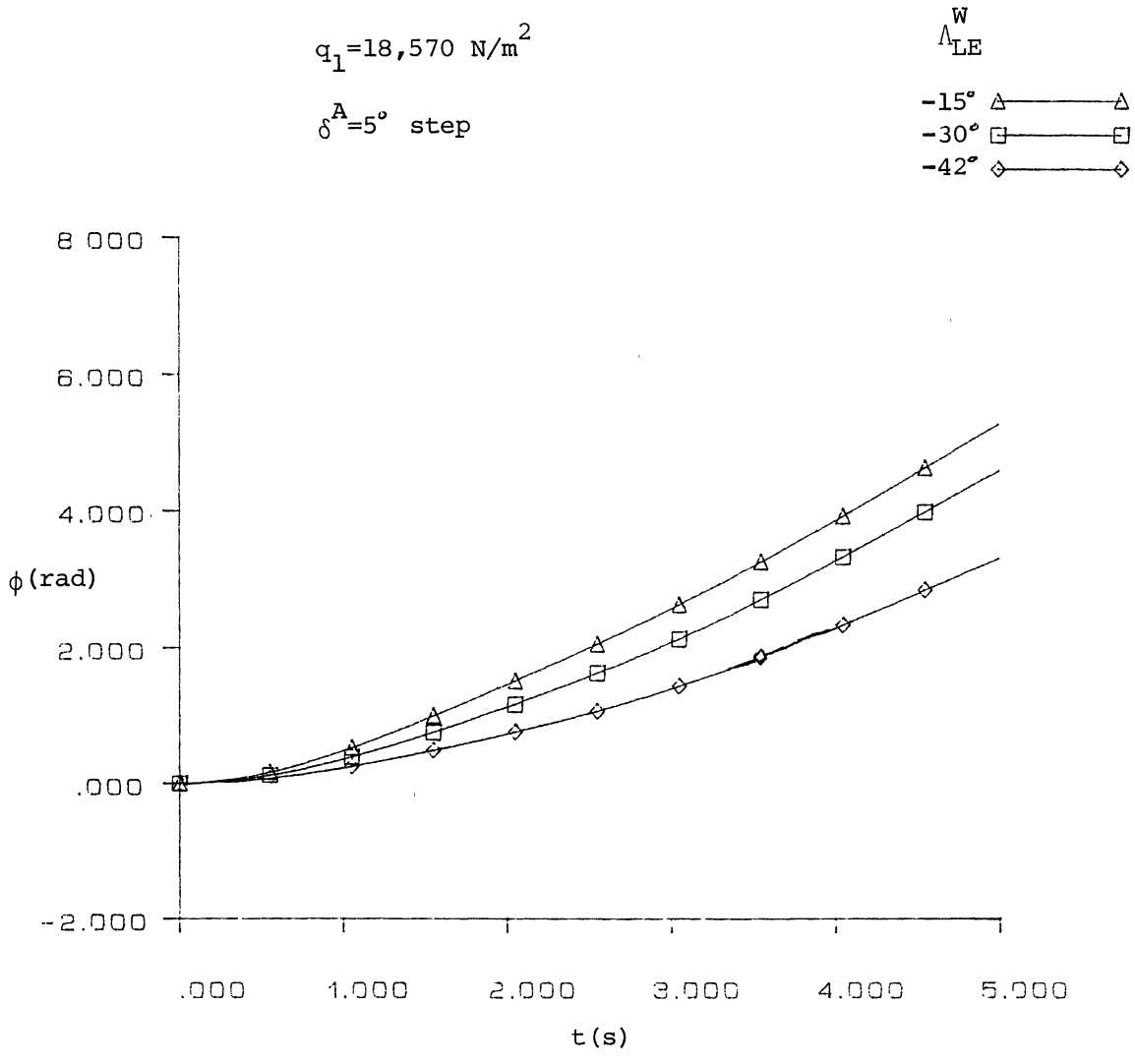

ϕ time response

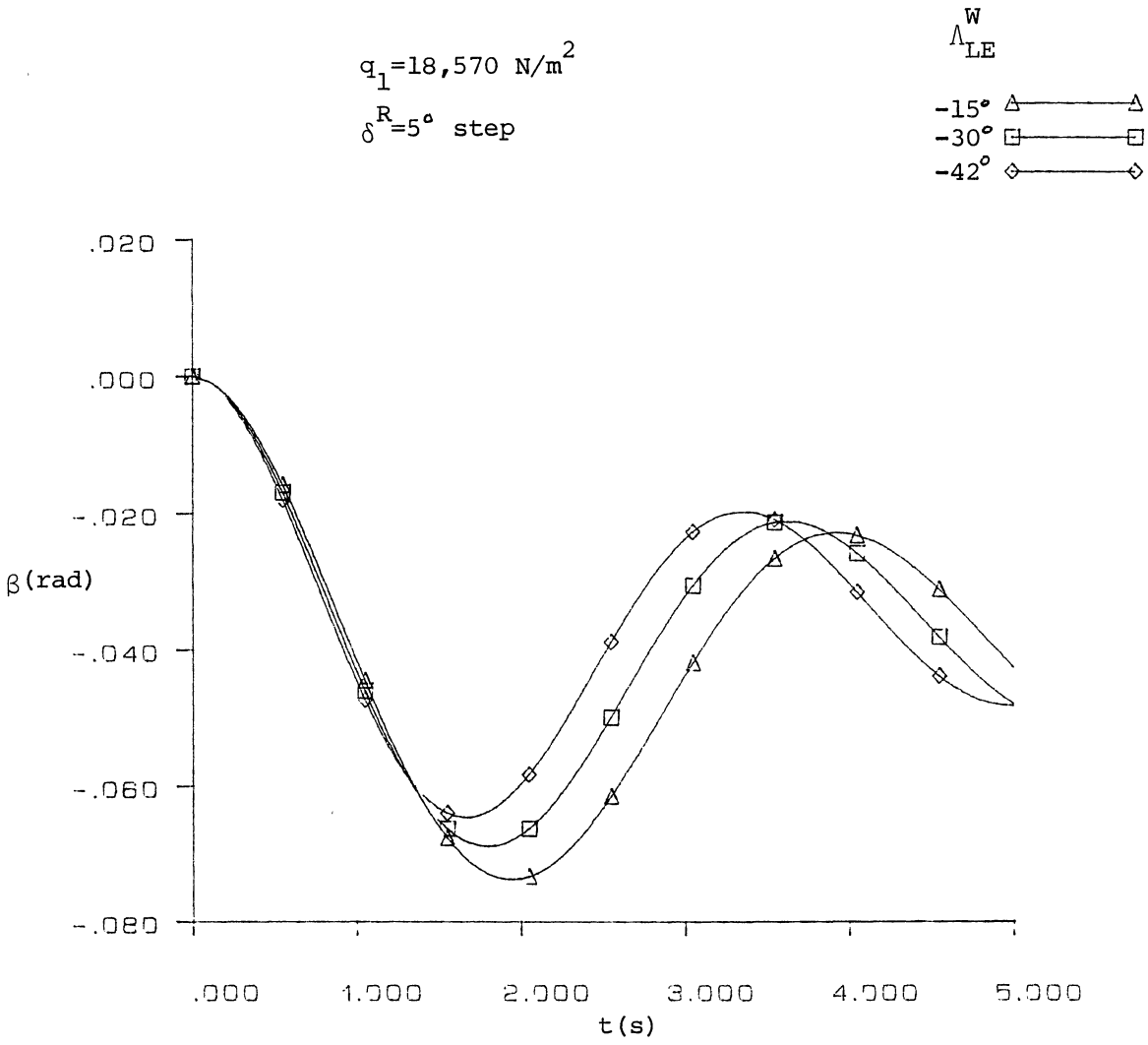

β time response

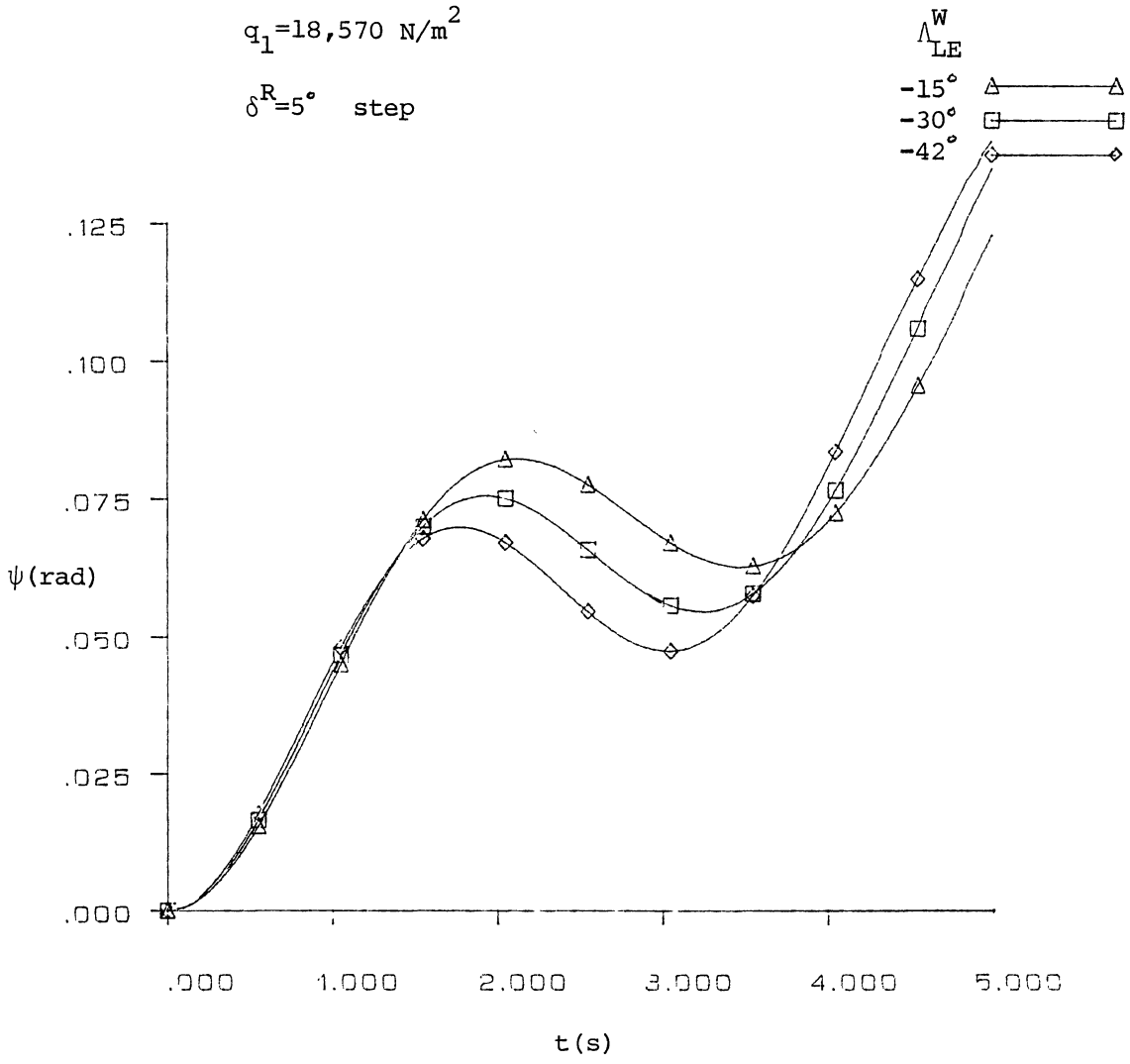

ψ time response

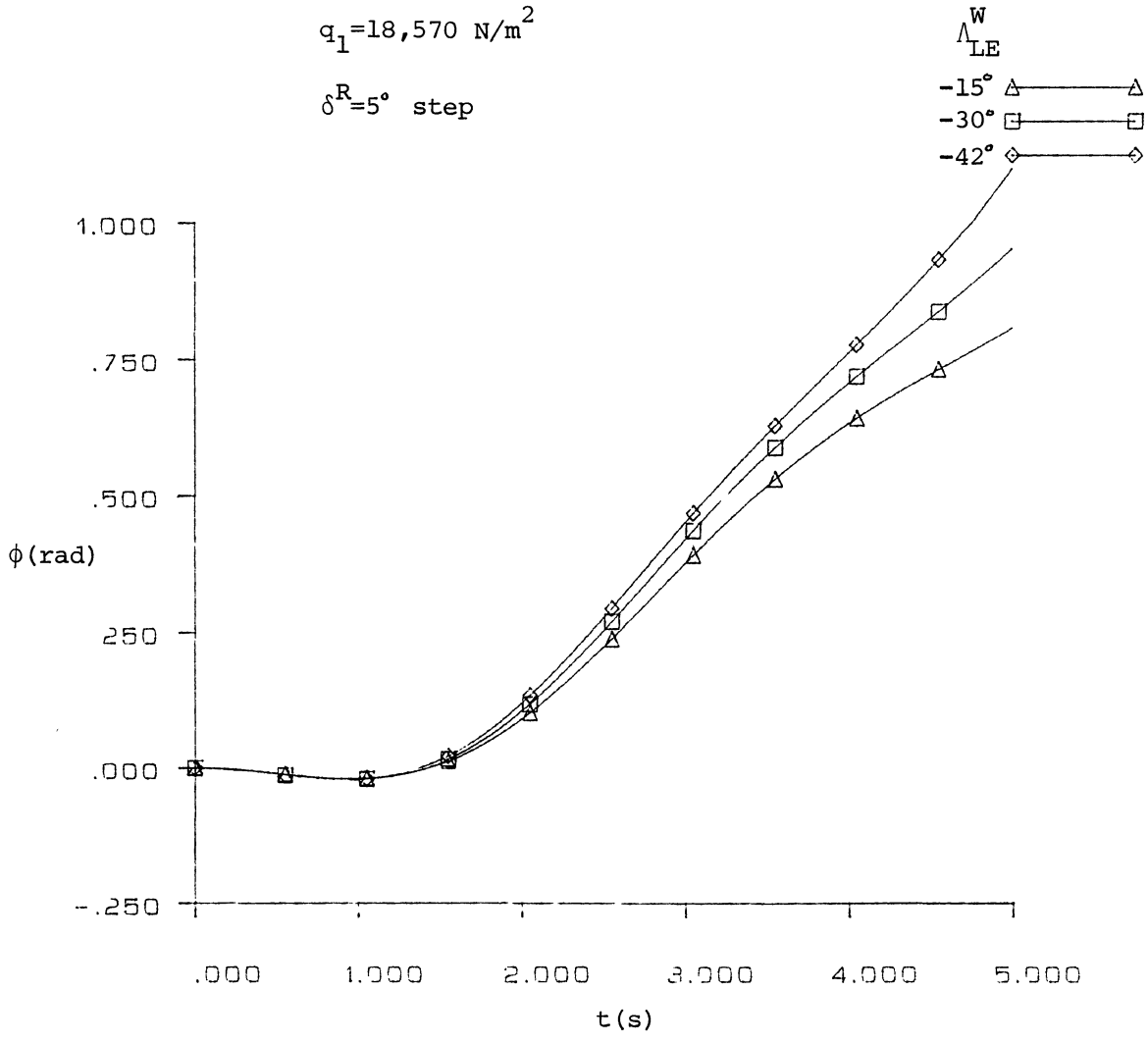

ϕ time response

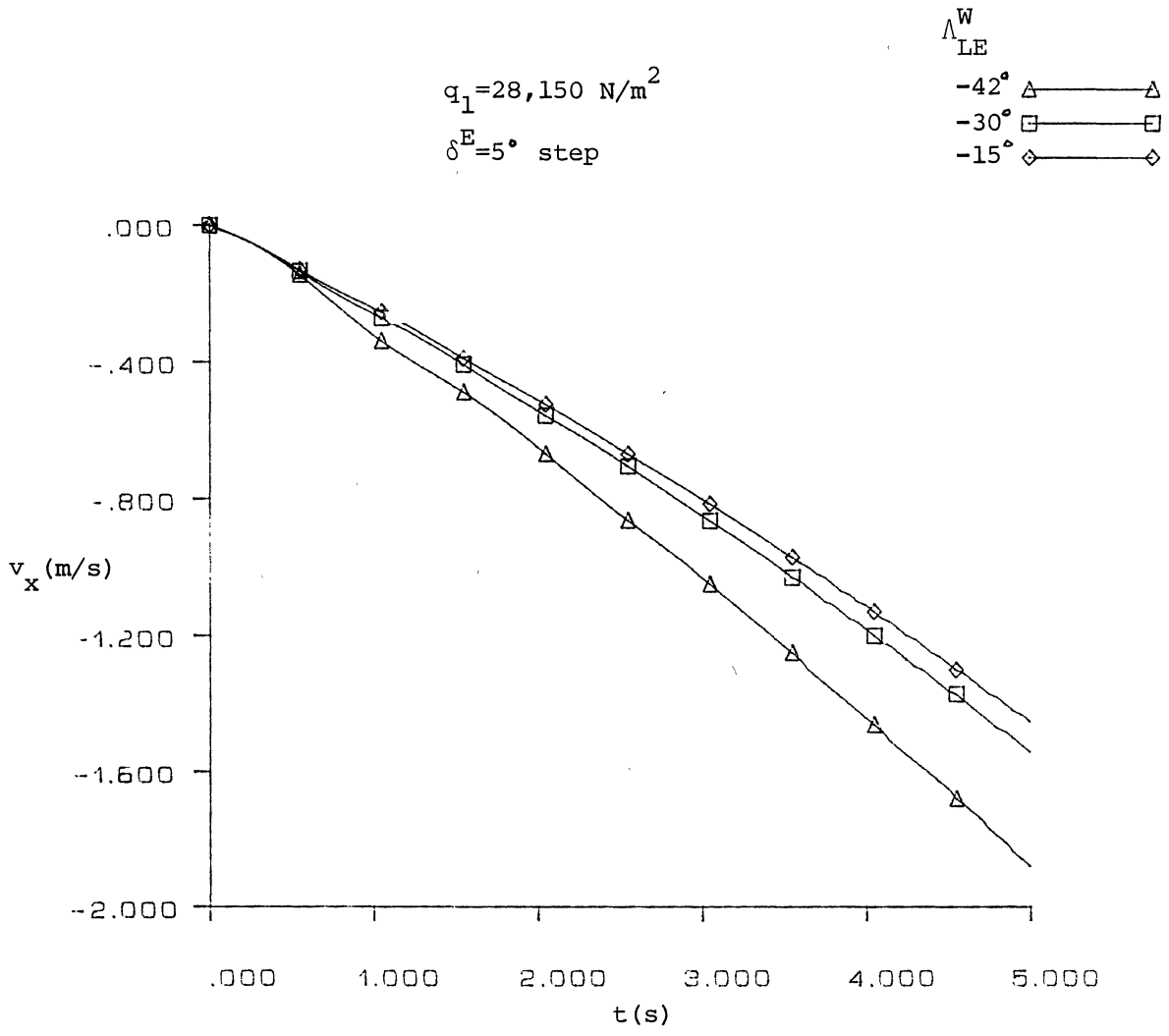

v_x time response

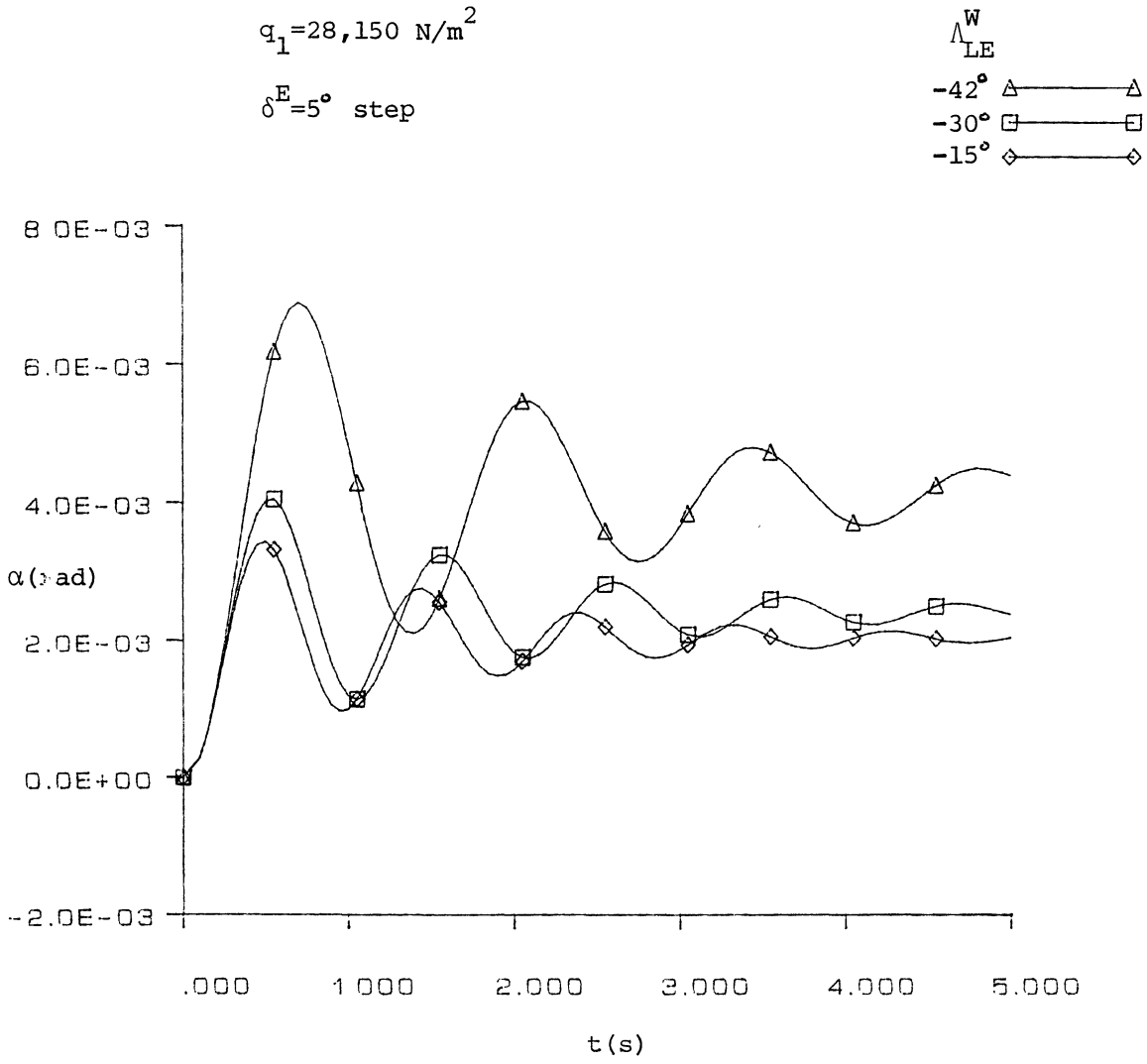

α time response

q_1=28,150 N/m^2

δ^E=5° step

Λ^W_{LE}

-42° △——△

-30° □——□

-15° ◇——◇

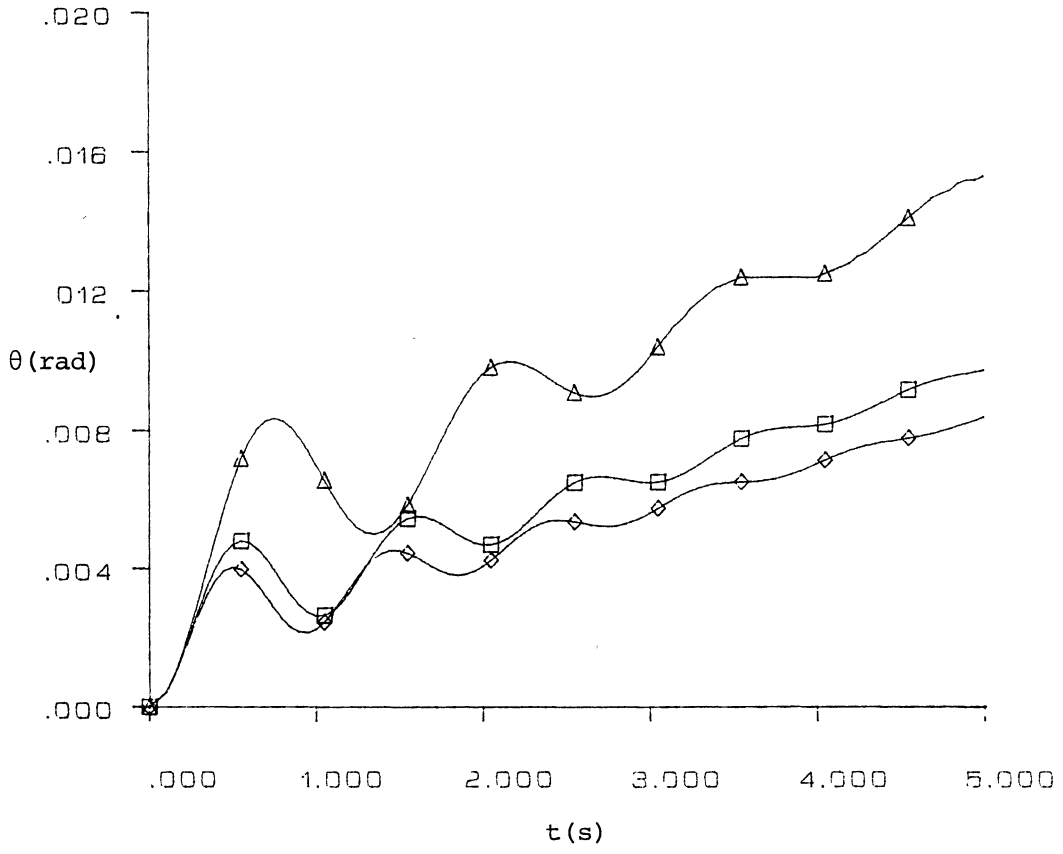

θ time response

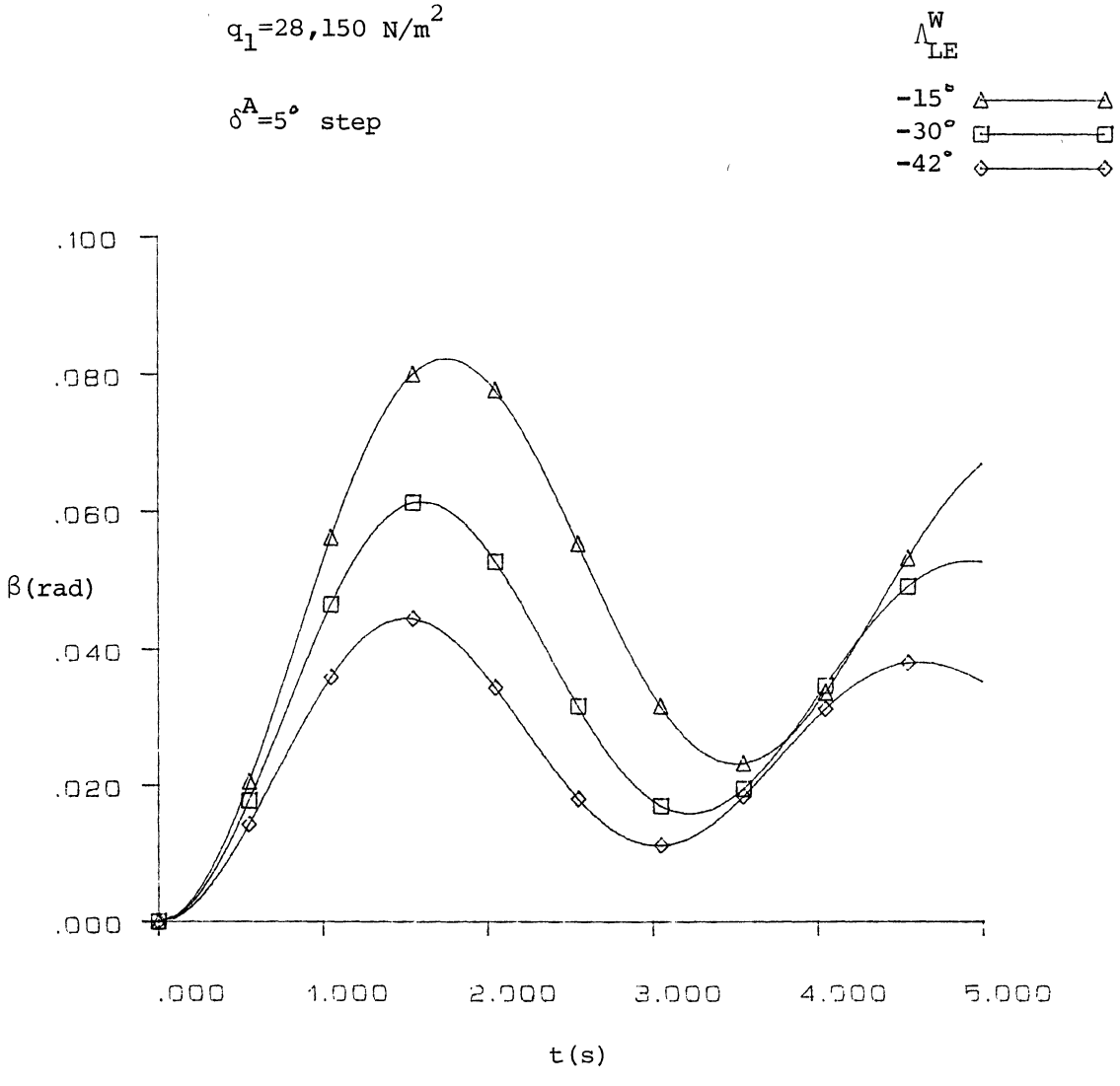

β time response

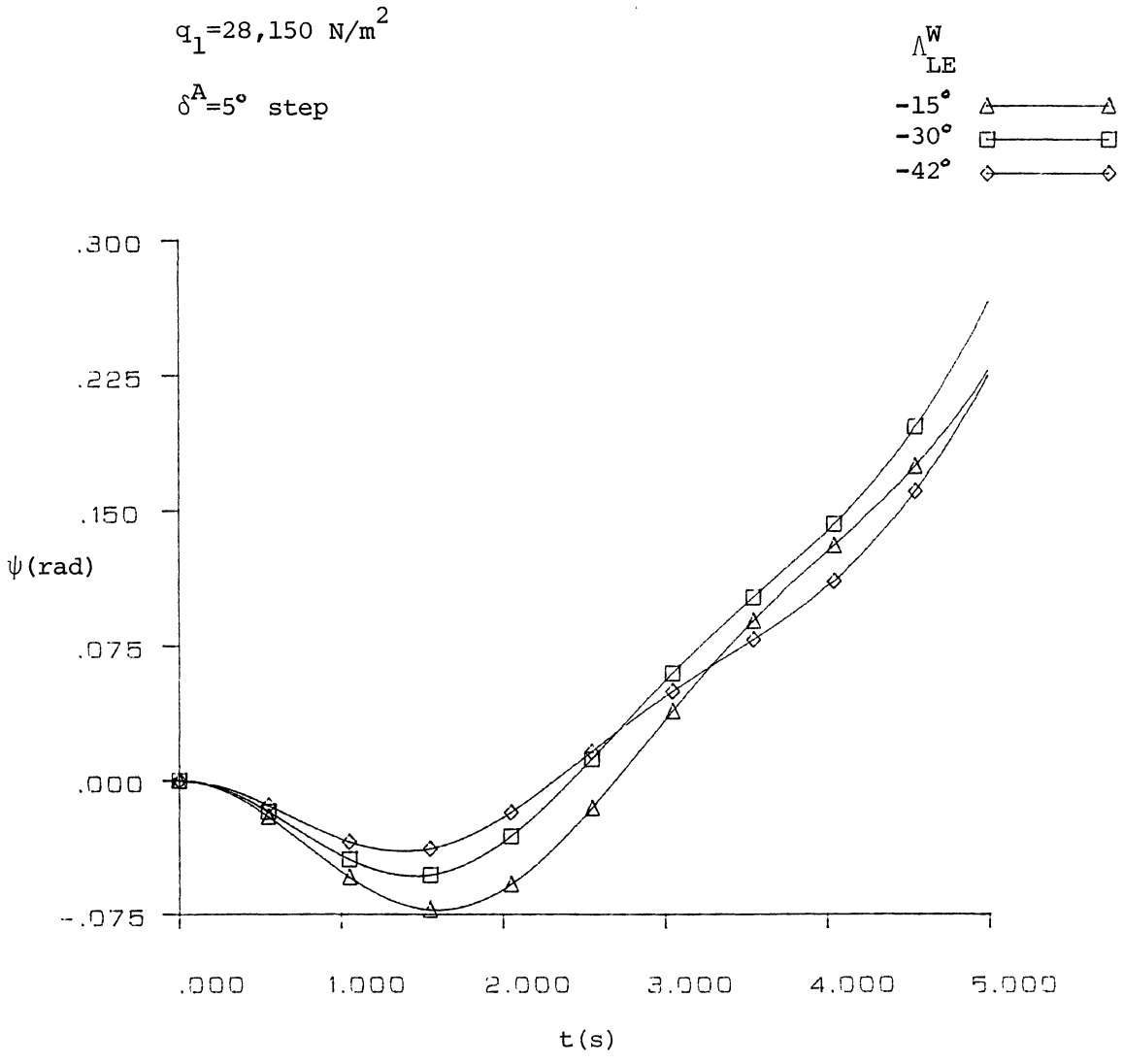

ψ time response

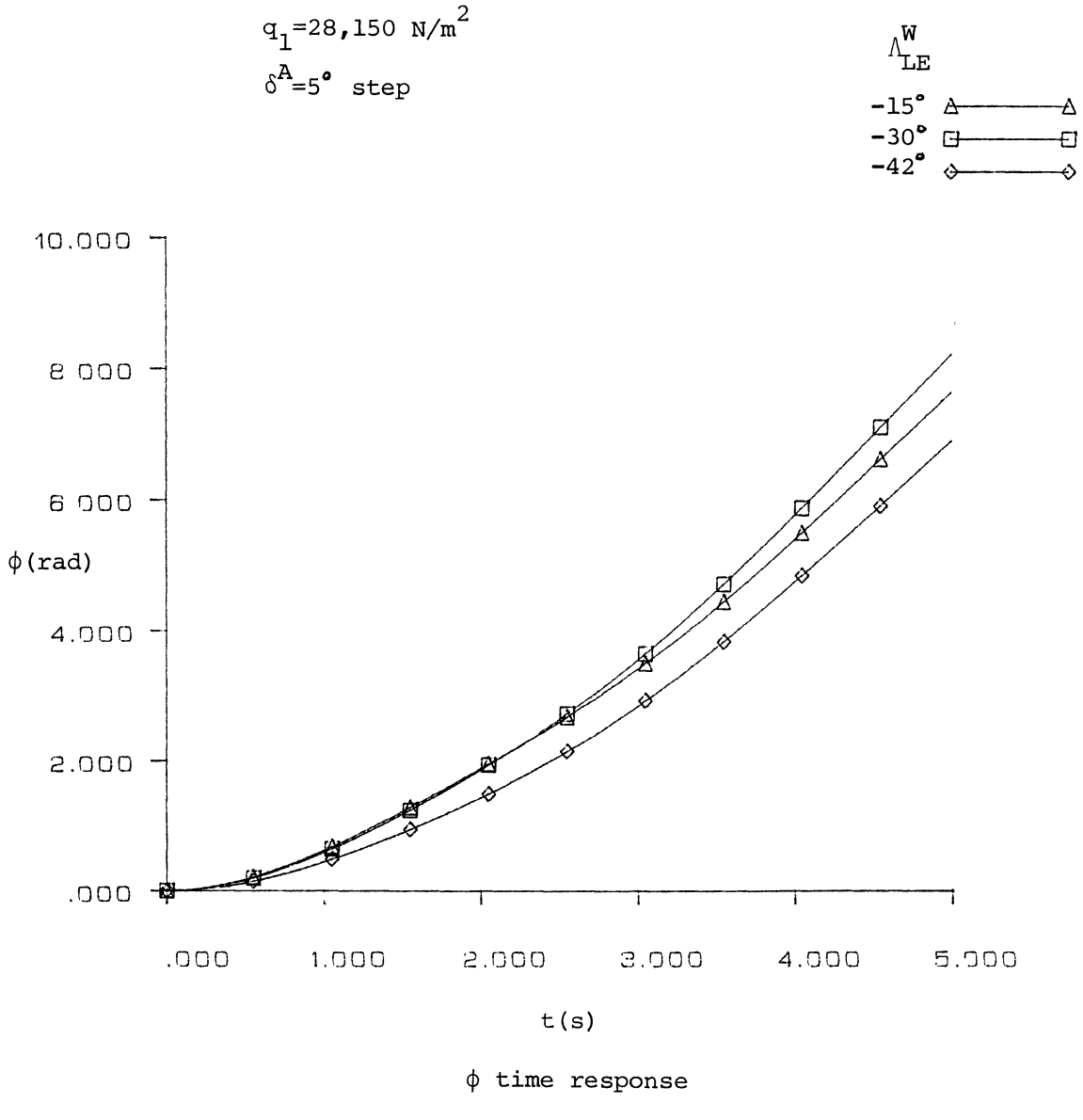

ϕ time response

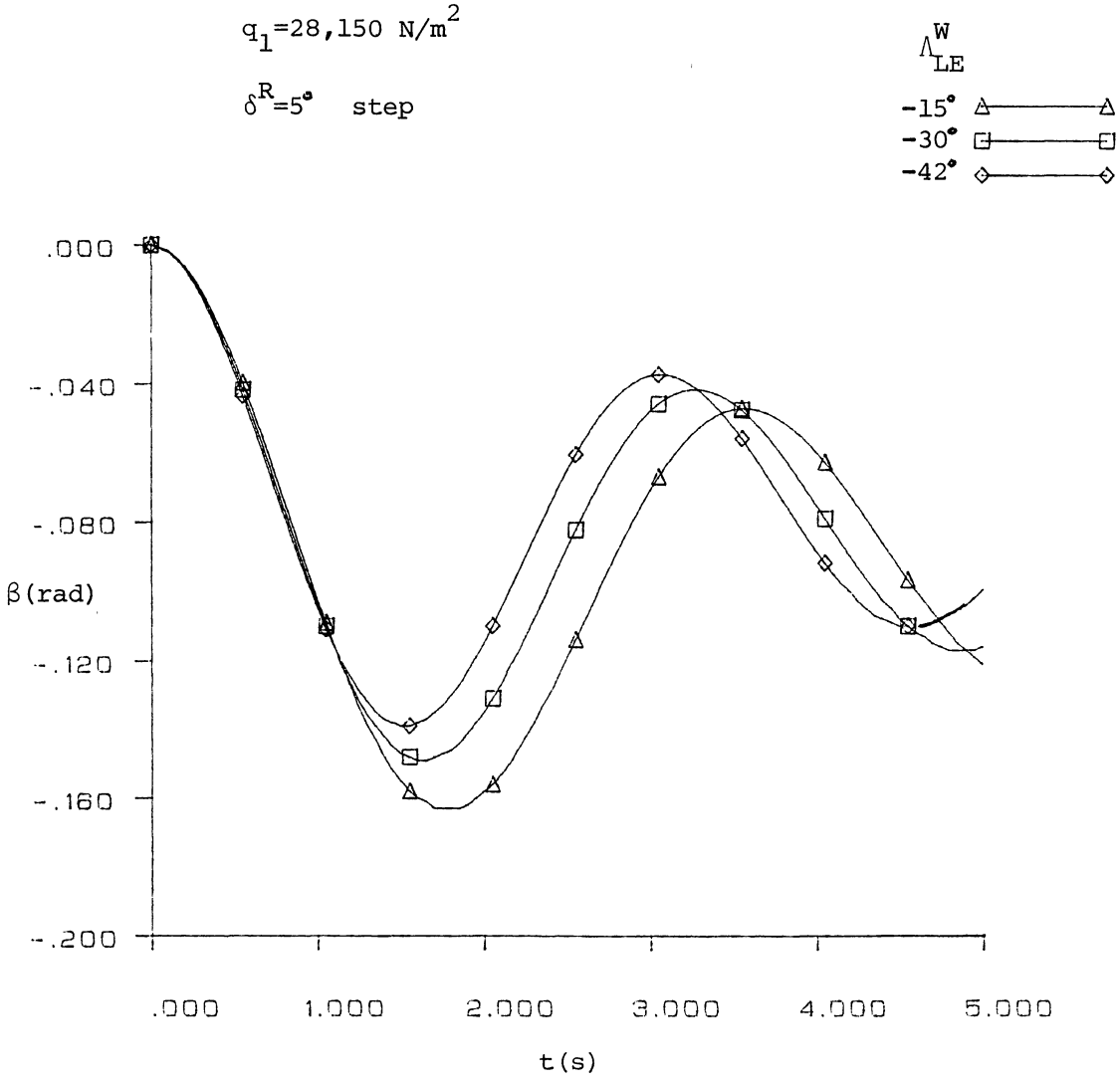

β time response

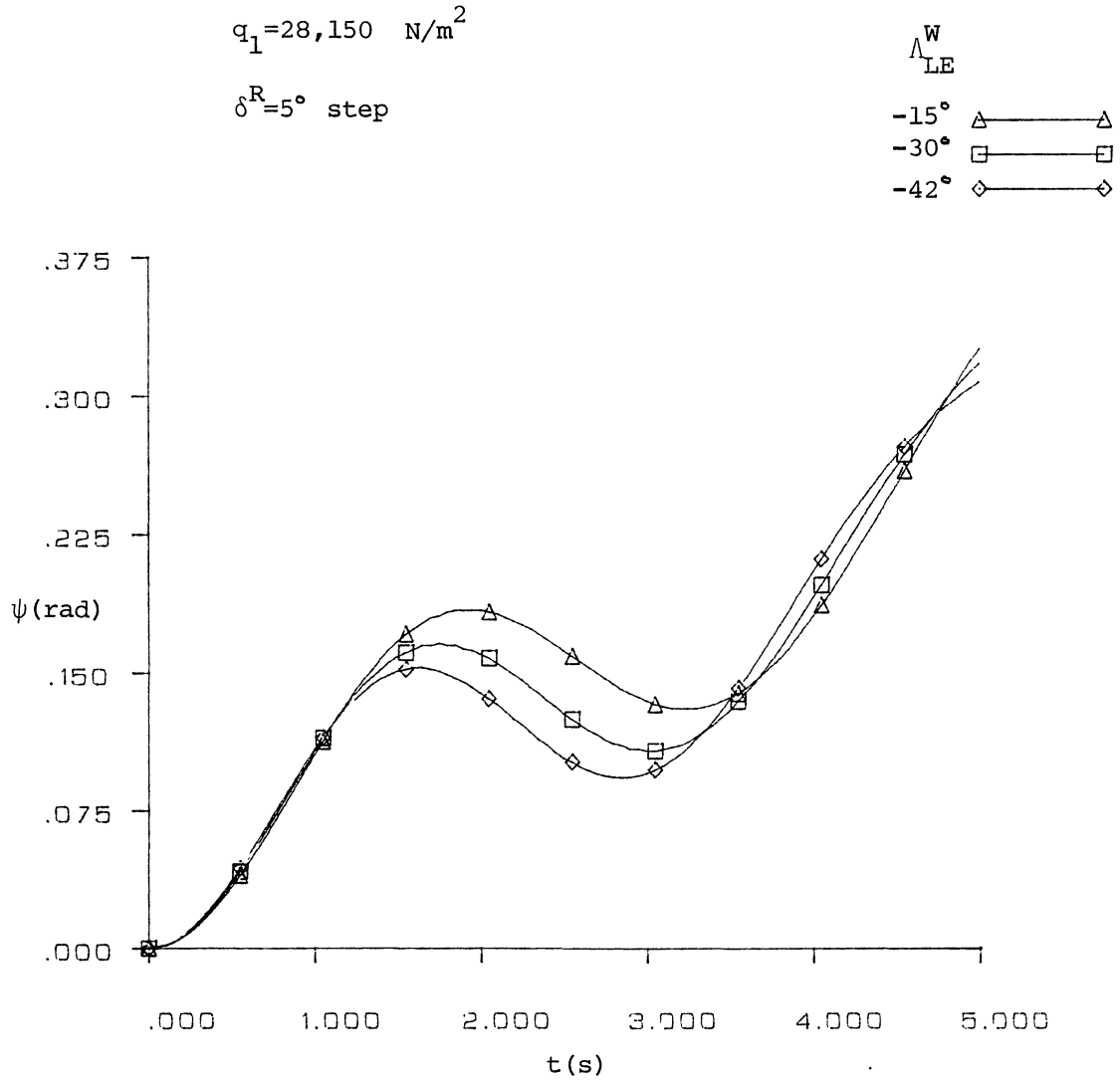

ψ time response

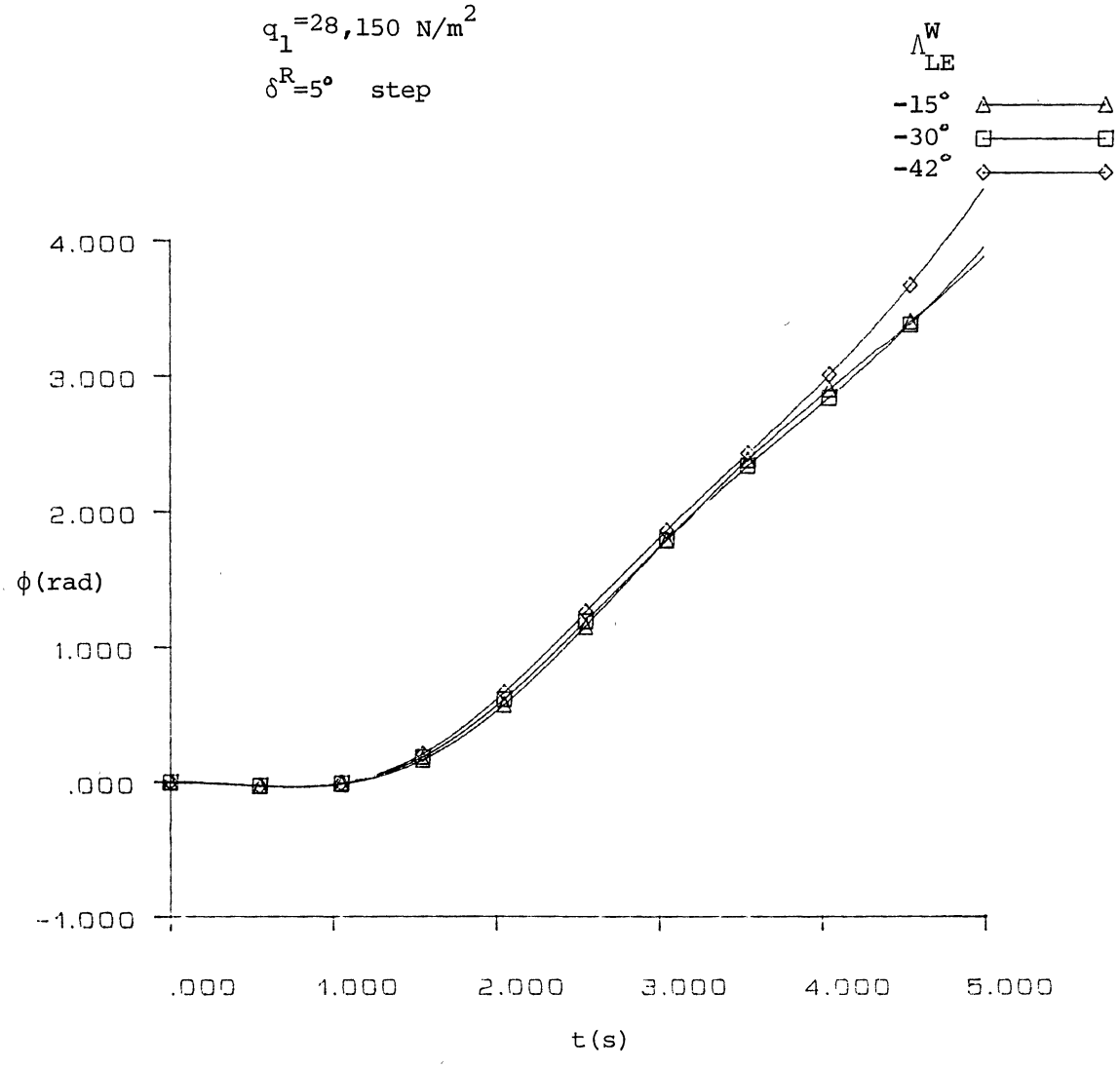

ϕ time response

VITA 2

BRETT ALAN NEWMAN

Candidate for the Degree of

Master of Science

Thesis: CLASSICAL FLIGHT DYNAMICS OF A VARIABLE FORWARD SWEEP WING AIRCRAFT

Major Field: Mechanical and Aerospace Engineering

Biographical:

Personal: Born in Oklahoma City, Oklahoma 23 October 1961. Single. Enjoy sports and outdoors.

Education: Graduated from Putnam City High School, Oklahoma City, Oklahoma, May, 1979. Received Bachelor of Science Degree in Mechanical and Aerospace Engineering from Oklahoma State University, May, 1983. Completed requirements for the Master of Science Degree at Oklahoma State University in May, 1985.

Experience: Research Fellow at Theoretical Mechanics Branch, Langley Research Center, NASA, during summer 1984. Engineering Technician at Materiel Management Engineering Analysis Reliability, AFLC, Tinker AFB during summer 1982. Teaching Assistant at School of Mechanical and Aerospace Engineering, Oklahoma State University duri g 1983-1985.

Organizations: Member of National Society of Professional Engineers and American Institute of Aeronautics and Astronautics.